TU Delft

Delft University of Technology

Document Version
Final published version

Licence
CC BY

Citation (APA)
Gaggero, M. B. (2026). *Autonomous masonry repair with a bacteria-based self-healing mortar: Research framework and multi-level experimental validation tailored to historical constructions.* [Dissertation (TU Delft), Delft University of Technology]. https://doi.org/10.4233/uuid:1bf71164-26a0-411c-80d3-7d67bad34fe7

Important note
To cite this publication, please use the final published version (if applicable).
Please check the document version above.

Copyright
In case the licence states “Dutch Copyright Act (Article 25fa)”, this publication was made available Green Open Access via the TU Delft Institutional Repository pursuant to Dutch Copyright Act (Article 25fa, the Taverne amendment). This provision does not affect copyright ownership.
Unless copyright is transferred by contract or statute, it remains with the copyright holder.

Sharing and reuse
Other than for strictly personal use, it is not permitted to download, forward or distribute the text or part of it, without the consent of the author(s) and/or copyright holder(s), unless the work is under an open content license such as Creative Commons.

Takedown policy
Please contact us and provide details if you believe this document breaches copyrights.
We will remove access to the work immediately and investigate your claim.

This work is downloaded from Delft University of Technology.



AUTONOMOUS MASONRY REPAIR WITH A BACTERIA-BASED SELF-HEALING MORTAR

Research framework and multi-level experimental validation tailored to historical constructions

Maria Belen Gaggero



AUTONOMOUS MASONRY REPAIR WITH A BACTERIA-BASED SELF-HEALING MORTAR

RESEARCH FRAMEWORK AND MULTI-LEVEL EXPERIMENTAL VALIDATION TAILORED TO HISTORICAL CONSTRUCTIONS

AUTONOMOUS MASONRY REPAIR WITH A BACTERIA-BASED SELF-HEALING MORTAR

RESEARCH FRAMEWORK AND MULTI-LEVEL EXPERIMENTAL VALIDATION TAILORED TO HISTORICAL CONSTRUCTIONS

Dissertation

for the purpose of obtaining the degree of doctor
at Delft University of Technology,
by the authority of the Rector Magnificus,
Prof.dr.ir. H. Bijl,
chair of the Board for Doctorates
to be defended publicly on
Monday, 28 September 2026 at 17:30

by

Maria Belen GAGGERO

This dissertation has been approved by the (co)promotors.

Composition of the doctoral committee:

Rector Magnificus		Chairperson
Em.prof.dr.ir.	J.G. Rots	Delft University of Technology, promotor
Dr.	R. Esposito	Delft University of Technology, copromotor
Dr.ir.	P. A. Korswagen	Delft University of Technology, copromotor

Independent members:

Prof.dr.	H.M. Jonkers	Delft University of Technology
Dr.	B.A. Lubelli	Delft University of Technology
Dr.	C. De Nardi	Cardiff University, UK
Prof.dr.	F. Ubertini	UniPG, Italy
Prof.dr.ir.	H.E.J.G. Schlangen	Delft University of Technology, reserve member

This research was funded by Topsectoren en Topconsortia voor Kennis en Innovatie (TKI) in connection with research for Nederlandse Aardolie Maatschappij (NAM).

Keywords: Unreinforced Masonry (URM), Lime, Heritage, Repair, Self-healing, Bacteria
Printed by: IPSKAMP
Cover by: M.B. Gaggero
Copyright: 2026 M.B. Gaggero
ISBN: 978-94-6518-420-3

An electronic version of this dissertation is available at: https://repository.tudelft.nl/

Table of Contents

1 SUMMARY V

1 SAMENVATTING XI

1 CHAPTER 1 1

1.1 Problem definition 3

1.2 Research objectives 5

1.3 Methodology 6

1.4 Outline of the thesis 8

2 CHAPTER 2 13

2.1 Masonry in the built environment 15

2.1.1 Masonry units 18

2.1.2 Masonry mortars 19

2.2 Damage in masonry structures: mechanisms and consequences 27

2.3 Repointing as repair strategy: practice and limitations 32

2.4 Innovation in repair: insights from self-healing concrete 34

2.4.1 Autogenous healing potential of mortars 35

2.4.2 Autonomous healing strategies 38

2.4.3 Healing agent based on poly-lactic acid (Basilisk Technology) 40

2.5 Towards self-healing solutions for masonry repair 41

2.5.1 Strategies under investigation 41

2.5.2 From concrete to masonry: first use of PLA-based mortar 42

2.5.3 Integrating PLA-based agent into cement-lime masonry mortars: early insights 44

2.6 Conclusions 46

3 CHAPTER 3 49

3.1 Framework structure 51

3.2 Recovery of performance 52

3.2.1 Performance definition and measurable properties 53

3.2.2 Controlled damage induction 57

3.2.3 Healing conditions 59

3.3 Identification of healing products 60

3.4 Impact on functional properties 63

3.5 Summary and implementation within this thesis 64

4 CHAPTER 4 69

4.1 Introduction 71

4.2 Materials and methods 72
4.2.1 Healing agent 72
4.2.2 Mortar mixtures 73
4.2.3 Bulk density and total water absorption at atmospheric pressure 76
4.2.4 Static modulus of elasticity in compression 76
4.2.5 Flexural tests 77
4.2.6 Compressive tests 81
4.2.7 Healing environments 82
4.2.8 Visual inspection 83
4.2.9 Fourier Transform Infrared Spectroscopy 83
4.3 Performance recovery 84
4.3.1 Mechanical recovery 84
4.3.2 Aesthetic recovery 90
4.4 Identification of healing products 94
4.5 Impact on functional properties 95
4.6 Conclusions 98

5 CHAPTER 5 101

5.1 Introduction 103
5.2 Materials and methods 104
5.2.1 Masonry mortars 104
5.2.2 Bricks 105
5.2.3 Masonry specimens 106
5.2.4 Bond wrench tests 106
5.2.5 Water permeability test 109
5.2.6 Shear triplet tests 111
5.2.7 Healing environment 113
5.2.8 Visual inspection 113
5.3 Performance recovery 113
5.3.1 Mechanical recovery 113
5.3.2 Watertightness recovery 116
5.3.3 Aesthetic recovery 117
5.4 Identification of healing products 119
5.5 Impact on functional properties 120
5.6 Conclusions 124

6 CHAPTER 6 127

6.1 Introduction 129
6.2 Materials and methods 130
6.2.1 Masonry materials and specimens 130

6.2.2 Compression tests on wallettes 131
6.2.3 In-plane four-point bending tests on spandrels 133
6.2.4 Healing environment 136
6.2.5 Visual inspection 136
6.2.6 Fourier Transform Infrared Spectroscopy 137
6.3 Performance recovery 137
6.4 Identification of healing products 138
6.5 Impact on functional properties 139
6.6 Conclusions 141

7 CHAPTER 7 143

7.1 Summary of main research findings 145
7.1.1 Formulation of the conceptual starting point and hypothesis for autonomous self-healing in masonry 145
7.1.2 Design of an experimental framework for exploring autonomous repair in masonry 146
7.1.3 Experimental validation of the effectiveness of a bacteria-based self-healing agent in historical masonry 147
7.2 Scientific and societal relevance 150
7.3 Recommendations for future research 151

2 BIBLIOGRAPHY 153

3 ACKNOWLEDGMENTS 161

4 CURRICULUM VITAE 163

5 LIST OF PUBLICATIONS 165

Summary

Unreinforced masonry structures constitute a substantial part of the global built environment and are inherently prone to **cracking** throughout their service life. Due to their limited tensile strength and high stiffness, cracking is an inevitable consequence of ageing processes and may be further aggravated by other actions such as ground movements or vibrations. Although cracks may initially be small, they can progressively compromise watertightness, mechanical performance, and aesthetic integrity. If not addressed in time, this damage can lead to accelerated deterioration, increased maintenance demands, and, in the case of historic masonry, the loss of cultural value. Conventional repair strategies, such as repointing, are effective, yet they rely on **repeated maintenance cycles** over the service life of a structure, thereby motivating the exploration of autonomous repair approaches. In this context, **self-healing mortars** offer a potential means of incorporating autonomous damage mitigation within the repair material itself. These mortars obtain their autonomous properties from engineered agents added during mixing, allowing the material to respond to damage without external intervention. While cement-based self-healing mortars have been extensively investigated for concrete repair, their application to masonry remains largely unexplored.

This thesis addresses this gap by evaluating the **technical viability of self-healing mortars specifically for masonry repair**, with particular attention to **heritage applications** and **lime-based mortars**, traditionally used in practice. As a first systematic investigation of this topic, the research establishes a scientific basis for future developments through three interconnected stages: (i) a comprehensive literature review and preparatory studies, (ii) the development of a dedicated research framework for assessing self-healing mortars for masonry repair, and (iii) its application to evaluate a specific self-healing mortar incorporating a commercially available bacteria-based poly-lactic-acid (PLA) healing agent. Rather than optimising the healing agent itself, originally designed for concrete repair, this work evaluates its application in lime mortars and masonry repair contexts. Given the focus on heritage structures, the agent is investigated using materials representative of historic masonry in the Netherlands. Although the framework is developed around bacteria-based self-healing mortars, reflecting the system studied

in this thesis, it is conceived as a flexible methodology that can be extended to other self-healing strategies, including crystalline admixtures and superabsorbent polymers, among others.

As a first step, the **literature review** (**Chapter 2**) established the conceptual starting point and underlying assumptions for self-healing masonry by linking masonry materials, degradation mechanisms, and repointing practice with insights from self-healing concrete research. **Autonomous self-healing** (induced by the activation of a healing agent) is framed as a technological extension of the **autogenous healing** capacity historically observed in lime-based mortars: a process mainly effective for microcracks. The review shows that, despite these historical roots, systematic research on self-healing has focused predominantly on cement-based materials for concrete applications, revealing a clear research gap for masonry, which relies instead on lime-based mortars. At the same time, it highlights how existing knowledge from self-healing concrete can be transferred to masonry, particularly for strategies based on calcium carbonate precipitation, which is inherently compatible with lime-based binders. For instance, preparatory studies conducted by the author prior to this thesis confirmed the feasibility of a bacteria-based poly-lactic acid (PLA) healing agent, while also highlighting the decisive influence of healing conditions and masonry porosity, thereby motivating the need for a structured assessment framework.

Building on this groundwork, **Chapter 3** proposes a **dedicated research framework** to assess self-healing performance for masonry. Recognising masonry as a composite material, the framework is structured across three levels: **mortar**, **brick–mortar**, and **masonry component**. At each level, three core aspects are systematically addressed: (i) **recovery of compromised performance**, namely watertightness, aesthetics and mechanical properties; (ii) **identification of healing products**; (iii) **impact of the agent on relevant functional properties**. This third aspect informs practical feasibility, as it indicates whether the agent can be used without compromising application-related requirements, such as workability. This approach allows governing parameters to be explored in smaller and more manageable specimens (e.g. mortar bars, couplets) before validating their relevance in larger masonry configurations (e.g. spandrels). Key variables include how damage is induced and its extent, together with healing environment and duration. The framework is intended as a first step towards a more consistent assessment of self-healing masonry and provides the methodological basis for the experimental investigation of the selected agent across Chapters 4-6.

On this basis, the experimental programme begins at the **mortar level** (**Chapter 4**), where the **PLA-based agent promoted calcium carbonate precipitation and crack filling in lime–cement mixtures without detrimental functional effects.** Using 40×40×160 mm³ mortar bars, the study assessed four mortar compositions with lime/cement ratios of 0, 0.33, 1, and 3.33, ranging from a pure cement mix to a composition aligned with

traditional Dutch masonry repair mortars. Mechanical and aesthetic recovery was quantified through CMOD-controlled three-point bending tests, followed by healing under different environmental conditions. In parallel, Fourier Transform Infrared Spectroscopy (FTIR) was used to identify the precipitated healing products, while complementary tests evaluated the influence of the healing agent on functional properties, including water absorption, compressive strength, and elastic modulus. Results show that **autogenous healing occurred alongside autonomous healing**: both mortars behaved similarly for fine cracks (≈0.07 mm), whereas for crack widths above 0.3 mm the bacteria-based mortars outperformed the reference, achieving **complete aesthetic crack filling**. This supports the need to evaluate crack widths above autogenous limits when quantifying autonomous healing effects. FTIR verified calcium carbonate precipitation, a low-solubility phase, supporting correct agent activation and indicating **potential for watertightness restoration**. Healing (autogenous and autonomous) occurred exclusively under wet conditions (20±2 °C, 95±5% RH) and wet–dry cycles (20±2 °C, 1h wet, 23h dry), while no recovery occurred under moderate humidity (20±2 °C, 80±5% RH). While further investigation is needed on healing duration, wider cracks, and realistic healing conditions, the results on mortar bars suggest that higher lime content improves healing efficiency. This confirms the agent's suitability for masonry mortars and supports further testing of the mortar with a 3.33 lime/cement ratio at the brick–mortar and masonry levels.

Progressing to the **brick–mortar level**, **Chapter 5** confirmed the feasibility of the **PLA-based agent in solid clay masonry built with cement–lime mortar, extending mechanical recovery beyond autogenous limits without adverse functional effects**. This stage evaluated performance using couplets (175×80×85 mm^3), triplets (175×140×85 mm^3), and cores (Ø75×85 mm) constructed with the selected high lime-to-cement ratio mortar (3.33) and solid clay bricks, a combination specifically chosen to represent historic Dutch masonry applications. Mechanical recovery was assessed by means of CMOD controlled bond wrench tests, which were used both to induce controlled cracking and to quantify flexural bond strength recovery. The experimental set-up, developed by the author in previous research, allows stable crack initiation and propagation. In parallel, watertightness restoration and aesthetics were evaluated on cores cracked in shear. This was performed using a permeability-based testing approach developed within this thesis, inspired by methodologies originally applied in self-healing concrete research. Performance recovery was assessed under wet healing conditions for 180 days. Concurrently, the influence of the agent on functional properties (including permeability, initial and residual shear properties, and flexural bond strength and energy) was evaluated to ensure no detrimental effects. Similar to the mortar level, results at brick-mortar level show that autogenous healing contributed to the recovery of flexural bond strength for fine cracks (≈0.07 mm); however, for crack widths above 0.16 mm,

the healing agent clearly outperformed the reference. **Flexural bond strength recovery averaged 27%, with peak values reaching up to 65% after 180 days**. Watertightness recovery was likewise observed, although results exhibited greater scatter due to the large crack width variability, as permeability specimens were cracked up to failure. These findings were supported by visual inspection, which revealed **localised crack filling and no evidence of leaching under wet healing conditions** representative of the masonry considered, indirectly indicating effective activation of the healing agent. Given the wide and variable crack widths (cracked up to failure), aesthetic recovery was only partial and healed shear properties could therefore not be assessed. Consistent with the mortar level, the presence of the healing agent also influenced material properties at the brick-mortar level, albeit without introducing major drawbacks. The results obtained primarily apply to cracks localised within the mortar (a potentially favourable scenario, as both crack faces are self-healing mortar), but they do not preclude interface cracking cases, for which pilot studies also indicated effective healing. Overall, tests on couplets, triplets and cores further confirm the potential of the healing agent, while highlighting the importance of controlled damage induction methods and supporting continued investigation into permeability-based testing approaches for their use in the investigation of self-healing masonry.

The final experimental stage (**Chapter 6**) addressed the **masonry component level**, with the aim of evaluating the performance of the selected self-healing agent in larger-scale specimens. Spandrels (1100x540x85 mm^3) were subjected to four-point bending to assess the recovery of performance (mechanical and aesthetics), while compression tests on wallettes (360x490x85 mm^3) were conducted to also evaluate the agent's impact on functional properties. In addition, FTIR analyses were performed in parallel to identify and verify the nature of the precipitated healing products. Despite using the same materials and comparable curing and healing conditions as in earlier levels, effective activation of the healing agent was not observed. FTIR analysis revealed **leaching of the PLA-based encapsulation material**, already evident after curing and intensified during subsequent healing under wet conditions (20±2 °C, 95±5% RH). This behaviour can be attributed to scale-dependent moisture gradients and internal water transport developing during early curing, which promoted the migration of the encapsulation material towards external surfaces. Crucially, these results do not suggest an intrinsic material incompatibility or improper healing conditions; instead, they highlight the vital role of scale-specific curing strategies, calling for further research to optimise these protocols and verify the agent's applicability at the structural level.

Overall, the results of this thesis demonstrate that **bacteria-based autonomous self-healing can be successfully activated in masonry materials** and a PLA-based healing agent originally developed for concrete can be transferred to masonry repair, provided that curing and healing conditions are carefully addressed. Beyond initiating the

validation of a specific PLA-based self-healing agent, the thesis contributes to a **structured experimental framework to support the systematic investigation of self-healing masonry** and identifies key parameters governing healing performance across material levels. Nevertheless, given the inherent variability of masonry materials and the limited number of specimens in some series, further testing on larger datasets is recommended to consolidate the trends observed. These contributions provide a scientific basis for future research and support the development of autonomous self-healing mortars as a complementary and potentially sustainable approach to masonry repair, particularly in the context of heritage conservation.

Samenvatting

Ongewapende metselwerkconstructies vormen een aanzienlijk deel van de wereldwijde gebouwde omgeving en zijn van nature gevoelig voor scheurvorming gedurende hun levensduur. Door hun beperkte treksterkte en hoge stijfheid is scheurvorming een onvermijdelijk gevolg van verouderingsprocessen en kan zij verder worden verergerd door andere invloeden, zoals bodembewegingen of trillingen. Hoewel scheuren aanvankelijk klein kunnen zijn, kunnen zij geleidelijk de waterdichtheid, mechanische prestaties en esthetische integriteit aantasten. Indien niet tijdig aangepakt, kan deze schade leiden tot versnelde degradatie, verhoogde onderhoudsbehoefte en, in het geval van historisch metselwerk, verlies van culturele waarde. Conventionele herstelstrategieën, zoals het opnieuw voegen (repointing), zijn effectief, maar vereisen herhaalde onderhoudscycli gedurende de levensduur van een constructie. Dit motiveert de verkenning van autonome herstelbenaderingen. In deze context bieden zelfhelende mortels een potentiële manier om autonome schadebeperking in het reparatiemateriaal zelf te integreren. Deze mortels verkrijgen hun autonome helende eigenschappen door toevoeging van speciaal ontworpen agentia tijdens het mengen, waardoor het materiaal zonder externe interventie kan reageren op schade. Hoewel cementgebonden zelfhelende mortels uitgebreid zijn onderzocht voor betonherstel, blijft hun toepassing in metselwerk grotendeels onontgonnen.

Dit proefschrift richt zich op deze kennislacune door de technische haalbaarheid van zelfhelende mortels specifiek voor metselwerkherstel te evalueren, met bijzondere aandacht voor erfgoedtoepassingen en kalkhoudende mortels, die traditioneel in de metselwerkpraktijk worden gebruikt. Als eerste systematische studie op dit gebied legt het onderzoek een wetenschappelijke basis voor verdere ontwikkelingen via drie onderling verbonden fasen: (i) een uitgebreide literatuurstudie en voorbereidende studies, (ii) de ontwikkeling van een specifiek onderzoeksraamwerk voor de beoordeling van zelfhelende mortels voor metselwerkherstel, en (iii) de toepassing daarvan om een specifieke zelfhelende mortel te evalueren. De specifieke mortel bevat een commercieel beschikbare bacteriegebaseerde poly-lactide (PLA) helingsmiddel, ook wel genoemd helingsagent. In plaats van het helingsagent, dat oorspronkelijk werd ontworpen voor

betonherstel zelf te optimaliseren, evalueert dit werk de toepassing ervan in kalkhoudende mortels voor metselwerkherstel. Gezien de focus op erfgoedconstructies wordt het agent onderzocht met materialen die representatief zijn voor historisch metselwerk in Nederland. Hoewel het raamwerk is ontwikkeld rond bacteriegebaseerde zelfhelende mortels, overeenkomstig het systeem dat in dit proefschrift wordt bestudeerd, is het opgezet als een flexibele methodologie die kan worden uitgebreid naar andere zelfhelende strategieën, waaronder kristallijne toevoegingsmiddelen en superabsorberende polymeren.

Als eerste stap stelt de literatuurstudie (Hoofdstuk 2) het conceptuele uitgangspunt en de onderliggende aannames voor zelfhelend metselwerk vast door metselwerkmaterialen, degradatiemechanismen en voegwerkherstel te verbinden met inzichten uit onderzoek naar zelfhelend beton. Autonome zelfheling (geïnduceerd door de activatie van een helingsagent) wordt gepositioneerd als een technologische uitbreiding van de autogene helingscapaciteit die historisch is waargenomen in kalkhoudende mortels: een proces dat voornamelijk effectief is voor microscheuren. De literatuurstudie toont aan dat, ondanks deze historische wortels, systematisch onderzoek naar zelfheling zich voornamelijk heeft gericht op cementgebonden materialen voor betontoepassingen. Dit legt een duidelijke onderzoekslacune voor metselwerk bloot, dat immers afhankelijk is van kalkhoudende mortels. Tegelijkertijd benadrukt zij hoe bestaande kennis uit zelfhelend beton kan worden overgedragen naar metselwerk, met name voor strategieën gebaseerd op calciumcarbonaatprecipitatie, die intrinsiek compatibel is met kalkhoudende bindmiddelen. Zo bevestigden voorbereidende studies, uitgevoerd door de auteur voorafgaand aan dit proefschrift, de haalbaarheid van een bacteriegebaseerd poly-lactide (PLA) helingsagent, terwijl zij ook de doorslaggevende invloed van helingscondities en metselwerkporositeit benadrukten, wat de noodzaak van een gestructureerd beoordelingsraamwerk motiveerde.

Voortbouwend op deze basis stelt Hoofdstuk 3 een specifiek onderzoeksraamwerk voor om de zelfhelingsprestatie in metselwerk te beoordelen. Metselwerk wordt erkend als een composietmateriaal en het raamwerk is gestructureerd over drie niveaus: mortel, steen–mortel en metselwerkcomponent. Op elk niveau worden drie kernaspecten systematisch behandeld: (i) herstel van aangetaste prestaties, namelijk waterdichtheid, esthetiek en mechanische eigenschappen; (ii) identificatie van helingsproducten; (iii) invloed van het agent op relevante functionele eigenschappen. Dit derde aspect is van belang voor de praktische haalbaarheid, of het helingsmiddel kan worden toegepast zonder praktische vereisten, zoals verwerkbaarheid, in het gedrang te brengen. Deze benadering maakt het mogelijk om bepalende parameters eerst te onderzoeken in kleinere en beter beheersbare proefstukken (bijv. mortelbalkjes, coupletten, tripletten) alvorens hun relevantie te valideren in grotere metselwerkconfiguraties (bijv. borstweringen). Belangrijke variabelen omvatten hoe schade wordt geïnduceerd en in

welke mate, evenals de helingsomgeving en -duur. Het raamwerk is bedoeld als een eerste stap richting een meer consistente beoordeling van zelfhelend metselwerk en biedt de methodologische basis voor het experimentele onderzoek naar het geselecteerde agent in Hoofdstukken 4–6.

Op deze basis begint het experimentele programma op mortelniveau (Hoofdstuk 4), waar het PLA-gebaseerde agent calciumcarbonaatprecipitatie en scheurvulling in kalk–cementmengsels bevorderde zonder nadelige functionele effecten. Met behulp van mortelbalkjes van 40×40×160 mm³ werden vier mortelsamenstellingen onderzocht met kalk/cement-verhoudingen van 0, 0,33, 1 en 3,33, variërend van een puur cementmengsel tot een samenstelling die aansluit bij traditionele Nederlandse metselwerkherstelmortels. Mechanisch en esthetisch herstel werd gekwantificeerd via CMOD-gestuurde driepuntsbuigproeven, gevolgd door heling onder verschillende omgevingscondities. Parallel hieraan werd Fourier Transform Infrared Spectroscopy (FTIR) gebruikt om de neergeslagen helingsproducten te identificeren, terwijl aanvullende proeven de invloed van het helingsagent op functionele eigenschappen evalueerden, waaronder waterabsorptie, druksterkte en elasticiteitsmodulus. De resultaten tonen aan dat autogene heling optrad naast autonome heling: beide mortels vertoonden vergelijkbaar gedrag voor fijne scheuren (≈0,07 mm), terwijl bij scheurwijdten groter dan 0,3 mm de bacteriegebaseerde mortels beter presteerden dan de referentie, met volledige esthetische scheurvulling als resultaat. Dit ondersteunt de noodzaak om scheurwijdten boven de autogene limieten te evalueren bij het kwantificeren van autonome helingseffecten. FTIR bevestigde calciumcarbonaatprecipitatie, een slecht oplosbare fase, wat correcte activatie van het agent ondersteunt en wijst op potentieel herstel van waterdichtheid. Heling (autogeen en autonoom) trad uitsluitend op onder natte condities (20±2 °C, 95±5% RV) en nat–droogcycli (20±2 °C, 1u nat, 23u droog), terwijl geen herstel werd waargenomen bij gematigde luchtvochtigheid (20±2 °C, 80±5% RV). Hoewel verder onderzoek nodig is naar helingsduur, bredere scheuren en realistische helingscondities, suggereren de resultaten op mortelbalkjes dat een hoger kalkgehalte de helingsefficiëntie verbetert. Dit bevestigt de geschiktheid van het agent voor metselwerkmortels en ondersteunt verdere beproeving van de mortel met een kalk/cement-verhouding van 3,33 op steen–mortel- en metselwerkniveau.

Voortgaand naar het steen–mortelniveau bevestigt Hoofdstuk 5 de haalbaarheid van het PLA-gebaseerde agent in baksteenmetselwerk opgebouwd met cement–kalkmortel. De experimenten tonen dat mechanisch herstel wordt gerealiseerd voorbij de autogene limieten zonder nadelige functionele effecten. In deze fase werd de prestatie geëvalueerd met coupletten (175×80×85 mm³), tripletten (175×140×85 mm³) en kernen (Ø75×85 mm), opgebouwd met de geselecteerde mortel met hoge kalk/cement-verhouding (3,33) en massieve kleibakstenen, een combinatie die specifiek werd gekozen om historisch

Nederlands metselwerk te representeren. Mechanisch herstel werd beoordeeld via CMOD-gestuurde bond wrench-proeven, die zowel werden gebruikt om gecontroleerde scheurvorming te induceren als om herstel van buigtreksterkte te kwantificeren. De experimentele opstelling, ontwikkeld door de auteur in eerder onderzoek, maakt stabiele scheurinitiatie en -propagatie mogelijk. Parallel hieraan werden herstel van waterdichtheid en esthetiek geëvalueerd op in afschuiving gescheurde kernen. Dit gebeurde met een op permeabiliteit gebaseerde testmethode, ontwikkeld binnen dit proefschrift en geïnspireerd door methodologieën uit onderzoek naar zelfhelend beton. Prestatieherstel werd beoordeeld onder natte helingscondities gedurende 180 dagen. Tegelijkertijd werd de invloed van het agent op functionele eigenschappen (waaronder permeabiliteit, initiële en residuele afschuifeigenschappen en buigtreksterkte en breukenergie) geëvalueerd om nadelige effecten uit te sluiten. Net als op mortelniveau droeg autogene heling bij aan het herstel van buigtrekhechting voor fijne scheuren (≈0,07 mm); voor scheurwijdten groter dan 0,16 mm presteerde het helingsagent echter duidelijk beter dan de referentie. Het herstel van buigtreksterkte bedroeg gemiddeld 27%, met piekwaarden tot 65% na 180 dagen. Herstel van waterdichtheid werd eveneens waargenomen, hoewel met grotere spreiding vanwege de aanzienlijke variabiliteit in scheurwijdten, aangezien permeabiliteitsproefstukken tot bezwijken waren gescheurd. Deze bevindingen werden ondersteund door visuele inspectie, die gelokaliseerde scheurvulling en geen aanwijzingen voor uitloging onder natte helingscondities liet zien, wat indirect wijst op effectieve activatie van het helingsagent. Gezien de brede en variabele scheurwijdten (gescheurd tot bezwijken) bleek esthetisch herstel slechts gedeeltelijk plaats te vinden, waardoor herstelde afschuifeigenschappen niet konden worden beoordeeld. Evenals bij het mortelniveau beïnvloedde de aanwezigheid van het helingsagent ook de materiaaleigenschappen op steen–mortelniveau, zij het in beperkte mate. De proeven toonden voornamelijk scheuren die in de mortel lokaliseerden (een potentieel gunstig scenario, aangezien beide scheurvlakken uit zelfhelende mortel bestaan), maar pilotstudies toonden eveneens effectieve heling voor scheuren die op het grensvlak tussen steen en mortel lokaliseerden. In het algemeen bevestigen de steen-mortel proeven op coupletten, tripletten en kernen het potentieel van het helingsagent. Ook benadrukken de proeven het belang het belang van gecontroleerde schade-inductiemethoden en verdere ontwikkeling van permeabiliteitsgebaseerde testbenaderingen voor toepassing in onderzoek naar zelfhelend metselwerk.

De laatste experimentele fase (Hoofdstuk 6) behandelde het metselwerkcomponentniveau, met als doel de prestatie van het geselecteerde zelfhelingsagent te evalueren in proefstukken op grotere schaal. Borstweringen (1100×540×85 mm³) werden onderworpen aan vierpuntsbuiging om herstel van prestaties (mechanisch en esthetisch) te beoordelen, terwijl drukproeven op kleine

muurtjes (360×490×85 mm³) werden uitgevoerd om de invloed van het agent op functionele eigenschappen te evalueren. Daarnaast werden FTIR-analyses parallel uitgevoerd om de aard van de neergeslagen helingsproducten te identificeren en verifiëren. Ondanks het gebruik van dezelfde materialen en vergelijkbare uithardings- en helingscondities als op de eerdere niveaus, werd in deze grotere proefstukken geen effectieve activatie van het helingsagent waargenomen. FTIR-analyse toonde uitloging van het PLA-gebaseerde inkapselingsmateriaal, reeds zichtbaar na uitharding en versterkt tijdens daaropvolgende heling onder natte condities (20±2 °C, 95±5% RV). Dit gedrag kan worden toegeschreven aan schaalafhankelijke vochtgradiënten en intern watertransport tijdens vroege uitharding, hetgeen migratie van het inkapselingsmateriaal het 'voedsel' voor de bacteriën naar uitwendige oppervlakken bewerkstelligen. Belangrijk is dat deze resultaten geen intrinsieke materiaalincompatibiliteit of onjuiste helingscondities suggereren; zij benadrukken daarentegen de essentiële rol van schaal-specifieke uithardingsstrategieën en de noodzaak van verder onderzoek om deze protocollen te optimaliseren en de toepasbaarheid van het agent op constructieniveau te verifiëren.

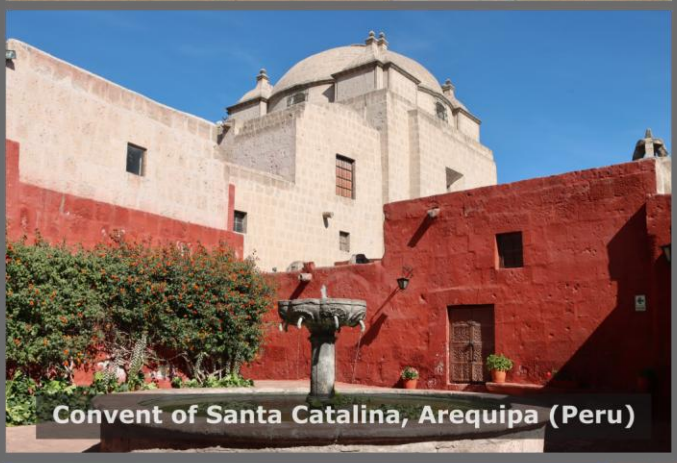
Chapter 1

Introduction

Research undertaken in this thesis is concerned with exploring the applicability of self-healing mortars, originally developed for concrete, to the repair of masonry structures. This introductory chapter sets the context by outlining the background and motivation for the research, followed by its objectives, scope, methodology, and a general outline of the dissertation.


Ziggurat of Ur, Ur (Iraq)


Colosseum, Rome (Italy)


Convent of Santa Catalina, Arequipa (Peru)


Kinderdijk windmills, Kinderdijk (The Netherlands)


Hamburg (Germany)


Cathedral of La Plata, La Plata (Argentina)

1.1 Problem definition

Extending the service life of the built environment is becoming a rising priority worldwide, driven by climate and resource-efficiency goals coupled with constrained public finances. The building and construction sector accounts for roughly 37% of the global CO_2 emissions and nearly one-third of the solid waste, much of the latter linked to demolition (Lei et al. 2023). Well-targeted repair is therefore an effective strategy to reduce this burden and avoid costly future interventions, as recognized in the European Union's 2050 climate-neutrality plan, which prioritizes action on the existing building stock (Dragonetti et al. 2025). The emphasis on repair extends to all construction materials, which naturally age and deteriorate over time. Among these materials is **unreinforced masonry** (hereinafter referred to as masonry), one of the oldest building traditions together with timber. From the earliest civilizations, masonry has been part of human culture worldwide, making its preservation an aspect of cultural relevance.

Since its origins in Mesopotamia, masonry has proven its remarkable durability; yet, due to its very low tensile and bond strength, **cracking remains an inevitable phenomenon** that challenges its long-term performance. This mechanical vulnerability makes masonry particularly susceptible to tensile and shear cracking at the mortar joints and at the brick–mortar interface, commonly constituting the weaker link. Over time, environmental exposure (wind, rain, snow and temperature) promotes crack formation and propagation, a process that may be further intensified by gradual actions (traffic and settlements) or by sudden events (earthquakes). Even if initially minor, cracks undermine watertightness, facilitating water ingress and accelerating degradation. With increasing crack extent, masonry performance is progressively affected, hindering also aesthetic appearance and mechanical performance.

As cracking is unavoidable, the long-term durability of masonry largely depends on its repairability. Historically, this has been supported by the flexibility and innate healing capacity of traditional lime-based mortars to self-repair microdamage (commonly referred to as **autogenous healing**), together with a modular construction system that enables the localized repair of units and joints before damage jeopardizes the structure's performance. Early identification of damage is therefore critical, as minor cracking can develop into more severe deterioration, leading to substantially higher repair costs when intervention is delayed. (Shiotani et al. 2024). Health monitoring and timely intervention are therefore crucial.

Intervention is usually carried out through **repointing**, a strategy that focuses on replacing the worn-out or damaged outer layer of the joints. When compatible units and mortars are used, deterioration is expected to concentrate in the joints and can thus be addressed in a localized manner. In repointing, the repair mortar is designed so that any

future damage occurs within the new mortar rather than in the existing material, ensuring that the repair layer is the part to be renewed when needed. When properly executed, repointing is minimally invasive and preserves the aesthetic integrity of masonry, qualities that make it suitable for heritage applications. However, the intervention must be repeated as damage reappears, demanding regular inspections and careful planning. This burden of **repetitive maintenance** is further exacerbated when the source of damage is recurrent rather than isolated. An example is the induced seismicity in Groningen, where frequent vibrations have caused accumulated damage and significant social and economic unrest. Whether the inherent need for repeated intervention fully satisfies conservation principles of minimal intervention and sustainability is therefore debatable. In any case, the need for clear monitoring and maintenance strategies is evident, unless autonomous approaches are developed and introduced to enable repair without external action.

The idea of **autonomous repair**, although innovative, is not new and has long been explored in the field of **concrete**. Decades of research have produced a large variety of self-healing solutions intended to limit maintenance costs and extend durability of concrete structures. The guiding principle is the damage management approach, which accepts that damage is inevitable and instead focuses on autonomous repair as it appears. In doing so, these engineered solutions extend the damage management concept beyond the narrow limits of autogenous healing. To this end, healing agents (HA) are incorporated into the repair material restore damage while in service through different mechanisms. Among these, one of the most studied involves “limestone-producing” bacteria, which activate in the presence of infiltrating water and precipitate calcium carbonate to fill up cracks. Research in this field has moved from early concepts to established research and even commercial solutions.

Building on these advances, interest in **applying autonomous self-healing approaches to masonry** has recently begun to emerge. References to “self-healing masonry” appear in the literature from around 2016 onwards (Figure 2-1), yet most of these early studies focused on autogenous healing phenomena in lime mortars rather than engineered solutions. Clear evidence of autonomous strategies only begins to surface after 2020, and even then, the number of dedicated publications remains very limited compared with the extensive bodies of research in the fields of “masonry repair” and “self-healing concrete”.

Given its novelty, research in this area is still at an early stage of development. To date, studies have focused on two main directions: the development of new agents specifically designed for lime-based mortars and masonry applications, and the adoption of an existing commercial **concrete repair agent containing bacteria and poly-lactic acid (PLA)**. In the first case, progress remains at an early development stage, with efforts still concentrated on designing and testing the agents themselves rather than on their

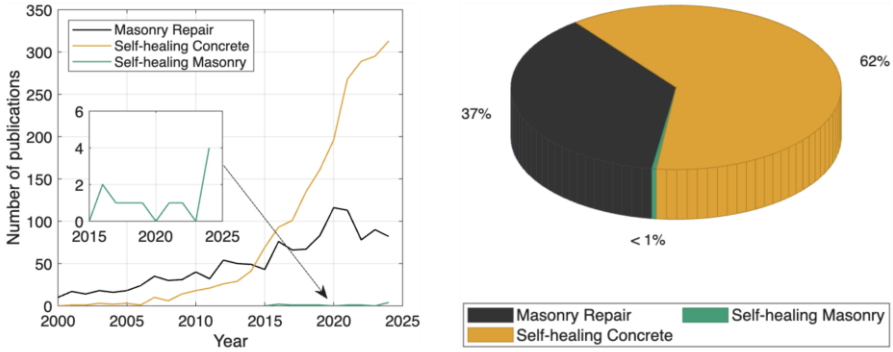


Figure 2-1 (a) Evolution of the number of publications per year between 2000 and 2024, retrieved from Web of Science in August 2024 using the keywords "Masonry Repair", "Self-healing Concrete" and "Self-healing Masonry"; (b) Proportion of total publications in each category as of August 2024.

performance in mortar or masonry specimens (De Nardi et al. 2024; Giordano 2025). In the second, only a few **pilot studies** are available, all conducted by the author of this thesis as preliminary work forming the basis for the research presented herein (Gaggero et al. 2024, 2025). These studies mainly focused on aesthetic recovery and bond restoration in small-scale masonry specimens. The performance of the agent in lime-based mortars, traditionally used in masonry repair, has not yet been systematically investigated, nor has the recovery of other critical properties such as watertightness. More broadly, systematic research efforts are lacking, and no comprehensive methods exist to assess autonomous self-healing strategies for masonry. This highlights both the novelty of the field and the substantial scope that remains for future research before autonomous self-healing can be considered a viable approach for masonry repair.

1.2 Research objectives

This study aims to evaluate the viability and effectiveness of bacteria-based self-healing mortars for the autonomous repair of cracks in masonry structures, particularly within the context of heritage conservation. The central research question guiding this work is, therefore:

To what extent are bacteria-based self-healing mortars a viable and effective solution for repairing masonry structures, including historical heritage?

To address the main question, the study uses a poly-lactic acid (PLA) self-healing agent, originally developed for concrete repair and commercialised in the Netherlands

(Basilisk®). Building on this premise, the research is structured around the following sub-questions:

- What insight from existing research can guide the study of self-healing strategies tailored to masonry repointing?
- How can bacteria-based self-healing mortars be systematically investigated for repointing masonry?
- What is the potential of a poly-lactic acid (PLA) self-healing agent to enable autonomous repair of masonry?

The use of the selected agent allowed the research to concentrate fully on assessing the applicability of the self-healing approach to masonry, whereas the development and optimisation of the agent lie beyond the scope of this work. For the same reason, although the strategy is examined within the context of repointing, the repointing process itself was not investigated and lies beyond the scope of this work. Nonetheless, this focus does not exclude the potential application of self-healing mortars in new masonry construction or their introduction through alternative repair strategies beyond repointing.

1.3 Methodology

To investigate the potential of self-healing mortars as a repair strategy for masonry structures, specifically through repointing interventions, this study followed three main steps: (I) knowledge foundation and preparatory studies, (II) the design of a dedicated research framework for assessing self-healing mortars in masonry repair, and (iii) its application to experimentally investigate the suitability of a specific self-healing mortar containing a bacteria-based poly-lactic acid (PLA) healing agent; each step provides answers to one of the research sub-questions formulated above.

In **step I (knowledge foundation and preparatory studies**), insights from the literature are combined with preparatory investigations to identify fundamental gaps, formulate key questions, and establish the basis for the methodological framework developed in the subsequent step. Given the emerging nature of the topic, the review encompasses **masonry materials**, **deterioration**, and **repointing**, alongside the established body of work on **self-healing concrete**, thereby bridging two previously separate domains. The first part delves into the material to be repaired, providing an overview of the mortars and bricks used throughout history, the types of damage that may be targeted by self-healing, and the repair method that offers an entry point for their application. The second part draws on self-healing concrete as inspiration, highlighting existing solutions that can be implemented or serve as models for new developments, and pointing to key aspects and methods for their investigation. This step also incorporates the **limited literature on self-healing masonry**, including the author's preparatory proof-of-concept studies

conducted prior to this thesis using the poly-lactic acid (PLA) based healing agent (Gaggero et al. 2024, 2025). The conclusions of this step informed both the design of the research framework in step II and the selection of masonry materials (mortars and bricks) adopted in step III.

In **step II (design of a research framework)** a methodological framework is developed to guide research on bacteria-based self-healing mortars for masonry repair and to provide the basis for the experimental campaign conducted in Step III. Given the complexity of both masonry repair and self-healing mortars, such a scheme is crucial to structure the study, ensure a comprehensive approach, and provide a reference point for future work (Figure 2-2). Grounded in the literature review (step I), the framework advances across the following levels: mortar (mortar alone), brick-mortar (bonding region), and masonry component (larger assemblies under more realistic stress states and crack patterns). At each level, the material is systematically investigated through three complementary aspects: recovery of performance, identification of healing products and impact on functional properties. The first two follow from the self-healing nature of the material, focusing on recovery and on verifying that the mechanism responsible for the recovery is the intended one. Confirming the mechanism is crucial, as healing might also result from components introduced with the agent sealing the cracks rather than from bacterial activity. These aspects are evaluated on specimens that are deliberately damaged and subsequently allowed to heal. Recovery is quantified by comparing measured properties before damage and after healing, whereas the identification of healing products is carried out on samples collected from precipitates on the crack surface post healing. The last aspect is considered to ensure the suitability of the repointing strategy and is assessed by comparing specimens with and without the agent. Key aspects considered in the framework include the method and extent of

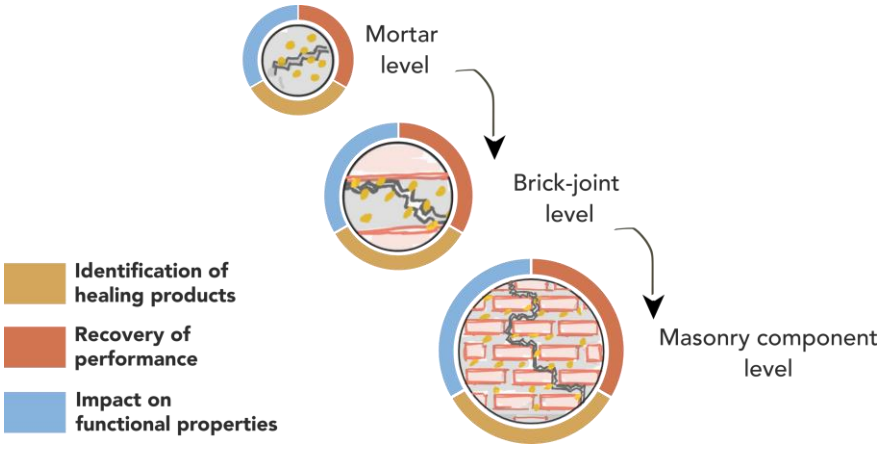


Figure 2-2 Schematic representation of the proposed research framework for the assessment of bacteria-based self-healing mortars for masonry repointing.

damage induction, healing environment and duration, and testing methods for each performance aspect. Besides contributing to the development of a more standardised methodology for investigating self-healing strategies in masonry repair, the proposed framework directly underpins the systematic experimental campaign conducted in step III using the selected PLA-based healing agent.

In **step III (experimental assessment with a selected self-healing agent)** a commercially available poly-lactic acid (PLA) based healing agent (Basilisk®), is experimentally assessed for the repair of cracked masonry, following the experimental framework proposed in the previous step (step II). A series of experiments on specimens ranging from small to medium size (Figure 2-3) are carried out to study the application of the agent at the mortar, brick–mortar, and masonry component levels. (Figure 2-3). At each level, the core assessment aspects defined in the framework are addressed by examining distinct mechanical and physical properties. Specimens were prepared with mortars and bricks representative of historic Dutch buildings, ensuring the relevance of the investigation to practical repair contexts. Beyond serving as an application of the proposed framework, this step provides a systematic experimental assessment of the proposed self-healing strategy and the selected agent, thereby supporting an informed evaluation of their applicability to cracked masonry repair.

Figure 2-4 summarises the three-step methodology, its objectives, and the research question addressed by each step. Details on the outline of each chapter follow in the next section.

1.4 Outline of the thesis

The thesis investigates the technical viability of self-healing mortars for the repair of cracked masonry. Its content unfolds across seven chapters, starting with the

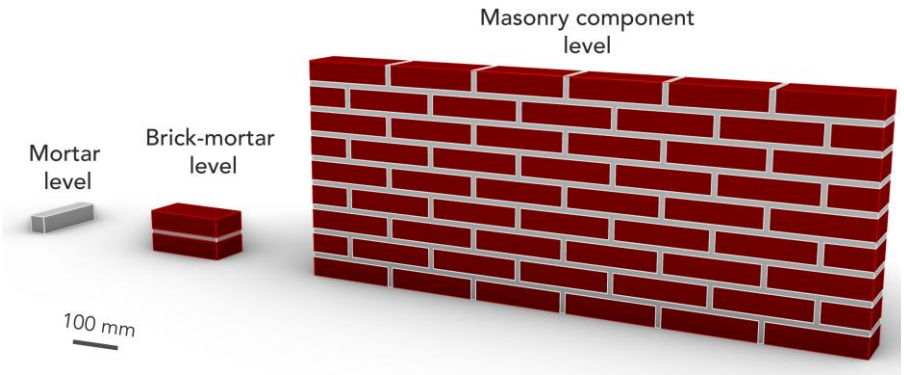


Figure 2-3 Examples of test specimens investigated at each level of the research framework, illustrating the differences in geometry and size.

Main step	Key objectives	Research question
I **Knowledge foundation and preparatory studies**	To define a clear research methodology, highlight key aspects for investigation, and guide the selection of both a suitable agent and representative materials for experimental evaluation	What insight from existing research can guide the study of self-healing strategies tailored to masonry repointing?
II **Design of a research framework**	To establish a framework for the systematic investigation of bacteria-based mortars for masonry repointing and guide the experimental assessment carried out in step III	How can bacteria-based self-healing mortars be systematically investigated for repointing masonry?
III **Experimental investigation with a selected self-healing agent**	To experimentally assess the potential of a poly-lactic acid (PLA) healing agent for cracked masonry repair at the mortar, brick-mortar and masonry component level	What is the potential of a PLA self-healing agent to enable autonomous repair of masonry?

Figure 2-4 Three-step roadmap to the research objective.

introduction (Chapter 1) and closing with the conclusions (Chapter 7). Figure 2-5 illustrates the structure and interrelation of the chapters. A brief synopsis of each is provided below.

Chapter 1 Introduction

This introductory chapter presents the background and motivation for the research, as well as the scope and structure of the current thesis.

Chapter 2 Groundwork and literature review for self-healing masonry

This chapter aims to establish the foundations for exploring the application of self-healing technology for masonry repair. In the first part, it reviews the different types of bricks and mortars used in masonry construction throughout history, highlighting their properties and, where relevant, referring to those typical of the Dutch context. It also describes common forms of damage and repointing as the established method for addressing joint deterioration. The second part, then, introduces self-healing technology as a novel approach to addressing durability challenges in concrete, outlining strategies developed to date, including the PLA bacteria-based healing agent used in this thesis. Finally, it considers the emerging literature on self-healing masonry, including the author's preliminary work leading up to this thesis.

Chapter 3 A framework for assessing bio-based self-healing performance for masonry applications

Building on the foundations established in Chapter 2, this chapter proposes a research framework for investigating bacteria-based self-healing mortars for masonry repointing. The framework builds progressively from the study of mortar to brick–mortar samples and ultimately to larger masonry assemblies, allowing both the healing conditions and the material's performance to be explored step by step. At each level, the material's performance is assessed through three complementary aspects: the recovery of key performance properties, whether this recovery results from the agent's intended healing mechanism and its effect on selected functional properties. Functional properties considered are those governing the applicability and compatibility of the mortar in repointing, e.g. workability, strength and deformability of the mortar, porosity and mechanical properties of the interface and masonry. Performance properties correspond to those that the self-healing mortar is designed to recover after damage, including aesthetic appearance, watertightness, and mechanical behaviour.

Chapter 4 Mortar level performance of bacteria-based agent

This chapter applies the framework introduced in Chapter 3 to the first level of investigation: the mortar level. To this end, a bacteria-based PLA capsule agent, developed and commercialised for concrete repair (Basilisk®), is tested in four cement–lime mortars with lime contents ranging from 0 to 80% of the binder content by volume; the latter representing a mix commonly used in masonry repair in the Netherlands. The recovery was assessed in terms of aesthetic and mechanical performance on mortar bars (40 × 40 × 160 mm³) tested in bending. Healing was carried out under wet conditions (20±2 °C, 95±5 %RH), moderate-humidity conditions (20±2 °C, 80±5 %RH) and wet–dry cycles (1h submerged in water, 23h dry at 20±2 °C and 65±5 %RH). Aesthetic recovery was evaluated using optical microscopy, while the formation of healing products was characterised by Fourier Transform Infrared Spectroscopy (FTIR) on fragments taken from the cracked regions. In parallel, the agent's effect on the bending and compressive properties (strength and elastic modulus), as well as on water absorption, was also assessed.

Chapter 5 Brick-mortar level performance of bacteria-based agent

This chapter advances the investigation to the next level of the framework proposed in Chapter 3: the brick–mortar interface. The composition with highest lime content (80% of the binder content by volume) and the PLA-based agent tested in Chapter 4 are further explored using solid clay bricks representative of historic buildings in the Netherlands. The recovery of performance is investigated in terms of aesthetic, mechanical properties, and watertightness. Mechanical recovery is assessed on brick–mortar couplets (110 × 50 × 50 mm³; length × height × width) in terms of flexural bond properties, while watertightness recovery is assessed on cores through permeability tests. Aesthetic recovery is evaluated on the same specimens using a portable microscope to observe

crack filling. After testing, healing is carried out under the selected environment identified in the previous chapter, i.e. wet conditions (20±2 °C, 95±5 %RH). In parallel, the effect of the agent on flexural bond behaviour, permeability and shear bond behaviour is investigated.

Chapter 6 Masonry component level performance of bacteria-based agent

This chapter extends the investigation to the masonry component level, the next scale of the framework (Chapter 3). The recovery of performance is investigated in terms of aesthetics and mechanical behaviour, through in-plane bending tests on masonry spandrels (110x440x85-mm^3; length x heigh x width). Specimens were tested under both monotonic and cyclic loading and monitored through digital image correlation (DIC) to capture the induced crack pattern. After testing, the specimens were left to heal under wet conditions (20±2 °C, 95±5 %RH) and were subsequently observed with a portable microscope to evaluate aesthetic recovery, before being re-tested to assess mechanical recovery. The formation of healing products was again characterised by FTIR on fragments taken from the cracked regions. In parallel, the agent's effect on the in-plane bending behaviour was investigated, along with its influence on the compressive behaviour, assessed on masonry wallets (360x390x85-mm^3; length x heigh x width).

Chapter 7 Conclusions and Outlook

The concluding chapter synthesises the conclusions of the three research steps and integrates the findings obtained with the selected agent at the mortar, brick–mortar, and masonry component levels. This integration supports an assessment on the technical viability of self-healing mortars for crack repair in masonry and enables reflection on the scientific contribution and societal importance of the thesis. The chapter concludes with an outlook on future research steps required to further develop the proposed strategy towards practical application.

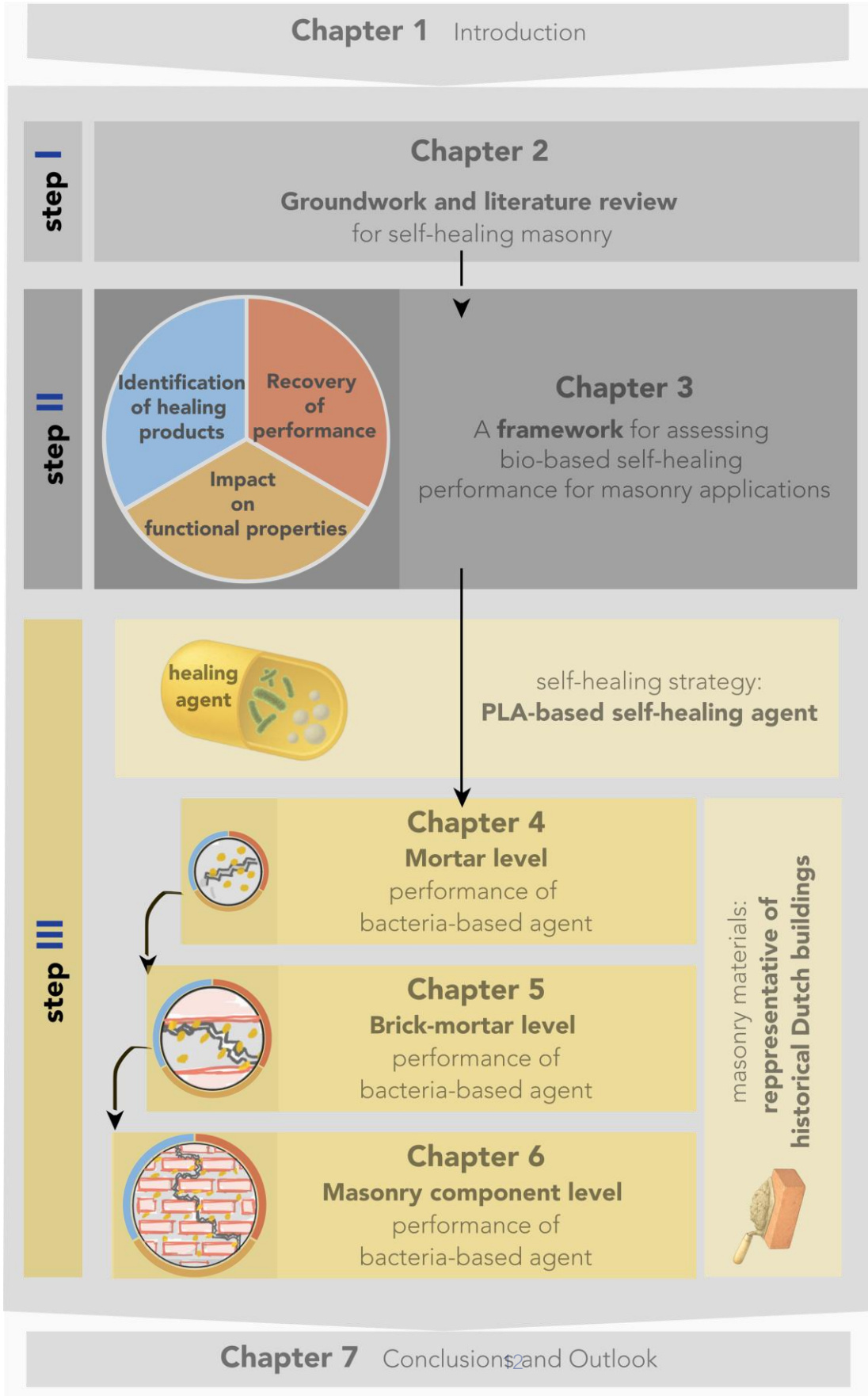


Figure 2-5 Visual outline of this thesis.

Chapter 2

Literature review and groundwork for self-healing masonry

As introduced in Chapter 1, this thesis aims to explore whether self-healing mortars can offer a viable solution for masonry repair. Before diving into hands-on research, however, it is essential to gather the background knowledge needed for making informed decisions: from designing a framework to test the concept, to selecting appropriate materials, and eventually conducting tests. This chapter aims to provide that foundation.

To do so, it is necessary to first understand the material system in question, masonry, along with its historical development and the types of damage that the self-healing strategy could address. Section 2.1 provides a brief historical overview of masonry and its constituent materials, offering the context needed to evaluate the compatibility of the healing agent with different mortar types and to select the materials used in the subsequent chapters. Section 2.2 discusses common damage mechanisms in masonry and their implications, helping to identify which properties need to be restored through healing. Section 2.3 focuses on repointing as a practical entry point for self-healing strategies.

With the material and repair strategy in place, in Section 2.4 the attention turns to what self-healing concrete research can offer as inspiration or guidance. This includes a review of self-healing mechanisms in cement-based systems, with a particular focus on the PLA-based bacterial agent used later on in this thesis. Section 2.5 concludes the chapter with an overview of the current state of research on the emerging field of self-healing masonry, including the author's early work, which contributed to laying the groundwork for this thesis.

Part of this chapter was previously published by the author in:

Gaggero, M. B., Korswagen, P. A., Esposito, R., & Rots, J. G. (2024). **Innovative Application of Self-Healing Technology to Masonry: A Proof of Concept**. International Journal of Architectural Heritage, 19(5), 598-608. https://doi.org/10.1080/15583058.2024.2380408

Gaggero, M. B., Korswagen, P. A., Esposito, R., & Rots, J. G. (2025). **Exploring Bacteria-Based Self-healing Potential in Cement-Lime Mortar Masonry**. In G. Milani, & B. Ghiassi (Eds.), 18th International Brick and Block Masonry Conference: Proceedings of IB2MaC 2024—Volume 2 (Vol. 2, pp. 1011–1020). (Lecture Notes in Civil Engineering; Vol. 614). Springer. https://doi.org/10.1007/978-3-031-73310-9_77

2.1 Masonry in the built environment

Masonry is a heterogeneous material obtained through the assemblage of units, such as stone pieces, bricks, blocks, or elements, usually (but not exclusively) with mortar. Its origins trace back to the earliest known human settlements, such as those in ancient Mesopotamia around 9000–8000 BCE, making it the oldest and one of the most enduring construction methods worldwide. Over the centuries, both materials and construction techniques have continuously evolved, shaped by shifts in knowledge, available resources, and functional demands.

Early masonry was rather rudimentary, using locally available raw materials like stone and sun-dried mud units, either dry-stacked or bonded with simple natural binders, such as clay, bitumen or even the mud itself. These primitive methods evolved with the first civilizations, introducing fired clay units, and later, under the Romans, a range of (non-hydraulic and hydraulic) lime-based mortars that dominated construction for over three thousand years. This long-standing tradition underwent a transformation during the Industrial Revolution in the late 19th century, with the introduction of new materials such as Portland cement, reinforced concrete and steel. While masonry continued to serve structural purposes, it increasingly assumed a new role as a non-structural element. Advances in materials and manufacturing brought significant changes to structural masonry itself, driving the shift from solid to cavity wall construction and from lime to cement-based mortars, while introducing reinforced masonry and new unit materials (concrete, calcium silicate). This period gave rise to what some authors describe as **modern, advanced or contemporary masonry** (Sandoval and Arnau 2016; Jessa), also characterized by the use of larger prefabricated units, and more industrialized assembly techniques. Meanwhile, the older forms are now often referred to as **traditional or historical masonry**.

Despite this change in role, masonry remains a predominant feature in the global building and infrastructure stock, appearing in many structures, including load-bearing walls, arches, aqueducts, bridges, earth retaining systems, and contemporary veneers around the world. Its role in contemporary construction is far from marginal: as Lourenço (Lourenço 2014) points out, unreinforced masonry is still used for 15% to over 50% of new housing in multiple European countries, both in low (e.g. Germany, Norway or Netherlands) and high seismicity zones. (e.g. Italy). Yet its significance goes well beyond modern use, as countless historical masonry buildings remain an integral part of the built environment. The Netherlands is a clear example, with masonry visible on every corner throughout its cities and a large portion dating back to before 1900. Figure 2-1illustrates one of many examples, Delft,

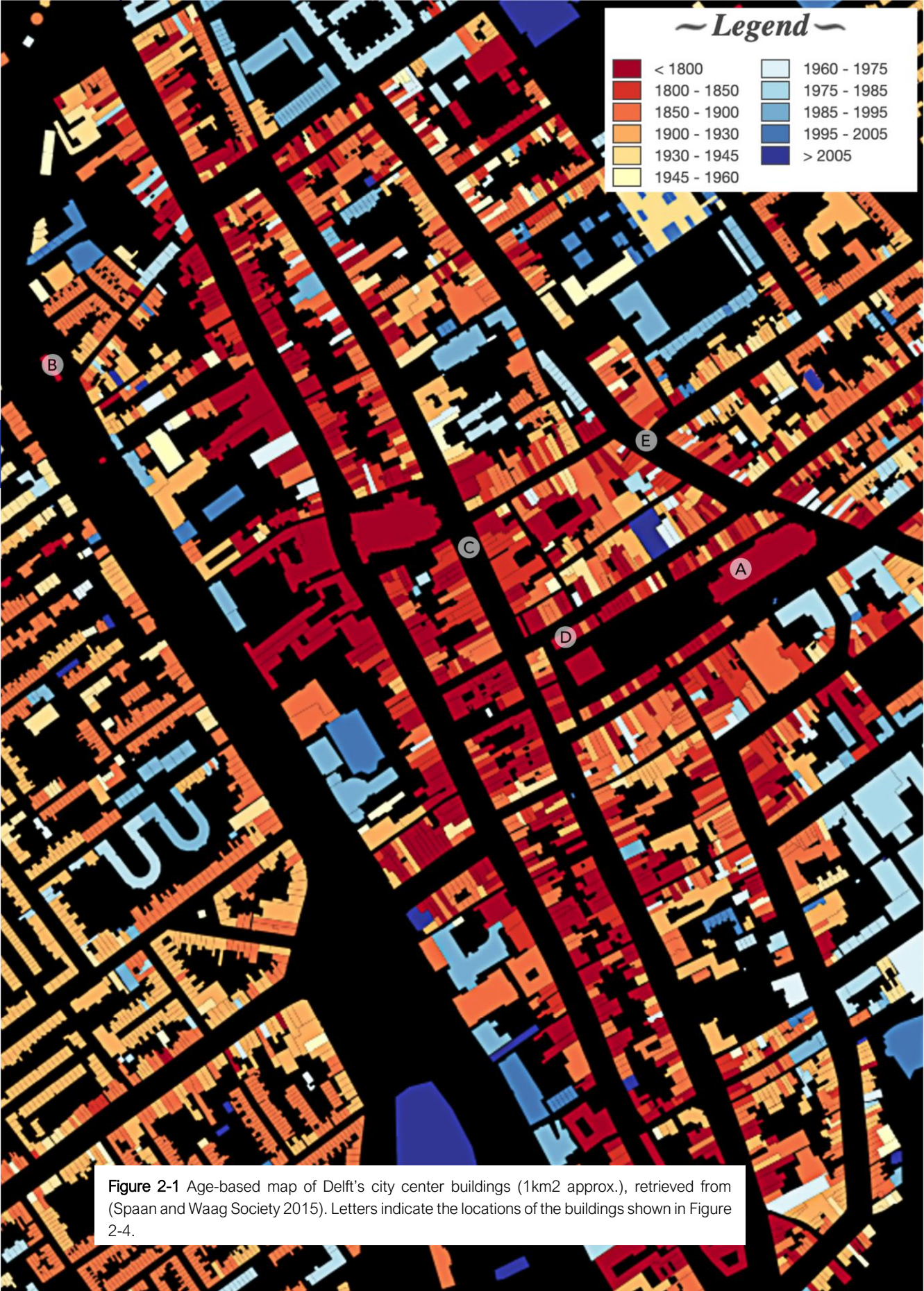


Figure 2-1 Age-based map of Delft's city center buildings (1km2 approx.), retrieved from (Spaan and Waag Society 2015). Letters indicate the locations of the buildings shown in Figure 2-4.

through a color-coded map retrieved from(Spaan and Waag Society 2015), showing the year of construction of buildings based on data from BAG, the Netherlands' national building database. Letters on the map indicate locations that are illustrated with photographs in Figure 2-2.

As masonry developed across time and regions, a wide range of units and binders came into use, giving rise to assemblages with markedly different physical and mechanical properties (Lourenço 2014; Kubica 2024). Understanding these constituents is therefore essential, as they determine the behaviour of the masonry targeted for self-healing. Such knowledge is crucial for assessing the compatibility of a healing agent with different masonry types, for delineating its potential field of application, for selecting representative materials in experimental campaigns, and for interpreting subsequent results. For instance, as will be discussed in Section 2.4.2, bacteria-based agents rely on environmental triggers such as water and, consequently, the physical properties of units and mortars play a key role in regulating the conditions that enable healing.

Since the properties of these constituents are strongly influenced by their raw materials and manufacturing processes, the following sections provide an overview of



Figure 2-2 Visual examples of Delft's built environment. Each location is marked with a letter in the map presented in Figure 2-1.

these aspects, focusing on traditional unreinforced masonry. While the discussion covers general developments, specific attention is given to the Dutch context where relevant.

2.1.1 Masonry units

Alongside natural stone, masonry units have historically been made from mud, clay, concrete, and calcium silicate, in formats ranging from small bricks (≈210 × 100 × 55 mm³) to larger blocks (200–300 × 100–600 × 100 mm³) and prefabricated elements (Ghiassi et al. 2019). Bricks and blocks may be solid, frogged, or perforated: solid units are fully compact, frogged units have an indentation to improve mortar bonding and handling, and perforated units feature through-holes to reduce weight. Solid and frogged formats dominated from antiquity until the late 19th century, when perforated bricks were introduced.

The materials used for masonry unit production have also evolved over time, reflecting both technological advances and the availability of local resources. Mud was the first material used: a mixture of local soil (clay, silt and sand) and water, also called adobe if reinforced with straw to reduce shrinkage and enhance strength (Almssad et al. 2022; Minke 2025). Bricks were formed by moulding the mix into regular units, which were then left to dry under the sun. Building upon the use of sun-dried bricks, the development of baked clay bricks followed around 3000 BCE as natural evolution aimed at improving strength and durability under wet conditions (Oliveira 2003; Almssad et al. 2022). This type marked traditional and historical masonry, being widely used for millennia. Only with the advent of new materials, new types were introduced 19th and 20th centuries: concrete and calcium silicate (CS). For instance, the abundance of sand for their production (Bowley 1994), CS units became a main structural building material in the Netherlands, Germany and the former Soviet Union. However, its susceptibility to moisture damage has limited its use in components exposed to water. For this reason, CS units are primarily employed as the inner structural component of cavity walls, and solid clay is still the preferable choice for the outer leaf.

Regardless of the format and material used, the properties of the final product are strongly dependant on the composition of the raw materials and the manufacturing process. Durability and mechanical performance are the most critical for long-lasting applications, and are commonly assessed through porosity and compressive strength (Fernandes 2019). As an indication, adobe bricks typically show compressive strengths of 0.45–5.20 MPa with density of 420 to 2550 kg/m³ (Sánchez et al. 2022); fired clay bricks present a large range of compressive strength from 1.5 up to 50 MPa with porosity ranging from 15–40% and water absorption between 10%-30% (Fernandes 2019; Almssad et al. 2022); calcium silicate units achieve 7–30 MPa with lower water absorption (6–16%) (Kamal 2023). Since clay was the primary material in traditional and

historical masonry, and its performance is highly dependent on the production process, further details on its manufacture are provided below.

Clay brick production involves the extraction and selection of raw material, its preparation with water and other additives, shaping, drying, and firing, with each stage influencing the final properties (Fernandes et al. 2010). The process begins with selecting suitable clay, a heterogeneous material composed mainly of silica (≈50%) and alumina (≈15–20%), and removing impurities. While iron oxides provide colour, calcareous materials such as limestone can cause expansion and early cracking after firing. In modern production, clays are carefully selected and cleaned before use, whereas historically such impurities were not always removed, increasing the risk of defects. After selection, the raw clay is stored in open-air deposits for days or weeks to reduce soluble salts and improve homogeneity, then crushed and mixed with water. Shaping was traditionally done by hand in sanded or wetted wooden moulds, producing bricks with irregular surfaces. The amount of water added aimed to produce an overly plastic mix to facilitate moulding, while sand (≈70% clay to 30% sand) was incorporated to limit shrinkage during drying. After the 19th century, moulding machines were developed and later on extruders, making the production more mechanical and industrialized. Compared to hand-moulded bricks, extruded bricks are characterized of very sharp edges and smooth surfaces. When desired, extruded brick were pressed afterwards in special machines to obtain bricks with a very high density. Before firing, bricks were air-dried to prevent shrinkage and cracking, a process traditionally carried out in open shelters until artificial drying was introduced in the late 19th century. The final stage involved either sun-drying or kiln firing, typically at about 800 °C, with ancient examples ranging from 600 °C to 950 °C (AtiKoğlu), higher temperatures markedly improved mechanical and chemical resistance. After firing, gradual cooling was essential, as rapid cooling could produce cracks that increased susceptibility to frost damage (see section 2.2).

The quality and properties of the final product are strongly influenced by the production process, particularly the quality of the raw clay, the water content, the shaping process and the firing conditions and temperature. Historical production methods yielded bricks with higher porosity than those produced today. For this reason, in restoration projects, specialised brick manufacturers are in charge of producing "restoration bricks", reproducing traditional methods to match the original properties as closely as possible.

2.1.2 Masonry mortars

The use of mortar for bedding, jointing, and bonding masonry units has also undergone significant changes throughout history. While the basic components of mortar remain largely the same (binder, sand, water, and optional admixtures), different types

of binders have been used to meet changing construction requirements. From the naturally occurring binders (bitumen and clay) used in the earliest human constructions to today's engineered high-strength cements, the evolution of binders reflects centuries of innovation and refinement. As illustrated by Elsen et al. (Elsen et al. 2012) in Figure 2-3, this historical evolution from natural binders can be broadly divided into two main phases: the introduction of air-hardening materials and the subsequent development of hydraulic binders. While air-hardening binders (lime and gypsum) slowly harden in air gaining limited strength, hydraulic binders (lime-pozzolan, natural hydraulic lime and cement-based mixtures) harden by chemical interaction with water.

The earliest binders used were natural materials like bitumen and clay, while air-hardening lime (also referred to as non-hydraulic lime or simply air lime) later became the most prevalent choice, dominating from antiquity until the late 19th century. While the first ones were readably available, the latter needed heating and mixing with water before application. Depending on the local availability of raw materials, either calcitic (also called high-calcium) or dolomitic (also called magnesian) lime mortars were used, with the former more common (Do Rosário Veiga and Santos Silva 2019). Calcitic limes derives from sources with less than 5% magnesium carbonate (pure limestone, chalk, calcitic marble), whereas dolomitic limes derives from sources with more than 20% (dolostone) (Elert et al. 2002). Regardless of the type, the transformation of the raw material into mortar comprises three main stages: calcination, hydration, and hardening. This process is known as the lime cycle and is illustrated for both calcitic and dolomitic

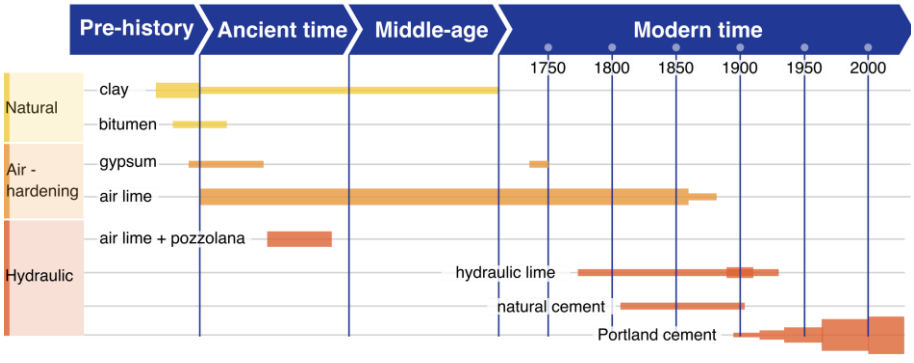


Figure 2-3 The evolution in time since prehistorical times of the different types of binders that have been used in Europe and their relative importance. Adapted from (Elsen et al. 2012).

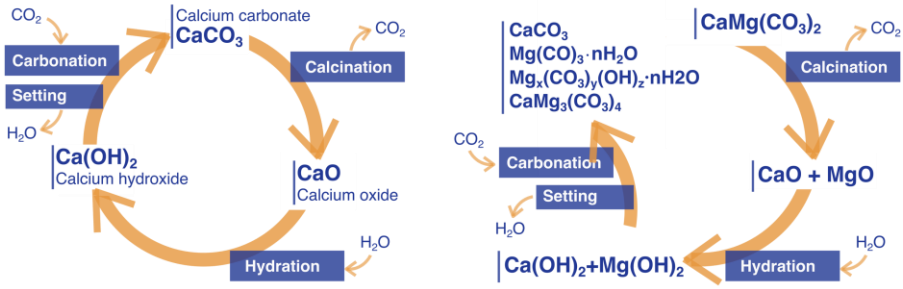


Figure 2-4 The lime cycle of (a) calcitic and (b) dolomitic lime. Retrieved from (Rodriguez-Navarro et al. 2023).

limes in Figure 2-4. As can be seen, the presence of magnesium (as magnesium oxide or, in hydrated lime, as magnesium hydroxide) in dolomitic limes makes the underlying chemistry more complex. Since dolomitic limes are generally not recommended for conservation due to late hydration of magnesium oxide and the risk of forming damaging sulphates (Elert et al. 2002), the focus here will be place on high-calcium limes; for further details on dolomitic lime, see (Rodriguez-Navarro et al. 2023).

The first step of the lime cycle, calcination, consists of heating the carbonate rock at 700-950 °C. This process, commonly miscalled burning, leads to the production of quicklime, which in the case of calcitic sources is composed of calcium oxide. This product becomes slaked lime when combined with water, a process known as slaking. This process, technically referred to as hydration, represents the second stage of the cycle and, in the case of calcitic sources, produces calcium hydroxide. Depending on the amount of water added, either a dry powder or a lime putty (a dispersion of portlandite crystals in water) can be obtained. Powdered lime, or dry hydrated lime, is the main product of modern industrial production, whereas lime putty was the most common traditional form historically used in construction. In either form, the material ultimately undergoes a final setting and hardening stage. Setting refers to the initial loss of mortar plasticity caused by water absorption into adjacent units and evaporation, without any chemical reaction. Hardening follows, with calcium hydroxide gradually reacting with atmospheric carbon dioxide to form calcium carbonate in a slow process called carbonation. It occurs in two stages: first, carbon dioxide dissolves in pore water to form carbonic acid; then, this reacts with calcium hydroxide to produce calcium carbonate crystals that bind the aggregate. Because water is essential for carbonation to occur, thorough curing is required for proper hardening (Young 2021). The chemical reactions involved in the lime cycle for calcitic limes are shown in Table 2-1. As can be seen, the end product is compositionally similar, (compositionally, but not texturally/structurally) to the original uncalcined carbonate rock used to produce the lime. For this reason, the

cycle in Figure 2-4 (a) is represented as closed. In contrast, in dolomitic lime the starting and end products differ, with the latter being a mixture of calcium and magnesium carbonates; hence, the cycle is not depicted as closed in Figure 2-4 (b).

Nowadays, carbonation is recognized for its environmental relevance, as it contributes to the reduction of atmospheric CO_2. It is further acknowledged as a main reason behind the long durability of lime mortars, as it underlies their innate ability to self-repair micro-damage, a process known as autogenous healing and discussed in section 2.4.1. From a practical standpoint, however, the process is very slow and highly dependent on ambient conditions. As highlighted by Lourenço et al. (Lourenço 2014), carbonation can take several years, especially in very thick masonry, and only occurs under specific humidity conditions, typically between 40% and 80% relative humidity (RH), as pointed out by do Rosário Veiga et al (Do Rosário Veiga and Santos Silva 2019). The result is a very porous and soft material that can accommodate large deformations, with apparent specific density generally below 2.0 and relatively low compressive strength, especially in the early stages, typically ranging from 1.5 to 2 N/mm² (Maria 2010; Lourenço 2014).

The slow setting and hardening of pure air lime mortars, particularly under humid conditions, along with their limited mechanical performance, prompted the transition to hydraulic binders. These materials set more rapidly, develop higher strength, and exhibit hydraulicity (i.e., the ability to harden under water). Their enhanced performance is mainly due to the formation of calcium silicate hydrate (C-S-H), with additional minor contributions from calcium aluminate hydrates (C-A-H). These compounds, also known as cementitious phases, develop through the hydration of clayey compounds present in the mix, primarily silica (SiO_2) and alumina (Al_2O_3). Initially, these compounds were

Table 2-1 Chemical reactions involved in the lime cycle for calcitic (air-hardening) limes.

Chemistry of air-hardening limes									
Calcination (burning)									
$CaCO_3$ calcium carbonate (limestone)	+	950°C heat	=	CaO calcium oxide (quicklime)	+	CO_2 carbon dioxide			(1)
Slaking (hydration)									
CaO calcium oxide (quicklime)	+	H_2O water	=	$Ca(OH)_2$ calcium hydroxide (slaked lime)					(2)
Hardening (carbonation)									
CO_2 carbon dioxide	+	H_2O water	=	H_2CO_3 carbonic acid					(3)
$Ca(OH)_2$ calcium hydroxide	+	H_2CO_3 carbonic acid	=	$CaCO_3$ calcium carbonate	+	$2\ H_2O$ water			(4)

added to slaked lime via pozzolanic additions and later incorporated directly through the raw material by using clay-rich limestones. In the latter case, depending on the clay content of the impure limestone and the calcination temperature used during production, various types of binders have been progressively developed throughout history. A closer look at the different hydraulic binders is presented below.

The earliest artificial form of hydraulic binder is lime–pozzolana, obtained by mixing slaked lime with reactive siliceous or aluminous materials. This binder is typically classified as an artificial or formulated hydraulic lime, as its hydraulic properties do not originate from the raw limestone itself but from the intentional addition of so-called pozzolanic compounds. The term derives from the volcanic material used by the Romans as early as 300–500 BCE to confer hydraulicity to air lime mortars when required, i.e. pozzolana. Today, it is used in a broader sense to indicate both natural and artificial siliceous or aluminosilicate compounds that react with calcium hydroxide ($Ca(OH)_2$) in the presence of water to form cementitious hydration products: calcium silicates hydrated (C-S-H) and calcium aluminates hydrates (C-A-H). Known as the pozzolanic reaction, this process co-occurs with carbonation when the material is exposed to atmospheric conditions. Throughout history, different types of additives have been incorporated to activate the pozzolanic reaction. Notable examples include Trass, a finely ground volcanic tuff from the Eifel region in Germany, widely used across northern Europe, including the Netherlands, northern Germany, and Denmark (Heinemann and Nijland 2009; Nijland). Alternatively, in the absence of natural pozzolanas, artificial ones such as crushed ceramic fragments from bricks or tiles were employed (called cocciopesto by the Romans). Modern artificial pozzolanas, by contrast, are often derived from industrial by-products such as fly ash, silica fume, and ground granulated blast furnace slag. Given the wide variety of materials used, with different compositions and water-to-binder ratios, a diverse range of mechanical properties can be achieved. To provide a reference to the reader, samples made with powdered hydrated lime and natural pozzolana from the island of Milos, with water-to-binder ratios between 0.6 and 0.8, showed porosity values ranging from 17% to 20% and compressive strengths between 2.5 and 5 N/mm² after 28 days of hardening (Papayianni and Stefanidou 2006). However, McCarthy et al. (McCarthy and Dyer 2019) report that compressive strength can triple over a two-year period due to the slow hardening rate of these mortars.

Building on centuries of experience with lime–pozzolana, the development of natural hydraulic lime around the mid-18th century introduced a new way to achieve hydraulicity directly from the raw material. In this case, the binder is produced via impure limestone containing approximately 6.5–20% clay. As with air lime, the production process involves calcination, hydration, setting, and hardening. However, each step presents key differences due to the presence of clayey compounds, and therefore to the material's hydraulic nature. For instance, carried out at around 1000 °C, calcination involves not

only the decomposition of limestone ($CaCO_3 \rightarrow CaO + CO_2$) but also the breakdown of clay into silica and alumina ($Al_2O_3 \cdot SiO_2 \rightarrow Al_2O_3 + SiO_2$), followed by their reaction with CaO to form hydraulic phases (mainly C2S (Lanas et al. 2004)). The final hydraulic performance depends on the composition of these phases, which is controlled by the clay content, kiln temperature, and residence time. In addition to the formed calcium silicate and aluminates, a portion of CaO (typically >3%) remains unreacted and is referred to as “free lime”, necessary to enable slaking. In this step, water is added in a controlled amount to hydrate the free CaO without prematurely activating the hydraulic compounds. The slaked material is then ground into a fine powder, sometimes with gypsum added to regulate the setting time. Setting and hardening occur in two stages: an initial hydraulic reaction, involving the hydration of kiln-formed calcium silicates and aluminates, followed by carbonation, where the remaining calcium hydroxide reacts with atmospheric CO_2 to form calcium carbonate ($Ca(OH)_2 + CO_2 \rightarrow CaCO_3 + H_2O$). This secondary reaction further contributes to strength development, with full mechanical performance typically reached after prolonged curing. According to Arizzi et al. (Arizzi and Parra-Fernández 2025), these mortars reach only about 50% of their final strength after 28 days, and a curing period of at least two years is required for a more accurate assessment. To provide a reference for the reader, samples prepared with binder-to-aggregate ratios between 1:1 and 1:5, using four different types of aggregates, achieved 365-day compressive strengths ranging from 2 to 15 MPa, with corresponding porosity values between 20% and 45% (Lanas et al. 2004).

Over time, limestones with higher clay contents began to be calcined, leading to the development of so-called natural cement, also known as Roman cement. This binder is made from limestone containing 75-60% carbonates and 25%-40% clay content, activated at temperatures between 1000 °C and 1300 °C. Being obtained from a single and un-modified rock source, means that each source yielded a cement with particular characteristics; hence this type of binders indicate the genre and not a unique material (Hughes et al. 2009). Unlike hydraulic lime, the calcined product (called clinker) contains insufficient free lime to be slaked, and therefore must be finely ground before use (Hughes et al. 2009). Due to the predominance of hydraulic phases and the minimal presence of free lime in the clinker, hardening occurs primarily through hydration, resulting in a material that sets and hardens simultaneously (Varas et al. 2005). This results in a fast-setting binder (30 min for lime-rich composition, usually called rapid natural cements) (Varas et al. 2005), with improved mechanical properties compared to earlier hydraulic limes. This enhancement in performance gave rise to the term "cement," a designation that distinguishes this new type of hydraulic binder from the traditional hydraulic lime.

Innovations in kiln design and firing temperatures in the late 1800s led to the development of artificial Portland cement, a material with superior mechanical properties compared to natural cements. This binder is manufactured following a rigorous procedure in which a homogeneous dosed mixture of finely ground limestone (approximately 75%) and clay (approximately 25%) is heated to approximately 1450 °C. In contrast to previous binders, the use of a dosed mixture leads to a unique material with specific characteristics. For detailed details on their production process, the reader is referred to (Costa 2015). After calcination, the obtained clinker is finely ground together with a small amount of gypsum, which regulates setting and promotes the early hydration of calcium silicates. Similar to natural cement, the resulting product is primarily composed of hydraulic phases and contains a minimal amount of free lime, specifically less than 0.5 to 1%. However, the addition of gypsum leads to a material in which setting time is longer than natural cements (> 1hour), as pointed out by (Varas et al. 2005). Due to the higher temperatures used during production, different hydraulic phases are formed with respect to natural hydraulic limes (Lanas et al. 2004). In this case, calcium silicates (mainly C_3S) and calcium aluminates (C_3A and C_4AF) are formed, with the final hardened paste contains 50-60% of calcium silicate hydrates (C-S-H). The remaining part consists mainly of calcium hydroxide and other hydration products that generally fill the pores, reducing porosity and thus increasing strength, which can range from 32 to 62 MPa at 28 days (Grosso Giordano et al. 2023). Some unhydrated particles may remain, depending on the water-to-binder ratio used.

To understand the fundamental differences between these binders, Young 2021 likens the mineral phases in hydraulic binders to needle-like crystals that weave through and lock adjacent particles, creating compact structures with low porosity (Figure 2-5). Air lime mortars remain far more open-textured, while hydraulic limes occupy an intermediate position. Consequently, the properties of different binders depend on the presence, quantity, and type of hydraulic phases, which is zero in the case of air lime. As

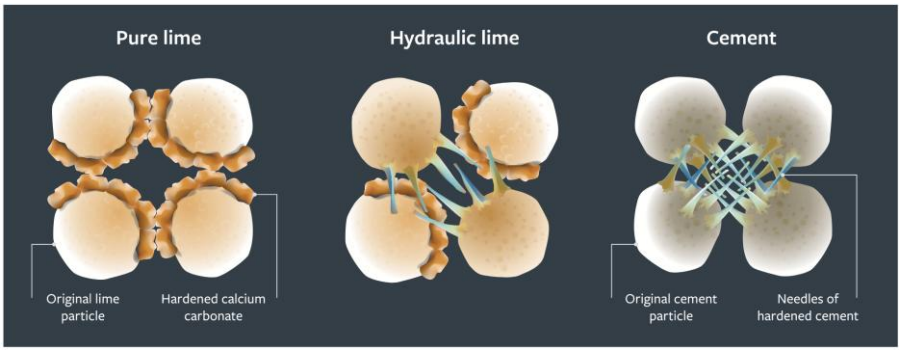


Figure 2-5 Schematic representation of the microstructure of pure lime, hydraulic lime, and cement binders. Retrieved from (Young 2021).

the proportion of hydraulic phases increases, strength (compressive, tensile, and bond) and elastic modulus also increase, while total porosity decreases significantly. This results in greater resistance to water penetration and reduced water transmission, aspects that play a fundamental role in the deterioration processes of masonry (see Section 2.2). To give the reader an overview, Figure 2-6 illustrates how the main technical properties vary across the different binder types. Providing precise values is difficult, as many binders represent a family rather than a specific product, and their properties depend on the raw materials used. Moreover, factors such as the binder-to-aggregate ratio, water-to-binder ratio, aggregate characteristics, and curing conditions also influence the final properties.

In the past century, cement has become the most widely used binder in new construction. However, growing concerns over CO_2 emissions and the environmental impact of cement production have prompted a search for more sustainable alternatives. In this context, many researchers have turned their attention back to traditional materials, with lime experiencing a renewed interest due to its lower carbon footprint and intrinsic compatibility with historic masonry. Unlike cement, lime hardens by reacting with atmospheric CO_2, offering potential as a carbon sink throughout the service life of structures. Moreover, the lower calcination temperatures required for lime production result in significantly reduced energy consumption compared to Portland cement. Yet, the very mechanism that makes lime attractive also presents a major limitation: carbonation progresses slowly, often requiring months or even years to develop sufficient mechanical strength. These limitations have motivated research into methods that could accelerate or enhance lime carbonation. In recent years, this has included the

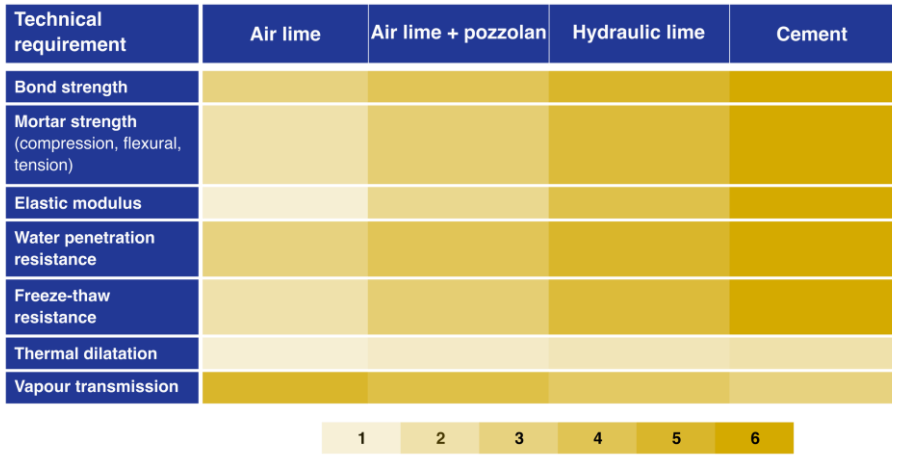


Figure 2-6 Relative comparison of binder properties, scored from 1 (low) to 6 (high); retrieved from (Válek et al. 2010).

exploration of bacteria-based approaches capable of promoting carbonate precipitation, to support the hardening of lime mortars (see section 2.5.1).

For restoration purposes in particular, air lime and natural hydraulic lime remain the preferred binders, valued for their physical, chemical and mechanical compatibility with existing masonry fabrics (Groot et al. 2022) (see section 2.3).

2.2 Damage in masonry structures: mechanisms and consequences

Masonry has been prevalent for centuries and, like any construction material exposed to the environment, undergoes a natural ageing process (Niedostatkiewicz and Majewski 2024). Driven by repeated physical actions (fluctuations in temperature and humidity, solar radiation, wind, and exposure to water), ageing can be further accelerated by other factors, such as human-induced activities, exceptional (incidental) events, inadequate or absent maintenance. These actions and conditions are referred to as deterioration factors, as their interaction can give rise to deterioration mechanisms that eventually causing degradation to the material, i.e. loss of performance. Such degradation may manifest in different forms and in various parts of the masonry: within the bricks, in the mortar joints, or along the brick–mortar interface. In historical masonry, commonly made with strong fired-clay bricks and weaker lime mortars, degradation tends to concentrate in the mortar and in the bond, which act as "sacrificial" zones: a desirable condition since replacing bricks is far more invasive and costly than renewing the joints. As the repair strategy explored in this thesis focuses on damage in the mortar and at the brick–mortar interface, this section provides an overview of the deterioration factors, the mechanisms through which they act, and the resulting forms of degradation, focusing in those areas.

Deterioration factors are conditions that contribute to the initiation and progression of damage in masonry structures by enabling harmful processes to develop. They are generally grouped into five main categories: environmental exposure, material characteristics, structural design, construction quality, and maintenance practices. A comprehensive overview of these factors is provided by Van Hees et al. (Van Hees et al. 2004) and summarised in Table 2-2. Rather than acting independently, these factors tend to interact, jointly influencing both the onset and rate of degradation. For example, the presence of water (an environmental factor) is a necessary condition for the development of many deterioration mechanisms, but not sufficient on its own. As explained by Lourenço et al. (Lourenço et al. 2014), the rate at which a material absorbs and releases moisture, governed by properties such as porosity and pore size distribution (material factors), also plays a critical role in determining whether degradation will occur. In addition, the building's design (e.g., orientation and detailing) and the quality of craftsmanship, further influence the structure's susceptibility to damage. The development of degradation is therefore a complex phenomenon, resulting

from the interplay of multiple interdependent factors. These interactions give rise to different types of deterioration mechanisms which can be broadly classified into three main categories: chemical, physical, and mechanical.

Chemical deterioration mechanisms arise from reactions between mortar constituents and aggressive substances in the presence of water. These substances may originate from (i) environmental pollutants (e.g., aerosols, de-icing salts) transported through air, soil, or water; (ii) residual contaminants from former building uses (such as salt storage or stables); or (iii) the original material composition (e.g., seawater or beach sand). The most common process is leaching, whereby slightly acidic rain or condensation dissolves components of the binder, increasing porosity and reducing cohesion and strength. The increased porosity renders the mortar more vulnerable to other forms of attack, such as frost, wetting–drying cycles, and further leaching. Loss of cohesion and strength typically manifests as sanding, powdering, or crumbling of the mortar, and makes it more susceptible to crack formation under subsequent actions. When the dissolved constituents migrate and precipitate at the surface, the resulting deposits are termed efflorescence, which commonly appears as a white coating once dry and is mainly aesthetic. Acid attack produces a similar but more intense effect, accelerating dissolution and resulting in pronounced “washing out” or erosion of the joints. In contrast, sulfate attack involves reactions between sulfate ions and binder phases (calcium hydroxide, calcium aluminates, or calcium silicates), forming expansive compounds such as gypsum, ettringite, or thaumasite, whose volumetric growth can lead to cracking and spalling of the mortar.

Physical deterioration mechanisms also involve volumetric changes, primarily driven by the presence of water in its liquid, vapor, or frozen states. The most relevant processes include freeze–thaw cycles, salt dissolution and crystallization, and water retention, the latter often promoting biological colonization. Freeze–thaw cycles occur when water-saturated pores freeze following rainfall. The formation of ice

Table 2-2 Summary of key factors involved in the degradation of masonry structures.

Environment	Moisture supply	Rain, snow
		Ground water
		Surface water
		Floods
	Salt supply	Soil or surface water
		Use (stable, salt storage)
		Air (aerosol)
		Floods
		De-icing salts
	Air pollution	
	Temperature factors	Variations
		Extremes
	Exposure to fire	
	Dynamic loads	Earthquakes
		Wind
		Traffic
		Vibrations
	Differential settlements	
Materials	Mortar composition	Binder type
		Binder quantity
		Grain size distribution sand
	Properties brick/stone and mortar system	Porosity
		Capillary transport
		Adhesion / bond
	Presence of salts in the materials	
Design	Original structural design of the building or modifications	
	Choice of combinations of materials	
	Detailing of the building	
	Choice of repair methods and materials	
Workmanship and construction procedures	Quality of execution	Quality of execution
		Mortar mixing on site
		Way materials are cured and curing conditions
		Protection of fresh mortars (masonry)
	Lack of knowledge on (traditional) workmanship	
Maintenance	Lack of maintenance	
	Inappropriate maintenance programme	

causes volumetric expansion, generating internal pressure that leads to cracking and surface crumbling. In salt dissolution and crystallization, internal pressure arises from repeated phase changes. It begins when soluble salts, present in the material itself or carried by infiltrating water as explained above, dissolve and migrate through the pore network. Upon evaporation, salts crystallize, generating pressure within the pores, particularly during repeated dissolution–crystallization triggered by wet-dry cycles and/or RH fluctuation. As a consequence, mortar can show damage in the form of sanding, scaling, exfoliation or crumbling and cracking. Eventually, water retention within the porous material can also lead to biological attack, fostering the growth of microorganisms such as algae and cyanobacteria. These can form a superficial layer that retains moisture and provides nutrients, creating favourable conditions for the development of other organisms. Although the primary consequence is often limited to aesthetic alteration in early stages, extensive colonization can induce mechanical stress, eventually leading to cracking.

Eventually, mechanical deterioration mechanisms may result from stresses induced by static and/or dynamic action. These may stem from long-term loads, such as additional elements introduced during renovations, or vibrations due to traffic, window, soil movement, mining activities, or accidental events like earthquakes and strong winds. The resulting damage typically manifests as the formation or widening of cracks, whose severity depends on the magnitude and frequency of the acting loads over time. In the context of Dutch buildings, for instance, this is especially relevant in the region of Groningen, where repeated low vibrations induced by anthropogenic activities have caused light damage to buildings (Korswagen et al. 2019). Nevertheless, mechanical deterioration is becoming a pertinent problem for the entire country due to climate-induced settlement activities (Prosperi 2025).

While degradation can manifest in various forms, cracks represent the most prevalent and pervasive manifestation of damage (Figure 2-7). Their impact is threefold, simultaneously affecting the aesthetics, watertightness, and mechanical performance of the masonry. First, aesthetically, cracks exceeding 0.1 mm become visible to the naked eye, constituting the threshold for 'light damage' that alters the building's appearance (Korswagen 2024). Second, this same threshold is critical for watertightness; cracks exceeding 0.1 mm are similarly recognised by several authors as sufficient to allow water ingress through masonry (Birkeland and Svendsen 1963; Grimm 1982, 1988). For the latter, Shahreza (Kahangi Shahreza 2024) demonstrated that 0.3 mm cracks in three-course masonry prisms resulted in a 1.7-fold increase in water penetration compared to undamaged samples when subjected to water spray. This highlights how seemingly minor forms of damage can increase water ingress, which in turn plays a central role in the initiation and progression of the deterioration processes described above. Finally, regarding mechanical performance, cracks disrupt the continuity of the material, locally

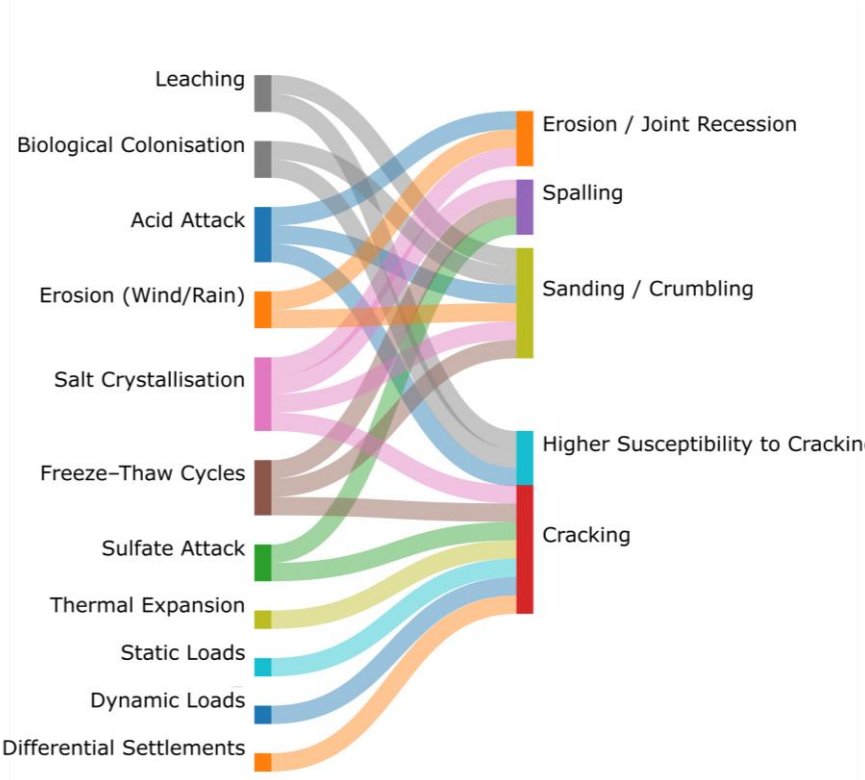


Figure 2-7 Conceptual mapping of deterioration mechanisms and their resulting degradation forms (made at SankeyMATIC.com)

reducing its stiffness and tensile capacity. This degradation alters the internal stress distribution, often creating stress concentrations at the crack tip that facilitate further crack propagation under repeated environmental or mechanical loading (Korswagen et al. 2019). As highlighted by Ghiassi and Lourenço (Ghiassi and Lourenco 2018), if these initial discontinuities are left unaddressed, they can worsen over time, leading to progressive degradation and potentially compromising structural stability. This highlights the importance of effective maintenance. Without timely and appropriate interventions, minor damage can worsen, especially if improper repair methods are applied. Regular maintenance and preventive measures are thus essential to ensure the long-term durability of masonry structures.

2.3 Repointing as repair strategy: practice and limitations

As discussed above, some degree of deterioration in masonry is unavoidable. For this reason, it is advantageous when damage localises in the mortar joints, which are easier to renew than the masonry units. Repointing has therefore become the traditional method for restoring the performance of deteriorated joints. As described by Mack et al. (Mack 1998), this technique (also referred to as 'pointing' or, less accurately, 'tuck pointing' (Shellenbarger 1991) involves the removal of the degraded mortar from the joints and its replacement with new, compatible material. The depth of intervention can vary depending on the damage. It is usually relatively superficial, 20 to 30 mm, with a rule of thumb minimum of the joint thickness but twice the thickness is often recommended to obtain an adequate key for the mortar. In special cases, if there are voids or the damage has extended further into the joint, it may go deeper, up to 50 or 70 mm (deep repointing), with structural assessment of the structure needed. Its minimal invasiveness and ability to preserve the original appearance make this technique particularly suitable for conservation interventions. When properly done, repointing restores the visual and physical integrity of the masonry. However, before implementation, accurate assessment of the cause of damage, the need for repointing and how to do it is of fundamental importance. As highlighted by (Maurenbrecher et al. 2016), successful repointing depends 50% on a proper design and 50% on-site execution. This section reviews the key aspects involved in the repointing process.

Developing an effective repair strategy for any existing structure, historic or modern, requires an initial assessment of its condition and a clear understanding of the mechanisms driving degradation (van Balen et al. 2010). Documentation plays a key role at this preliminary stage, not only in guiding the current intervention, but also in providing a valuable record for future repair or maintenance efforts. Understanding the damage, and especially its underlying causes, is crucial in defining an effective course of action. As noted by Mack et al. (Mack and Askins 1979), repointing is unlikely to be effective if underlying causes of damage, such as leaking roofs, or gutters, differential settlements of the building, capillary actions causing rising damps, or extreme weather exposure are not addressed first. Tackling these issues, if present, in advance is essential to reduce the risk of future deterioration and to ensure the long-term success of the intervention. Together with the building assessment, relevant data must be gathered to inform the selection of a suitable mortar mix. This ranges from evaluating the type and severity of climatic exposure to documenting, sampling, and analysing the original components of the masonry, namely the original mortar and any previous applied repair mortars (colour, form, and composition) and masonry units (Lindqvist 2009).

Following the assessment phase, the focus turns to designing a compatible repair strategy, guided by core principles such as authenticity, which ensures the repair

preserves cultural and material identity; compatibility, to guarantee the intervention does not trigger or worsen deterioration processes; and retreatability, ensuring that the current repair does not hinder future interventions (Van Balen 2005). These conceptual requirements, along with considerations like durability, the use of locally sourced or low-energy materials, and aesthetic compatibility, form the foundation of the repair design process. Fulfilling most of them often depends on selecting a repair material that closely mimics the original. This, in turn, requires a thorough characterisation of both the original and repair mortars, translating the guiding principles into measurable technical requirements tailored to the function of the element. For example, harmonization relates to the visual match between the new repair mortar and original masonry, and can be evaluated through surface features like colour, texture and surface finish. According to Mack et al. (Mack and Askins 1979), using similar sand as the existing is key, as it defines much of the final look in terms of color and texture. Yet, the final surface finish is also shaped by the techniques and craftsmanship employed.

Besides surface features (colour, texture, and surface finish) and composition (type of binder, type of aggregates and grain size distribution), the most decisive technical characteristics for ensuring the above-mentioned principles and an acceptable application are: (i) strength (compressive, tensile and bond), (ii) elasticity (modulus of elasticity, deformability) and (iii) porosity properties (total porosity, app. specific gravity, pore size distribution, water absorption by capillarity and vapour transport). On the one hand, the strength and flexibility of the new mortar must be carefully calibrated. It should be strong enough to bind the masonry units and support the structure, yet soft and deformable enough to protect the historic materials by failing first when overstressed. This sacrificial behaviour ensures that stresses are absorbed by the mortar rather than transferred to the original units, which could otherwise suffer permanent damage. if the new mortar is improperly selected, for instance, being too stiff or strong compared to the original masonry, it will not accommodate these stresses. Instead, it will transfer the load to the softer masonry units, leading to cracking or spalling of the bricks, which are far more difficult and costly to replace than the mortar itself. Moreover, a softer mortar allows for future removal without harming the original masonry (retreatability/repairability). On the other hand, porosity properties play an equally decisive role. They determine the mortar's hygric response to environmental actions, influencing both water absorption and vapour transmission. Ideally, the porosity and pore size distribution of the new and old mortar should align to ensure a good interface and prevent incompatibility. The mortar should promote evaporation and facilitate the outward migration of moisture and salts, thereby protecting the masonry units. If the repair mortar is too dense or impermeable, it will trap moisture within the wall, leading to salt crystallization and accelerated decay within the bricks or at the brick-mortar interface.

Besides an appropriate mix design, proper application is essential to ensure both the effectiveness and durability of the repair. Key aspects include scheduling, skilled execution, proper joint preparation, correct mortar handling, and both on-site quality control and post-application monitoring. Nothing should be left to chance, as Groot et al. (TC 203-RHM (Main author: Paul Maurenbrecher) 2012) point out: low-strength repair mortars, commonly used in historic masonry, are particularly unforgiving of errors. For instance, carrying out the work under unsuitable seasonal conditions may result in freezing damage or excessive drying, both of which can compromise the mortar's performance. For this reason, interventions are preferably scheduled for spring or early autumn, a practice already recognised by the Romans. Likewise, during the early stages of curing, the mortar must be kept moist to ensure proper carbonation. This can be achieved by covering the masonry with plastic sheeting and regularly re-wetting the burlap before it dries. For further guidance on these aspects, the reader is referred to Groot et al. (TC 203-RHM (Main author: Paul Maurenbrecher) 2012).

It is important to note that, even if repointing restores the strength, watertightness, and aesthetic condition of the masonry, it cannot prevent future damage, as all buildings are in a constant process of deterioration (see section 2.2). As Mack et al (Mack and Askins 1979) explain, this aspect is accounted in masonry design and its repair: in well-designed walls, mortar joints are intended to bear most of the stresses that cause deterioration and can be repointed repeatedly. This, however, still requires repeated interventions over time, increasing maintenance costs and undermining the principles of restoration, which aim for minimal intervention and long-term sustainability. In this context, self-healing repair mortars could offer a novel solution to tackle these challenges by extending the service life of the intervention. As research on this specific application remains limited, the following sections explore established strategies in self-healing concrete to identify potential approaches for masonry.

2.4 Innovation in repair: insights from self-healing concrete

The widespread occurrence of cracking in masonry, discussed in Section 2.2, mirrors challenge long recognised in concrete structures. For this reason, research on self-healing concrete, a field that is now well-established, offers valuable insights for developing self-healing strategies tailored to masonry repair. Over the past two decades, numerous mechanisms, healing agents, and assessment frameworks have been explored in cement-based systems, providing a solid foundation from which masonry-oriented adaptations can be derived.

Self-healing materials originate from a shift in design philosophy: instead of preventing damage at all costs, materials are conceived to manage damage by restoring functionality after cracking. This concept, articulated by van der Zwaag (van der Zwaag

2007) and later adopted in concrete research, redefines damage (or cracking) as a tolerable event, provided that the material is equipped with mechanisms to autonomously repair it.

Although the idea of materials capable of repairing themselves may seem recent, the phenomenon has long been observed in historical constructions. Roman lime mortars exhibited autogenous healing properties that are believed to have contributed to their exceptional durability, with many structures surviving over 2000 years. This healing, however, occurs spontaneously and not intentionally engineered. The modern development of man-made self-healing materials began with the pioneering work of White (White et al. 2001), who embedded microcapsules filled with liquid adhesive into concrete and epoxy matrix. When cracks formed, the capsules ruptured, releasing the adhesive into the damaged area, where it filled the crack and subsequently hardened, restoring the materials' integrity, a solution deeply explored for concrete. Variations of this concept have since been extensively explored for concrete.

Before examining the specific strategies developed for construction materials, it is important to clarify the terminology. According to De Rooij et al (De Rooij et al. 2013), self-healing refers to "any process by the material itself involving the recovery and hence improvement of a performance after an earlier action that had reduced the performance of the material." The concept is further classified into two types:

- Autogenic healing: "the self-healing process is autogenic when the recovery process uses materials components that could otherwise also be present when not specifically designed for self-healing (own generic materials)" (De Rooij et al. 2013).
- Autonomic healing: "the self-healing process is autonomic when the recovery process uses materials components that would otherwise not be found in the material (engineered additions)" (De Rooij et al. 2013).

A large variety of engineered additions have been developed, either to enhance the intrinsic autogenous capacity of concrete or to introduce novel autonomous healing systems. In the following sections, these approaches are presented, starting with autogenous healing, and continuing with autonomous healing strategies, with a particular focus on the poly-lactic acid (PLA) based healing agent investigated agent in this thesis.

2.4.1 Autogenous healing potential of mortars

Autogenous healing is the term commonly used to describe the spontaneous ability of materials to repair micro-damage that can develop during their service life, thereby contributing to the material's long-term durability. The phenomenon, already documented in the late 19th and early 20th centuries for both cement-based and lime-based mortars, has since been studied extensively.

Regardless of binder type, autogenous healing is predominantly driven by the dissolution and subsequent carbonation of calcium-bearing compounds, primarily calcium hydroxide ($Ca(OH)_2$) due to its higher solubility compared to other phases. While this compound persists in all types of lime mortars due to slow carbonation, in hydraulic mortars it forms during hydration along with C–S–H phases that provide strength. This carbonation-driven self-healing is essentially the same as the one responsible for the hardening of lime mortars, reported in Table 2-1.

Initiated by the ingress of water, whether from rain or atmospheric moisture, the process follows a sequence of reactions outlined in Table 2-3. On the one hand, $Ca(OH)_2$ dissolves in the pore solution, releasing calcium ions (Ca^{2+}), Eq. (5). These ions then migrate from binder-rich zones toward the damaged region. At the same time, the atmospheric carbon dioxide (CO_2) dissolves in the pore water, forming carbonic acid (H_2CO^3), Eq.(6), which is further dissociated into bicarbonate (HCO^{3-}), Eq.(7) and carbonate (CO_3^{2-}) ions, Eq.(8). Depending on the pH of the pore solution, the dominant carbonate species reacts with Ca2+ to precipitate calcium The extent of these chemical reactions is governed by the presence of water and the availability of calcium hydroxide. While dry mortars cannot carbonate, in fully saturated ones, carbonation is inhibited due to limited gas diffusion, and leaching of calcium hydroxide may prevail instead. For this reason, wet-dry cycles are considered to be more favourable. Equally important is the availability of calcium hydroxide present in mortar, whose amount depends on several factors, including its composition (binder-to-aggregate ratio, binder type, presence of reactive components such as fly ash or pozzolana), and the degree of carbonation, often

Table 2-3 Sequence of carbonation reactions underlying the full or partial hardening of lime mortars and autogenous self-healing across all mortar types.

Chemistry behind carbonation								
Dissolution of calcium hydroxide								
$Ca(OH)_2$ calcium hydroxide	+	H_2O water	=	Ca^{2+} calcium oxide	+	2 OH^- carbon dioxide		(5)
Dissolution of carbon dioxide								
CO_2 carbon dioxide	+	H_2O water	=	H_2CO_3 carbonic acid				(6)
H_2CO_3 carbonic acid			=	H^+	+	HCO_3^-		(7)
H_2CO_3 carbonic acid			=	$2H^+$	+	CO_3^{2-}		(8)
Hardening (carbonation)								
Ca^{2+} carbon dioxide	+	CO_3^{2-} water	=	$CaCO_3$ calcium carbonate				(9)
Ca^{2+} calcium hydroxide	+	HCO_3^- carbonic acid	=	$CaCO_3$ calcium carbonate	+	H^+		(10)

linked with the age at which cracking occurs. While mortars with higher binder content typically contain more $Ca(OH)_2$, pozzolanic or fly ash additions can gradually consume part of it through secondary hydration reactions, thus reducing the amount available for self-healing (De Rooij et al. 2013). Furthermore, as carbonation progresses over time, calcium hydroxide is gradually consumed and transformed into calcium carbonate, a 100 times less soluble compound. Since dissolution is essential for transport and reprecipitation to occur, the process is more effective in less carbonated mortars. That said, carbonation is a slow process that moves inwards from the exposed surface. For this reason, uncarbonated regions can still be found even in old structures.

Evidently, the dissolution of $Ca(OH)_2$ plays a fundamental role in the efficiency of self-healing. Therefore, any factor that influences its solubility or dissolution rate becomes highly relevant. Among these, the presence of certain organic or inorganic phases, often introduced as impurities or through the mortar composition, can have a significant impact. For instance, ammonium chloride (NH_4Cl), commonly found in industrial or agricultural environments, has been shown to considerably increase the solubility of $Ca(OH)_2$.

The process itself typically proceeds in two distinct stages. Immediately after cracking, Ca^{2+} ions are more prone to be directly available on the crack surfaces, leading to faster recrystallization growth. After an initial layer of calcium carbonate is formed in the cracks, Ca^{2+} ions must travel through diffusion through the matrix and form a $CaCO_3$ layer to precipitate on the face of the crack. This phase is much slower than the initial one. The concentration of CO_3^{2-} and HCO^{3-} near the crack mouth is higher than that inside the crack, leading to the formation of calcium carbonate first near the crack mouth, as observed in the Figure 2-8.

Contributing to autogenous healing in hydraulic binder mortars, there is also swelling of hydrated paste near crack surfaces due to the absorption of water by the paste.

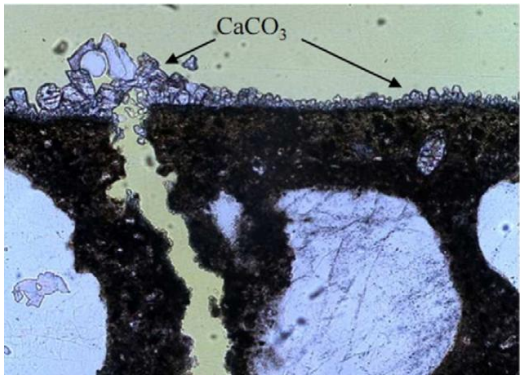


Figure 2-8 Localized $CaCO_3$ precipitation at the crack tip in cement-based mortars. The crack interior shows no healing. Retrieved from (Huang et al. 2016).

Particles that did not hydrate because of lack of water can hydrate because of leaked water. This phenomenon is more common

in young mortars and depends on the w/c ratio: lower w/c leads to more unhydrated cement particles that would theoretically increase the self-healing capacity of the material at a later stage. Additionally, this mechanism is highlighted as being of minor importance in the whole process.

Alongside the processes described above, minor mechanisms like the obstruction of cracks by waterborne debris or loose particles can contribute to healing. Yet, autogenous healing is largely confined to small cracks (likely less than 50 µm (Huang et al. 2016)). To achieve faster and more extensive concrete repairs, engineered autonomous strategies have been proposed and are discussed in the next section.

2.4.2 Autonomous healing strategies

Autonomous healing refers to the deliberate incorporation of engineered additives, either to enhance the material's intrinsic autogenous healing capacity or to introduce entirely new repair mechanisms. While the former can enhance the healing of cracks up to 100-150 µm, new mechanisms allow for the healing of larger cracks of 300 µm (De Belie et al. 2018) or even around 1 mm (Wang et al. 2014), and typically act faster. This section provides a brief overview of the main strategies, with further details available in (Van Tittelboom and De Belie 2013; Muhammad et al. 2016; Tziviloglou 2018; De Belie et al. 2018).

In the first subset, research focuses on additives that support and enhance the material's intrinsic autogenous capacity. As reported in the previous section, autogenous healing is more effective when crack widths are limited, water is available, and hydration or crystallization are promoted. Therefore, various design strategies have been developed to support these conditions: restricting crack width (e.g., by incorporating fibers such as PVA, steel, or polypropylene), maintaining internal moisture (e.g., through superabsorbent polymers, nanoclay, or encapsulated water), or stimulating further hydration (e.g., with fly ash or slag, which contain unhydrated particles that react over time). In addition, more advanced admixtures like crystalline products or encapsulated expansive agents have been used to induce swelling or form crystalline products (e.g., ettringite) upon water ingress, facilitating crack closure.

The second category, developed intensively over the last decade, includes encapsulated or vascular networks containing healing agents that are released upon cracking. Capsules can vary in shape (spherical or cylindrical) and size, ranging from micro (<1 mm) to macro. Macro-capsules are sometimes preferred as they can store larger amounts of healing agent and potentially enable multiple healing events. Vascular systems, on the other hand, consist of hollow tubes, often 3D-printed, filled with healing agents. These can be single-channel, containing a one-component healing agent, or

multi-channel, for multi-component systems. Compared to capsule-based approaches, vascular systems offer the advantage of a continuous supply of healing agent to damaged areas, can address varying degrees of damage, and may be pressurized to enhance distribution, enabling multiple healing cycles.

Regardless of the delivery method, the healing agent itself can vary widely in nature and mechanism. Examples include polymers that flow into and seal cracks upon release; mineral precursors that react to form solid phases; calcium hydroxide, which carbonates upon exposure to CO_2, leading to additional limestone precipitation; tung oil, which hardens when in contact with air; and carbonate-precipitated bacteria, supplied with nutrients, that activate under specific conditions depending on the bacteria strain used.

Extensive research has been conducted for the latter case, usually referred to as bio-concrete or biogenic concrete, due to its high potential for long-term performance. Unlike other strategies where the healing agent is consumed during the repair process, thereby limiting the number of healing events, bacteria act as mediators of the reaction, producing the repair material rather than constituting it. In addition, the calcium carbonate produced during bacterial activity acts as an effective bonding agent and is fully compatible with concrete, being usually part of the concrete matrix. Research efforts have concentrated on selecting the most suitable microorganisms and nutrients, as well as on strategies to protect them. This latter aspect is crucial, as both bacteria and nutrients must withstand mixing procedures, high alkalinity, a dense matrix (with small pores), and unsuitable humidity conditions. As a result, numerous solutions have been explored, some of which are already commercially available. One example is the healing agent used in this thesis, developed by Jonkers et al. since 2006 at TU Delft, which will be described in more detail in the next section.

It is worth noting that although numerous testing methods have been developed over the past decades to evaluate the self-healing efficiency of these strategies (Çopuroğlu et al. 2013), no standardised protocol has yet been established. Regardless of the strategy, self-healing behaviour is influenced by numerous factors, including mix design (composition and water-to-binder ratio), cracking procedures, age and morphology of cracks, and healing duration and conditions. Without a standardised protocol to account for these variables comparing results and generalising findings remains challenging, as many authors have pointed out (Muhammad et al. 2016; Van Mullem et al. 2020). In addition, verifying healing efficiency alone may be insufficient, and as highlighted by Rossi (Rossi 2022), a comprehensive assessment of the engineered material's functionality should be carried out. For this reason, Tziviloglou et al. (Tziviloglou et al. 2015) proposed a framework within the context of bio-concrete, which can be extended to other self-healing agents by tailoring it to their specific mechanisms. The methodology comprises three performance requirements that must be verified simultaneously to ensure proper applicability of a bacteria-based self-healing agent: (i) evidence of bacterial activity, (ii)

mineral formation induced by bacterial metabolic processes, and (iii) recovery of the material's performance. This approach allows for a more comprehensive assessment by not only evaluating the healing behaviour of the material but also demonstrating that the enhanced performance originates from the proper functioning of the healing agent, in this case, through bacterial activity. Tziviloglou et al. (Tziviloglou et al. 2015) explain that "recovery of performance" must be clearly defined. In the case of concrete, this can be divided into mechanical properties, durability, and aesthetic appearance, with durability often linked to water ingress and therefore commonly assessed through watertightness measurements. Since the latter aspect is the most important one, "recovery of performance" is often substituted directly with "crack sealing". Rossi (Rossi 2022) later refined this framework by including the evaluation of the agent's effect on the mortar's functional properties, such as hydration, air void content, setting time, workability, and both compressive and flexural strength. As highlighted by the author, many studies have reported negative effects of the healing agent on certain functional characteristics of concrete, underscoring the importance of systematically verifying this aspect.

2.4.3 Healing agent based on poly-lactic acid (Basilisk Technology)

Among the solution exposed above, a bacteria-embedded poly-lactic-acid (PLA) agent has been developed after years of research at TU Delft (Jonkers et al. 2010, 2015; Wiktor and Jonkers 2015; Tziviloglou et al. 2016; Mors and Jonkers 2020) and is commercialized in the Netherlands (Basilisk, Delft, The Netherlands). Initially commercialized as a cement-based repair mortar, the agent later became available as a granular additive for direct incorporation into any concrete/mortar? mix. In both forms, the agent consists of 0.1–1.0 mm PLA capsules (density: 1200 kg/m³) enclosing bacterial spores from alkaliphilic (alkali-resistant) *Bacillus cohnii*-related strains, along with nutrients required for bacterial activation during germination. As explained by Jonkers in (Mors and Jonkers 2020), this bacterial species was selected for its ability to survive casting and to form spores resistant to high pressure, aggressive chemicals, elevated temperatures, and dehydration. In addition, the PLA capsules serve a dual role: protect the bacterial spores and, upon hydrolysis to calcium lactate, provide a precursor for calcium carbonate formation. PLA is transformed to derive the actual food for the bacteria, i.e., calcium lactate $Ca(C_3H_5O_3)_2$. The rate of this process is strongly influenced by the pH, with alkaline conditions being the optimal (pH 12-13).

The sequential steps of the PLA-based healing process are outlined in Table 2-4. Once the material cracks, and water infiltrates, the pH drops below 11.5 activating bacteria. Once activated, the bacteria convert the precursor in the presence of oxygen (aerobic activity), producing calcium carbonate and carbon dioxide following Eq.(11). Bacteria-produced carbon dioxide near the crack enhances autogenous healing through carbonation, further reacting with calcium hydroxide present in the matrix, Eq.(12). As a

Table 2-4 Sequence of reactions involved in the healing mechanism of PLA? bacteria-based agent.

Chemistry behind PLA-based based healing agent										
Biological conversion of calcium lactate										
$Ca(C_3H_5O_3)_2$	+	6 O_2	=	$CaCO_3$	+	5 CO_2	+	$5H_2O$	(11)	
calcium lactate		oxygen		calcium carbonate		carbon dioxide		water		
Carbonation from metabolically generated CO_2										
5 CO_2	+	5 $Ca(OH)_2$	=	5 $CaCO_3$	+	5 H_2O			(12)	
carbon dioxide		calcium hydroxide		calcium carbonate		water				

result, massive precipitation of calcium carbonate is obtained with the production of six equivalents of calcium carbonate from one equivalent of calcium lactate, optimizing the healing process.

The idea behind this type of agent is that the limestone formed fills cracks, reducing water permeability and helping to restore lost strength. While no evidence of strength regain has been observed in the literature, lab studies showed complete sealing of up to 0.8 mm cracks after two months of healing when 15kg/m^3 of healing agent was introduced into the mix (Wiktor and Jonkers 2011; Mors and Jonkers 2017). The authors explained that the efficiency is strongly dependent on the agent's dosage. For instance, samples containing a third of the latter amount (5 kg/m3) showed complete sealing of cracks of up to 0.4 mm after 100 days of submersion in water. Reference samples tested in parallel showed that cracks of up to 0.18 mm could be healed under the same conditions through autogenous healing, the agent significantly enhancing the healing efficiency.

2.5 Towards self-healing solutions for masonry repair

Despite increasing attention to self-healing materials in the concrete field, the application of such technologies to lime-based mortars and masonry applications remains in a nascent stage. Only in recent years, specific strategies have been proposed to enable self-repair in masonry through the incorporation of healing agents, with very few experimental studies dedicated to this domain.

2.5.1 Strategies under investigation

Among the first investigations explicitly targeting lime-based mortars and masonry, De Nardi et al. (De Nardi et al. 2024) proposed the use of 3D-printed mini-vascular networks (m-MVNs), small PLA units designed to lie within the thickness of a mortar joint. Adapted from systems developed for concrete, these units are engineered to store and protect the healing agents, releasing them when a crack forms. Their geometry and

external ribs help anchor them within the lime matrix and increase the likelihood of rupture when intersected by a crack. To date, research has focused on optimizing printability and watertightness of the systems, with a wax coating successfully applied to prevent leakage of the agent. Although promising, the system remains at a conceptual stage, and its actual self-healing performance in masonry has yet to be experimentally verified.

A different research direction, also inspired by developments in self-healing concrete, focuses on the implementation of bacteria to enhance carbonation-based processes in lime-based mortars. In this context, Giordano et al. (Giordano et al. 2024) investigated specific bacterial strains capable of accelerating calcium carbonate precipitation, with the aim of improving both early hardening and autonomous healing capacity. As the authors note, the slow strength development of lime mortars has historically limited their use and contributed to their replacement by faster-hardening binders. Preliminary results indicated that bacterial addition could increase the degree of carbonation in lime mortars, although the approach remains in a developmental phase and has not yet been tested in combination with bricks.

A third direction is the one investigated in this thesis and consists of direct application to masonry of a healing agent already established for use in concrete. The focus, therefore, is not on the development of the agent itself, but on its application to masonry. For this purpose, the PLA-based healing agent described in section 2.5.3 was selected and examined in two pilot studies to demonstrate the feasibility of the research approach and to identify potential challenges. The first (Gaggero et al. 2024) used the technology's original commercial formulation: a ready-to-mix cement mortar with the agent pre-incorporated by the manufacturer. In contrast, the second study (Gaggero et al. 2025) transitioned to a pre-bagged cement-lime mortar (1:2:9), a mix widely used in masonry research and more compatible with historical structures. In this case, the healing agent was manually added to the fresh mix during preparation. Both studies relied on masonry couplets to evaluate healing performance in terms of flexural bond strength recovery and visual crack closure. Details on the two studies are provided in the following sections.

2.5.2 From concrete to masonry: first use of PLA-based mortar

In 2020, a feasibility study was undertaken to examine whether bacteria-based self-healing mortar technology, proven effective in concrete, could be applied to masonry repair. The investigation focused on the commercially available PLA-based healing mortar described in section 2.5.3, testing its potential for repairing induced cracks in small-scale masonry couplets (Gaggero et al. 2024).

The testing programme compared the healing capacity of the innovative mortar with that of a reference mix when applied to different brick types and curing conditions. The commercial product was a ready-to-mix cement-based mortar containing 5% healing agent by binder mass, tested alongside an identical mix without the agent to distinguish autonomous from autogenous healing. Both mortars were applied to solid clay and calcium silicate bricks to build couplets, two bricks joined by a mortar joint (Figure 2-9). These brick types were selected for their different porosity and absorption properties, factors expected to influence internal moisture conditions and, consequently, the healing process. Controlled cracks of around 0.1 mm were introduced using a crack-mouth opening-controlled bond wrench test. After a 65-day healing period under high humidity (RH 95%), wet–dry cycles, or dry conditions (RH 70%), mechanical recovery was assessed using the same test configuration. Crack closure was also qualitatively evaluated through photographic comparison before and after healing. The main findings can be summarised as follows.

Specimens containing the bacterial agent consistently outperformed reference specimens, confirming its ability to enhance autogenous healing. In calcium silicate specimens, the self-healing mortar nearly restored its original peak force capacity (90%) after two consecutive crack–healing cycles, compared with less than half (40%) for the reference mortar when cracks were up to 0.1 mm. Effective crack closure and full or partial mechanical recovery was observed even when damage occurred at the brick–mortar interface, with visible calcium carbonate precipitation contributing to aesthetic restoration, and successful recovery after multiple damage–healing cycles. For instance, calcium silicate couplets with 0.1 mm cracks recovered 240%, 90%, and 60% of their original strength over three successive cycles (Figure 2-10 (a)). Reduced healing efficiency was observed with increased crack width (Figure 2-10 (b)) and cycle repetition

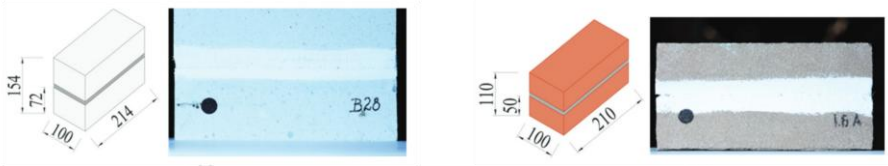


Figure 2-9 (a) Calcium-silicate and (b) clay brick masonry couplets.

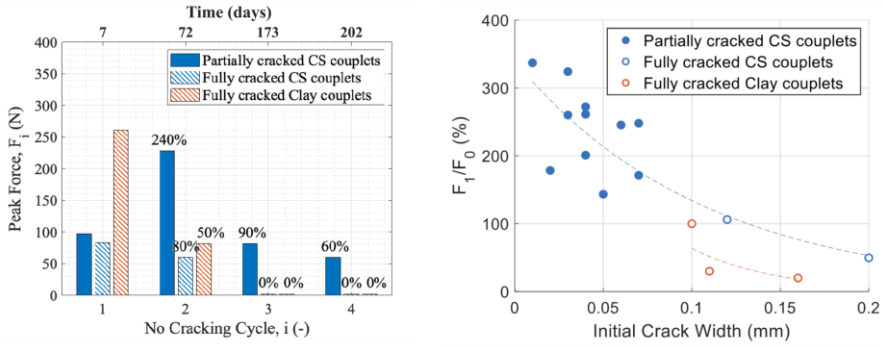


Figure 2-10 (a) Peak force after successive crack–healing cycles for calcium silicate and clay couplets. (b) Healing efficiency as a function of initial crack width for specimens tested after the first healing period.

(Figure 2-10 (a)), likely due to nutrient depletion. This highlights the role of the agent dosage to match the expected damage conditions.

The agent performed effectively across both brick types, demonstrating broad applicability despite their differing porosity and surface roughness. However, performance varied according to brick type and curing regime: calcium silicate bricks exhibited superior healing efficacy under high humidity, while more porous clay bricks performed better under wet–dry cycles. This is mainly attributed to brick porosity, which mediates the interaction between the environment and the crack, thereby exerting a strong influence on the local conditions near the crack. This result highlights the importance of identifying suitable healing conditions prior application of the strategy based on the materials used.

As in concrete, the presence of the agent, even when inactive, affected the material's properties, with masonry bond strength at 28, 56, and 98 days consistently higher than in the reference specimens. This finding underlines the importance of investigating the agent's effect on mortar functional properties and its constituents to ensure the correct application of the strategy.

2.5.3 Integrating PLA-based agent into cement-lime masonry mortars: early insights

Building on the promising results obtained with the commercial PLA-based mortar described above, a second pilot study explored the integration of the healing agent into a more porous, lime-rich matrix, more compatible with the built heritage. The aim was to assess its healing potential for repairing induced cracks in small-scale masonry couplets (Gaggero et al. 2025).

The testing programme used a pre-bagged cement–lime mortar (1:2:9 ratio) with three agent dosages: 0% (reference), 5%, and 15% by binder mass. Couplets were built

using solid clay bricks and tested with a force-controlled bond wrench setup. Damage was induced at 7 days, followed by a 30-day healing period under wet–dry cycles.

Results confirmed that the self-healing agent influenced masonry bond properties, improving initial bond strength: mortars with 5% and 15% agent content achieved values up to 4.5 times higher than the reference at 7 days, with no significant difference between the two dosages (Figure 2-11 (a)). After healing, only samples containing the agent showed partial strength recovery, while all references remained completely separated (Figure 2-11 (b)). However, surface leaching, likely due to calcium lactate migration within the porous lime matrix, was observed, indicating the need to optimise curing environments (Figure 2-11 (c)(d)).

From this study, no clear evidence of agent activation was detected under the applied conditions, highlighting the importance of understanding the interaction between the healing environment, the lime-rich matrix, and the porous clay bricks. These findings emphasise the need to tailor curing regimes to the specific brick–mortar system, as well as the need for a coherent framework to assess healing performance for traditional masonry applications.

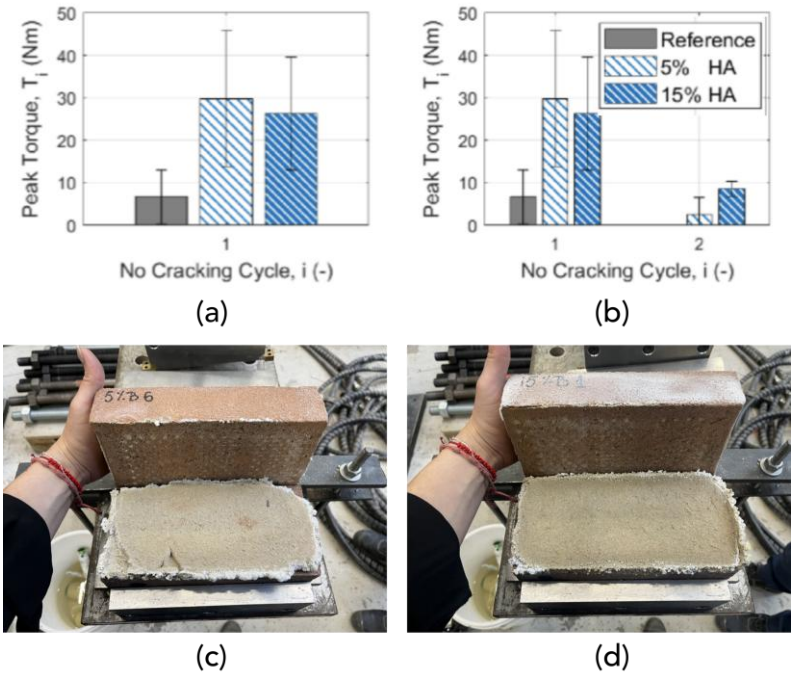


Figure 2-11 (a) Peak torque for reference and agent-containing measured at (a) 7 days (before cracking) and (b) at 7 days (No cracking cycle = 1) and after a 30-day healing period under wet–dry cycles (No cracking cycle = 2). (c)(d) Visual evidence of surface leaching observed on

2.6 Conclusions

This chapter aims to lay the groundwork for exploring self-healing mortars as a repair strategy for masonry. It begins by revisiting the materials historically employed, and the various deterioration mechanisms to which these systems are inherently susceptible. Repointing is considered next, grounded in the design principle that damage should concentrate in the mortar joints, which can be periodically replaced throughout a building's service life. While this logic enables effective maintenance the approach is not fully efficient and does not entirely align with conservation principles such as minimal intervention and long-term sustainability. In this regard, the field of masonry could benefit from a similar evolution to that seen in concrete technology, where the development of self-healing materials has redefined maintenance and durability practices. Although research has recently begun to explore the applicability of self-healing materials to masonry, the field is still at an early stage, with only a few experimental pilot studies conducted to date.

The literature on self-healing concrete constitutes a robust foundation for research to build upon, through devising new approaches, adapting established ones to masonry, or directly applying them. For instance, the chemistry of a commercialised PLA-based agent aligns with the hardening of both non-hydraulic and hydraulic lime mortars, suggesting strong theoretical compatibility that may even surpass performance observed in cement systems. Since the bacterial by-product is $CaCO_3$, the principal binding phase in carbonated lime mortars, material compatibility (chemical, physical, and mechanical) should be met. In addition, CO_2 generated by bacterial metabolism could accelerate autogenous healing through carbonation deeper within cracks, potentially enabling a degree of mechanical restoration not verified in cement-based systems (where C–S–H is the primary binding phase, significantly stronger than $CaCO_3$). It could therefore be expected that the implementation of the agent would lead to massive precipitation, restoring watertightness in all lime mortars. Mechanical recovery may also occur, likely to a greater extent in air lime mortars than in hydraulic limes, where the presence of C–S–H phases results in higher intrinsic mechanical properties. This compatibility and material performance, however, still require targeted verification.

Proceeding along this line, pilot studies with the PLA-based agent in masonry couplets have shown promise while exposing clear research gaps. Beyond implementation in lime-based mortars, future research should prioritise: (i) establishing suitable healing conditions based on the substrate and mortar used, (ii) verifying watertightness recovery, paramount for durability, in addition to mechanical and aesthetic recovery; (iii) verifying proper functioning of the healing mechanism by characterising precipitate nature; and (iv) quantifying the agent's impact on material properties to ensure compatibility and appropriate use in conservation practice.

Before exploring these aspects, however, it is opportune to draw on the lessons from self-healing concrete and prioritise the development of a framework for evaluating this nascent strategy in masonry. This is essential given the complexity of both the self-healing material itself and its application as a repair strategy, with numerous interdependent variables that must be understood to ensure proper performance and practical implementation. Beyond providing a structured basis for assessment, it would facilitate comparison and reproducibility. The following chapter addresses this task, proposing an initial draft of such a framework.

Chapter 3

A framework for assessing bio-based self-healing performance for masonry repair

The previous chapter established the basis for applying self-healing mortars in masonry repair, highlighting the promise of the technology and the limited research conducted so far. Existing pilot studies, mainly focused on aesthetic and mechanical recovery of brick–mortar specimens, confirmed its feasibility but also highlighted key knowledge gaps. The decisive influence of healing conditions calls for a better understanding of healing products, while watertightness recovery, crucial for durability, remains unaddressed. These encouraging, yet preliminary findings underline the need for a structured approach to guide research systematically and comprehensively.

Building on these considerations, this chapter proposes a structured framework for assessing self-healing mortars in masonry repair. Inspired by methodologies developed for biogenic concrete, the framework is adapted to the specific features and requirements of masonry, integrating both the principles of self-healing materials and the practical constraints of repointing interventions. Section 3.1 presents the overall structure of the framework, introducing three core aspects (recovery of performance, identification of healing products, and impact on functional properties) and showing how these can be assessed across different masonry levels: mortar, brick–mortar, and masonry component. Sections 3.2–3.4 then address each aspect in depth, providing practical guidance and outlining relevant testing methods. The chapter concludes with Section 3.5, offering a concise summary of the framework and a preview of its practical application in the remainder of this thesis, where it is used to evaluate the performance of a PLA-based bacterial healing agent.

3.1 Framework structure

The study of self-healing mortars for masonry repair requires a structured approach that integrates the requirements of compatible repair with the principles of self-healing materials. Investigating this strategy therefore requires making several methodological choices, including what parameters to evaluate, which tests to perform, and under which conditions. To support these choices, this chapter proposes a framework that organises the assessment of self-healing mortars in a systematic manner.

The structure of the framework builds upon the evaluation principles introduced by Tziviloglou (Tziviloglou 2018) and Rossi (Rossi 2022) for biogenic concrete, which distinguish three core dimensions of analysis:

- Recovery of performance, quantifying whether, to what extent, and under which conditions the material autonomously regains the functions compromised by damage.
- Identification of healing products, verifying the mineralogical nature and (where possible) the biogenic nature of the precipitates to confirm the proper operation of the healing mechanism.
- Impact on functional properties, assessing how the agent affects relevant physical and mechanical properties that govern compatibility between original and repair mortar, and, therefore, applicability.

Although these principles stem from the field of biogenic concrete, their structure and objectives can be effectively transposed to masonry repair, provided that the characteristics of masonry systems are taken into account. In doing so, it is convenient to consider the composite nature of masonry and structure the analysis across different levels. This approach allows healing-related variables to be first investigated in a more manageable way in smaller specimens, before verifying their relevance in larger specimens.

Accordingly, the proposed framework is organised into three material levels, characterised by increasing specimen size:

- Mortar level: this level provides controlled conditions to verify the functioning of the healing agent within the mortar and to identify suitable healing conditions. The development and evaluation of new healing agents is commonly conducted at this level.
- Brick–mortar level: this level introduces the interface between the mortar and the bricks, allowing the investigation of interfacial cracking. The presence of the brick makes the porosity closer to that of masonry, so the most suitable healing environment, identified at mortar level, can be verified.

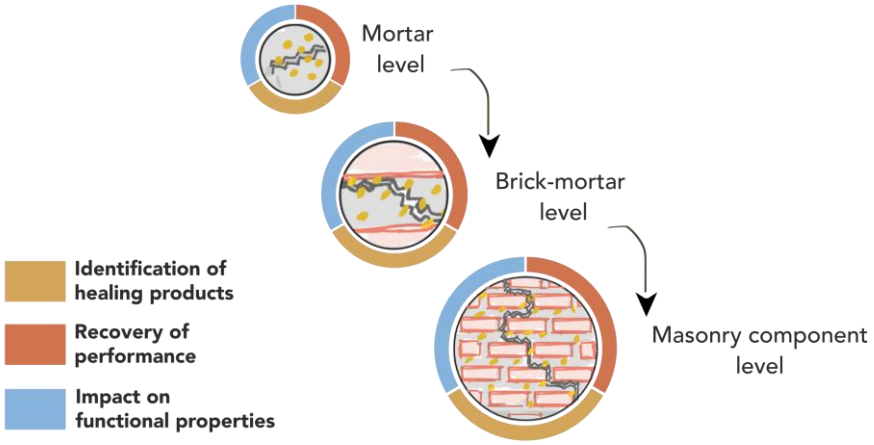


Figure 3-1 Evaluation dimensions (Recovery, Identification, and Impact) applied across the mortar, brick–mortar, and masonry levels.

- Masonry component level: this level uses larger specimens placing multiple bricks in a certain bond pattern, therefore bringing closer to real composite masonry. Crack patterns become more representative of actual masonry damage, and exposure to the healing environment is no longer uniform (as in small-scale specimens) but limited to external faces. This level allows linking the recovery observed at the previous levels (mortar and brick-mortar) to the recovery of the component.

By progressively increasing level, the framework allows early-stage verification to be carried out on simpler configurations, where controlled tests can be carried out on a larger number of smaller specimens. Once the healing agent has been validated at the mortar level, the complexity is gradually increased by extending the investigation to brick–mortar specimens and, subsequently, to masonry components, verifying at each stage whether the observed effects are maintained. The progression across these levels and the associated performance criteria are schematically illustrated in Figure 2-2.

In the following sections, each of the three dimensions introduced above is explored in greater detail.

3.2 Recovery of performance

Self-healing mortars are designed to autonomously recover the performance of the material once degradation has reduced it. Measuring this recovery is therefore the first logical step in evaluating the effectiveness of the strategy. It also serves as a prerequisite for subsequent analyses: without measurable recovery, there is no basis to examine the healing products or assess the influence of the agent.

Verifying whether this recovery occurs, requires a systematic approach involving several steps:

I. Define performance: identify the functional aspects to be recovered and select properties that can adequately quantify it.
II. Establish reference values: measure the chosen property in the intact material.
III. Introduce controlled damage: define the method, timing, and extent of the induced damage.
IV. Specify the healing conditions: determine conditions such as humidity, temperature, and exposure duration.
V. Measure recovery: repeat the property measurement and compare it with the reference value to evaluate the level of recovery.

In the following sections, the recovery of performance is examined in detail, including how performance is defined and measured, how damage is introduced and controlled, and under which healing conditions recovery can be expected. These aspects are considered across the different material levels introduced in the framework: mortar, brick–mortar, and masonry component.

3.2.1 Performance definition and measurable properties

Performance refers to the set of functions that damage compromises and therefore is correlated to the consequences of the targeted damage. In the context of this thesis, repairing masonry with self-healing mortars, the targeted damage develops gradually within the mortar joints or at the brick-mortar interface (typically through cracking) and compromises three key aspects of the material: (i) aesthetic appearance, (ii) watertightness, and (iii) mechanical performance. Accordingly, recovery of performance can be evaluated through the recovery of these three aspects. Within each dimension, it is essential to define measurable properties that can be monitored over time and to select appropriate tests capable of quantifying them.

Although the term self-healing is often used broadly to encompass recovery across all these dimensions, this thesis distinguishes between self-sealing and self-healing. Self-sealing refers to crack filling sufficient to reduce fluid ingress and restore barrier properties without necessarily re-establishing mechanical continuity. Self-healing requires in-depth crack filling and rebonding of the fractured surfaces, resulting in the recovery of mechanical properties such as strength. Consequently, superficial crack filling may provide a visual indication of self-sealing but does not demonstrate it, as watertightness recovery requires sufficiently continuous filling by low-solubility products. Moreover, neither superficial crack closure nor restored watertightness provides evidence of mechanical self-healing. This distinction underpins the definitions of performance recovery presented below.

Recovery of aesthetics involves the superficial filling of cracks, which re-established the visual continuity of the material. It can be documented with fixed or portable microscopes or with high-resolution cameras, depending on the sample size, taken before (Figure 3-2 (a)) and after (Figure 3-2 (b)) the healing period. The resulting images can be analysed qualitatively or quantitatively; in the latter case, threshold-based image analysis allows detecting the cracked area before and after healing and quantifying its reduction as a measure of recovery. The black-and-white areas in Figure 3-2 (a)(b) illustrate the binary images obtained through this process. Beyond quantifying aesthetic restoration, observing the superficial filling of cracks provides valuable insight into how healing progresses and how it relates to other performance aspects. For instance, surface filling can be correlated with the recovery of watertightness and therefore provide evidence of self-sealing, while it may also offer indications of mechanical self-healing. In the latter case, such indications are only partial, since superficial closure does not guarantee that cracks are filled in depth and thus cannot be considered evidence of mechanical restoration. Since both autogenous and bacteria-induced healing typically progress from the surface inward (Section 2.4.1), verifying complete filling requires complementing surface observations with observations of the crack interior. In studies on self-healing concrete, crack interior observations are commonly performed on transversal sections using optical or electron microscopy, which allow the presence, morphology, and continuity of healing products to be assessed. However, this approach involves cutting the specimens after the healing period, which can be particularly challenging when dealing with weak lime mortars and is inherently destructive, preventing the reuse of the same specimens for further testing. A non-destructive alternative is provided by X-ray computed tomography (X-ray CT), which allows crack filling to be assessed in depth without cutting the specimen. Nevertheless, phase discrimination remains challenging, as healing products and matrix exhibit similar density and atomic composition. Before–after scan subtraction has been proposed to address this limitation (Wang et al. 2014).

Superficial crack filling is therefore the primary indicator of aesthetic restoration, but it also serves to monitor healing progress. Consistent with previous studies on self-healing concrete and masonry, aesthetic recovery cab be assessed on the same

specimens used for watertightness and mechanical recovery, as this assessment is non-destructive and allows the specimens to be reused for subsequent tests.

Recovery of watertightness, corresponding to self-sealing, occurs through superficial crack filling with low-solubility precipitates that seal the openings and interrupt the pathways for water ingress. This regained impermeability is a key aspect of durability, since water acts as the main driver of many chemical and physical deterioration mechanisms in masonry (Section 2.2). Watertightness recovery can be quantified through parameters that describe the material's ability to resist water flow or penetration (water permeability coefficient, the rate or depth of water penetration, or the time to leakage). Experimental methods to evaluate these parameters in masonry, however, remain limited. ASTM (ASTM E514/E514M-20 2020) provides laboratory procedures to evaluate water penetration in full-scale masonry panels exposed to simulated wind-driven rain, while more recent studies have proposed simplified approaches. For instance, (Kahangi Shahreza 2024) tested three-course prisms (≈250 × 218 × 120 mm) with artificial cracks subjected to continuous water spray, demonstrating that the method can capture the influence of crack width and repointing on water penetration. However, both methods depend on specialized equipment and relatively large specimens, which makes them impractical for early-stage studies where simplified and more controllable setups are preferable. One possible alternative is the Karsten pipe method, or simply the pipe method (RILEM TC 25-PEM 1980; CEN 2013; ASTM E2167-01 2008), which measures local water absorption on the exposed surface by monitoring the drop in water level within a sealed tube over time. Despite its simplicity, the Karsten pipe method is highly sensitive to surface irregularities and sealing quality, which may limit reproducibility and comparability. This is particularly relevant for self-healing assessment, as repeated measurements require the pipe to be attached to and removed from the same surface at different testing stages, potentially introducing variations in the sealing conditions.

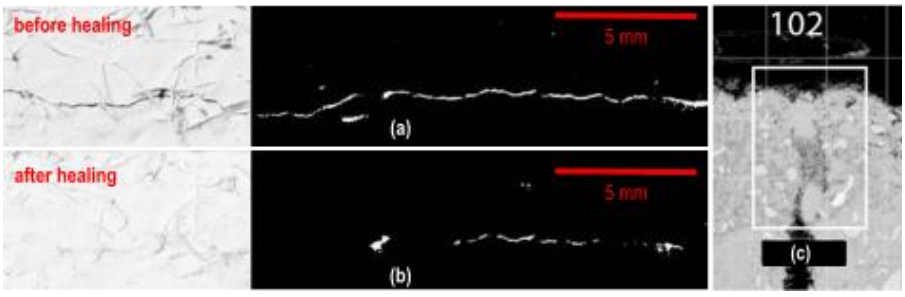


Figure 3-2 Surface images of a masonry couplet (a) before and (b) after healing, with threshold analysis used to quantify crack closure (Gaggero et al. 2024); (c) ESEM cross-section of a ~100 µm crack in a cement-based dog-bone shaped specimen after 8 weeks in a mist room, showing healing products forming from the exterior towards the crack interior (He et al. 2023).

Adapting pressure-based water permeability tests, as commonly used for concrete, to masonry cores represents a promising yet unexplored direction. This approach could also be combined with subsequent shear testing, allowing both watertightness and mechanical recovery to be assessed. Regardless of whether the Karsten pipe method, a pressure-based permeability test, or a combination of both is used, the brick–mortar level appears to be the most suitable for investigating watertightness recovery. It captures crack development both within the mortar and along the brick–mortar interface while still allowing the use of relatively small specimens. Once the relationship between crack sealing and watertightness recovery is established at this level, aesthetic recovery may be considered a qualitative or indirect indication of sealing efficiency at larger scales.

Recovery of mechanical performance, corresponding to self-healing, involves the in-depth filling of cracks and rebonding of fractured surfaces, restoring the material's ability to resist loads and transfer (tensile and shear) stresses. Mechanical recovery prevents the easy re-opening of cracks and limits the propagation of damage within the structure, thereby mitigating potential structural consequences. Mechanical recovery can be quantified through parameters that describe the ability of the material to resist and transfer stresses, such as stiffness, strength, and toughness. Tensile and shear stresses, in particular, are the critical ones as they govern joint failure within the mortar or along the brick–mortar interface. To assess the effects of self-healing, it is therefore appropriate to first investigate recovery under these individual loading conditions, where controlled cracking and healing can be more reliably evaluated.

Tensile loading results in joint opening, while shear loading produces sliding accompanied by friction. Of the two, tensile failure offers the clearest indication of healing capacity, as it directly reflects the recovery of cohesion between the crack faces. This behaviour can be investigated either directly, through direct tension tests, or indirectly, through bending tests. Given the complexity of the former and the practicality of the latter, bending tests are generally preferred. Under displacement control, bending tests allow cracks to be introduced in a consistent and repeatable manner without reaching complete failure, enabling their subsequent recovery to be monitored after healing. This aspect is of fundamental importance, as crack dimensions have a strong influence on healing performance (the reader is referred to Section 3.2.2 for further details). In addition, such controlled tests can be performed at the three different levels considered in this work (Figure 3-3): at the mortar and masonry component level through three- or four-point bending tests, and at the brick–mortar level through bond wrench tests (Gaggero and Esposito 2023). In all cases, crack formation is controlled by performing the tests under crack mouth opening displacement (CMOD) control.

Investigating these different levels serves two main purposes. First, the mechanical behaviour of masonry depends on the properties of its constituents: brick, mortar, and the brick–mortar interface; therefore, the overall recovery of mechanical performance is influenced by the recovery of each constituent, particularly the mortar and the brick-mortar interface. Second, starting from simpler cases and smaller specimens allows testing a larger number of samples in the early stages of research, when the optimal healing environment still needs to be identified. Once recovery under individual loading conditions is confirmed, more complex loading scenarios can be investigated to understand how tensile, shear, and compressive stresses interact in the healing process.

Investigating the recovery of all performance aspects requires controlled damage induction and the definition of appropriate healing conditions. Since both strongly influence the reproducibility and extent of recovery, they are discussed in detail in the following sections.

3.2.2 Controlled damage induction

The evaluation of self-healing requires the introduction of damage that is both controlled and reproducible, ensuring that the subsequent recovery can be quantified and compared across specimens. Three aspects are particularly important in this regard: (i) the method used to induce the damage, which should allow controlled formation of cracks both within the mortar and along the brick–mortar interface; (ii) the timing of damage introduction, which affects the relative contribution of autogenous and autonomous healing; and (iii) the extent of the induced damage, as healing efficiency depends strongly on crack width. Each of these factors must therefore be carefully defined to ensure that the measured recovery reflects the self-healing potential of the material.

Cracks can be introduced either through mechanical testing or artificially, by creating controlled cuts. Other approaches, such as inserting strips during casting and removing them after hardening, are generally unsuitable for self-healing studies, since most healing

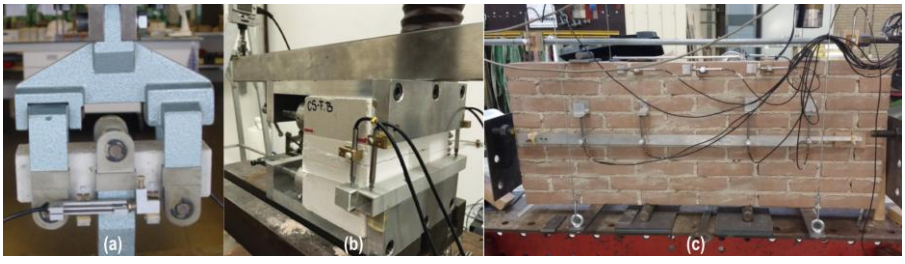


Figure 3-3 Examples of CMOD-controlled bending test configurations at the three material levels: (a) mortar prism under three-point bending (De Rooij et al. 2013); (b) brick–mortar couplet tested through a bond-wrench setup (Gaggero and Esposito 2023); (c) masonry spandrel tested under four-point bending (Korswagen et al. 2019).

agents require the rupture of their carrier system to enable the release of the agent. Mechanical testing allows the reproduction of realistic stress conditions and the formation of crack morphologies closer to those found in practice. Among the options available at the considered levels (mortar, brick–mortar, and component), tensile, shear, and bending tests can be employed. However, as discussed in Section 3.2.1, bending tests allow a better control of crack initiation and propagation, and are therefore preferred for inducing cracks of measurable width. While tensile tests were discussed above, in shear tests the imposed displacement primarily governs crack sliding rather than crack opening, increasing the difficulty of avoiding full detachment. Uncontrolled crack opening or loading until failure hinders the reassembly of the fractured specimen, leading to wide and irregular fractures that are not representative of the damage levels typically addressed by self-healing strategies. Nevertheless, the exclusive use of bending tests constrains the geometry and size of the specimens, which may limit their applicability for certain evaluations, such as watertightness. As an alternative, cracks can be produced by cutting the specimen and inserting spacers of controlled thickness (widely used for concrete). This method allows for uniform and measurable crack widths, but the resulting cracks lack the irregular and tortuous morphology typical of real damage. Moreover, for soft lime-based mortars, the cutting process may damage the specimen and performing precise cuts along the brick–mortar interface also remains technically challenging. Nevertheless, this approach could be further explored for specimen configurations not compatible with bending tests, such as those used for assessing watertightness.

The timing of damage introduction also plays a crucial role: as in specimens damaged at earlier ages, a greater contribution of autogenous healing can be expected. In the case of cement-based mortars, it is generally established that tests should be performed after 28 days, ensuring that most of the cement has hydrated. Lime-based mortars, however, require a longer curing period before testing, due to the slower carbonation process that (fully or partially) governs their hardening. If tests are carried out too early, a considerable amount of free lime may still be present and, given its high solubility, can migrate toward the crack, resulting in crack filling unrelated to the healing agent. Moreover, the recovery of strength would not reflect the full maturity of the material, as the mortar strength is still developing. This introduces a time-dependent contribution that must be accounted for, for instance by testing undamaged specimens in parallel. To reduce the total number of specimens, plain reference ones are typically preferred, allowing autogenous healing to be quantified. These samples are also useful for characterizing the healing products, as explained in Section 3.3. Where possible, the appropriate testing age can be established through preliminary trials (e.g., at 28, 60, 90, and 120 days). Otherwise, as a general guideline, 28 days are suitable for cement-based

or cement–lime mortars (with lime <30% of the binder), around 90 days for lime–pozzolana mortars, and at least 12 months for pure lime mortars.

Finally, the extent of cracking plays a role on the healing performance of the material. Beyond the existence of a maximum crack width that the material can effectively heal, smaller cracks tend to heal faster and reach a higher degree of recovery within the same healing period than larger ones. To allow meaningful comparison of performance recovery across different properties and studies, it is therefore advisable to maintain fixed criteria for both crack width and healing time. Defining the target crack width is, however, not straightforward and, considering its correlation with healing time, selecting smaller cracks could be a reasonable strategy to reduce testing durations. As a practical recommendation, crack widths between approximately 100 µm and 1 mm may be considered suitable, as cracks around 100 µm correspond to just-visible light damage, whereas widths up to about 1 mm fall within the range of easily observable and easily repairable light damage (Korswagen 2024). Beyond this interval, damage becomes more costly to repair: a condition that the strategy seeks to prevent by autonomously intervening before crack propagation reaches this stage. In addition, the effectiveness of self-healing mortars tends to decline, as the material approaches its maximum healable crack width; for the poly-lactic acid agent used in this thesis, literature indicates an upper limit of approximately 800 µm.

3.2.3 Healing conditions

Healing efficiency in bacteria-based self-healing mortars strongly depends on the environmental conditions and duration of exposure during the recovery period. These factors control whether bacterial activity can be activated and sustained, and to what extent healing products can form and remain stable. Among other parameters, humidity plays a decisive role in promoting calcium carbonate precipitation and in maintaining bacterial viability within the mortar.

In the literature on bacteria-based self-healing concrete, particularly those employing aerobic bacteria, the presence of both oxygen and water is identified as essential for healing activation (e.g. (Mors and Jonkers 2017; Cappellesso et al. 2023)). Water enables calcium ion dissolution, nutrient transport and bacterial activation, while oxygen supports bacterial metabolism. For this reason, three main exposure regimes are most frequently investigated in the literature to assess healing in biogenic concrete: wet–dry cycles, continuously humid conditions (20°C, RH>95%), and water submersion. Given, however, the higher porosity and water absorption of masonry (lime mortars and bricks) with respect to concrete samples, continuous submersion can be excluded, as it may lead to excessive water uptake and hinder oxygen availability. Instead, a slightly less humid environment (e.g. 80% RH) can be advantageous, providing sufficient moisture for bacterial activity while maintaining air access. Therefore, wet–dry cycles, humid

conditions, and a less humid environment (≈80% RH) are recommended as starting points to assess suitable healing environments for the masonry materials considered. Analyses under different exposure conditions should first be conducted at the mortar level, where smaller specimens allow a larger test set, and subsequently confirmed at the brick–mortar level to account for the influence of the brick substrate. Finally, verification at the masonry component level is also necessary, as the exposure of the specimen changes with the scales: unlike smaller samples, where all faces are directly subjected to the healing environment, only the external surfaces of masonry components (and especially the mortar joint) are exposed, which can significantly affect moisture distribution and, consequently, the overall healing process.

The healing time is another key parameter in the evaluation of self-healing mortars, as it defines the duration over which recovery processes can occur. It is inherently correlated with crack width, since wider cracks generally require longer exposure periods to achieve comparable degrees of filling or performance recovery. Despite its importance, no consensus exists in the literature regarding the healing time to be adopted when assessing the efficiency of bacteria-based self-healing materials. Reported studies show considerable variation, with crack widths ranging from 250 to 970 µm and healing periods spanning from approximately 50 to over 100 days, without a consistent relationship between these two parameters. For instance, cracks of about 250 µm were in some cases monitored for up to 70 days, whereas cracks approaching 970 µm were healed for only 56 days. In most studies involving the PLA-based bacterial agent used in this work, a healing period of 56 days is adopted, which can thus be considered a lower reference limit for the evaluation of performance recovery. However, conducting tests with different healing durations remains advisable to investigate the influence of exposure time on the extent and rate of healing, and to identify potential trends in the evolution of recovery under prolonged exposure.

3.3 Identification of healing products

Identifying the products formed inside the cracks or at their surface is essential to verify the proper functioning of the healing agent within the system considered (masonry, concrete). The mere observation of performance recovery does not provide sufficient evidence that the agent is operating as intended, as it may also result from other processes, such as autogenous healing or agent-derived compounds that block the crack without triggering the designed healing mechanism (the reader is referred to Section 2.5.3 for an example). Verifying the proper functioning of the agent under analysis is therefore essential to justify its application.

The aim is therefore to verify that the healing products have the expected mineral composition and originate from the designed mechanism, namely bacterial activity in the

case of bacteria-based agents. A range of techniques, including Optical Microscopy (OM), Scanning Electron Microscopy (SEM) or Environmental Scanning Electron Microscopy (ESEM), X-ray Diffraction (XRD), Raman spectroscopy, and Fourier-Transform Infrared Spectroscopy (FT-IR or FTIR), have been predominantly employed in the concrete field to characterize the mineral composition of the precipitates (Çopuroğlu et al. 2013). Among these, ESEM and FTIR may also provide indirect evidence of bacterial activity, since bacterially induced calcite is not identical to purely inorganic calcite: it may display distinctive crystal morphologies (observable with SEM/ESEM) or contain occluded organic matter detectable by FTIR and Thermogravimetric Analysis (TGA). However, it is worth emphasizing that such bacterial evidence is difficult to detect and usually requires the analysis of a considerable number of samples. This could be related to the prevalence of indirect carbonation mechanisms, whereby bacterially produced CO_2 reacts with portlandite in the matrix, yielding $CaCO_3$ precipitates that may not display distinctive biogenic signatures.

One possible way to address this challenge is to complement the characterization of precipitates with direct measurements of bacterial activity. For instance, in the case of aerobic bacteria, Wiktor et al. (Wiktor and Jonkers 2011) monitored oxygen consumption in an alkaline buffer solution simulating the concrete environment, using optical oxygen microsensors to quantify bacterial activity. However, such oxygen sensors measure dissolved oxygen and can therefore only operate in fully saturated environments and are thus unsuitable for mortar or masonry specimens and more realistic conditions. Therefore, it is good practice to include reference samples and compare them with agent-containing counterparts, so that differences in the quantity of precipitates can serve as an indirect indication of bacterial activity. Reference samples are in any case required to evaluate the effect of the agent on the functional properties of the system (see Section 3.4) and can thus serve a dual purpose. Once the mineral composition is confirmed, visual comparisons of the extent of precipitation between the two sets of samples can provide an indirect indication of bacterial enhancement. It is therefore advisable to employ methods that allow both the identification of the mineralogical composition and, where possible, indirect evidence of bacterial activity, so that a double confirmation of the agent's functioning can be obtained.

Among the techniques employed in self-healing studies, microscopy (whether optical or electron-based) is among the most widely used, both to observe the extent of precipitation (as explained in Section 3.2.1) and to characterize the healing products. While surface observations can only provide indications of aesthetic restoration and the overall healing process (Figure 3-4 (a)), the examination of thin sections allows following the process inside the crack and identifying the minerals formed (Figure 3-4 (b)). Comparable information can also be obtained from cross-sections observed with ESEM (Figure 3-4 (b)), where backscattered electron (BSE) imaging, combined with energy-

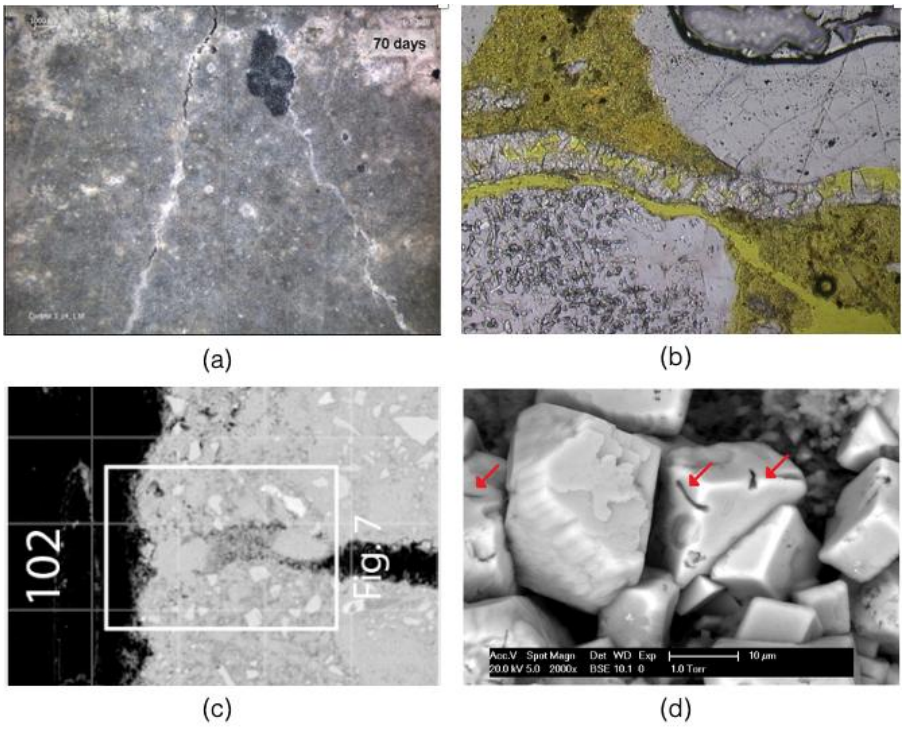


Figure 3-4 (a) Stereomicroscopic view of crack healing on the surface of bacterial concrete (Wiktor et al 2011); (b) Plane-polarized thin-section view of a crack filled with re-precipitated $CaCO_3$ (Lubelli et al 2011); (c) ESEM cross-section of a ~100 µm crack after 8 weeks in mist room showing healing products sealing the crack (He S 2025); (d) ESEM image of crack-surface precipitates after healing; arrows indicate possible bacterial imprints (Tziviloglou et al. 2015).

dispersive X-ray spectroscopy (EDS) mapping provides insight into both the morphology and chemical composition of the precipitates. In addition, scrapings from healed cracks may be examined to further characterize crystal morphology and, reveal traces of bacterial activity such as surface imprints (Figure 3-4 (d)). It should be noted, however, that preparing polished thin sections and cross-sections is a demanding task requiring specialized expertise, and that ESEM instrumentation is not widely accessible, which may restrict the broader use of this approach. In lime mortars, the high porosity and fragile nature of the matrix make the process especially delicate, while in larger specimens such as masonry couplets the heterogeneity of mortar and brick renders thin-section preparation considerably more challenging.

Compared to microscopy, FT-IR spectroscopy offers a much simpler alternative, as it requires only very small amounts of material and almost no sample preparation. It is a chemical technique used to identify many types of organic and inorganic compounds by measuring how they absorb infrared light. As a result, FTIR has become a common tool

to study healing products in self-healing concrete and has more recently been extended to lime-based mortars, including efforts to detect bacterial activity. Giordano (Giordano 2025) has shown that calcium carbonate precipitating bacteria mediate the formation of calcite crystals through metabolically derived organics. These organics influence crystal orientation and remain occluded within the $CaCO_3$ lattice, producing additional absorption bands (e.g. 950–1150, 1190–1350 and 1500–1700 cm^{-1}). Given the low proportion of organics relative to the total carbonate mass, such signatures can be difficult to detect and may require a large number of samples. However, even when bacterial organics are not identified, FTIR remains a powerful tool for characterizing the mineralogical composition of healing products. For example, FTIR spectra reported by Jonkers et al. (Wiktor and Jonkers 2011), obtained from material scraped from healed cracks in cement-based specimens containing bacterial healing agents, revealed the presence of calcium carbonate polymorphs. In their study, calcite was identified by the characteristic carbonate bands corresponding to the C–O asymmetric stretching vibration (ν_3), the out-of-plane bending vibration (ν_2), and the planar bending vibration (ν_4), cantered at approximately 1390, 871 and 712 cm^{-1}, respectively. In addition, spectral features associated with aragonite were observed in some bacterial samples, including broadening of the ν_3 band in the 1500–1300 cm^{-1} region, the appearance of the symmetric stretching vibration ν_1 (1040–1120 cm^{-1}), and splitting of the ν_2 and ν_4 bands. As noted by Navarro et al. (Rodriguez-Navarro et al. 2023), calcite is the stable end-product of carbonation, usually preceded by metastable phases such as vaterite and aragonite, following the Ostwald rule of stages (vaterite → aragonite → calcite). All three polymorphs, however, are also widely reported in the literature as products of bacterial mineralization (Wei et al. 2015). The detection of these phases in healed cracks of bacterial samples, together with the very limited precipitation occurred in the reference specimens, suggests early-stage carbonation and bacterial activity, in line with the mechanism of the healing agent. A further advantage of FTIR is that it can be applied to larger specimens without the demanding preparation required by microscopy, making it particularly useful in masonry contexts. Nonetheless, its combination with complementary approaches remains desirable to achieve a more conclusive identification.

3.4 Impact on functional properties

Once the healing agent has been verified in terms of performance recovery and identification of healing products, the final step is to evaluate its impact on the functional properties. This evaluation encompasses both the individual constituents (mortar and brick-mortar level) and the composite material (masonry component level), whose overall behaviour inevitably depends on the former. This step is essential to determine the

practical feasibility of the self-healing agent. In fact, effectiveness alone does not guarantee applicability: if the agent modifies essential properties such as workability, setting time, or strength development in a bad or incompatible way, it becomes unsuitable for practical use. Moreover, ensuring compatibility with the existing masonry remains a key requirement in conservation practice. Understanding how the healing agent affects the physical and mechanical properties masonry is therefore essential to guarantee its suitability for heritage repair.

For this purpose, both physical and mechanical properties must be examined on plain reference samples and on samples containing the healing agent, across the different levels. At the mortar level, relevant parameters include workability, elastic modulus, and compressive strength, flexural strength and porosity. While porosity-related properties can be initially estimated using standard mortar bars (e.g., through water immersion tests), these do not reflect those of the actual masonry as the influence of the brick is not considered. The substrate's suction alters the water-binder ratio at the interface, modifying the pore structure. Therefore, a more accurate characterization requires moving to the brick–mortar level, either by casting mortar specimens against bricks using a permeable filter in between or by performing MIP on mortar fragments extracted directly from masonry samples. The effect of the agent on key porosity parameters of the mortar include total porosity, pore size distribution, water absorption by capillarity, and vapour transport. In addition, the mechanical characterisation at this level should focus on the bond capacity between mortar and brick, evaluated in tension (commonly through flexural testing) and in shear. Finally, at the masonry component level, the mechanical response can be characterized through compression and flexural tests (e.g., three- or four-point bending, in-plane or out-of-plane).

Some of the specimens tested to evaluate these effects can also be used to verify the mechanical recovery, allowing a more efficient experimental design and reducing the overall number of samples required across the different levels.

3.5 Summary and implementation within this thesis

This chapter proposed a structured framework for assessing self-healing mortars for masonry repair, building upon methodologies developed for bio-concrete and adapting them to the specific characteristics of masonry. The framework adheres to the same three dimensions, namely recovery of performance, identification of healing products, and impact on functional properties, but translates them into the masonry context through three corresponding material levels: mortar, brick–mortar interface, and masonry component (Figure 3-5). This structure allows the different aspects of self-healing to be explored in a progressive and interrelated manner, while accounting for the composite nature of masonry.

At the mortar level, the framework supports controlled testing on small specimens, enabling the identification of suitable healing environments. Once these conditions have been established, the brick–mortar level serves as an intermediate step where healing can be verified also at the brick-mortar interface and under more realistic hygric constraints. Finally, the component level extends the investigation to larger specimens, where cracks and exposure conditions are more representative for existing masonry constructions. In this way, the framework provides both a methodological structure and a practical roadmap for designing and conducting the experiments. It facilitates comparability across studies and supports the identification of key influencing parameters (such as crack width, healing time, and exposure regime).

Table 2-1summarises the comprehensive set of tests and variables identified as suitable for each material level. The entries reported in italic correspond to those specifically explored in the next chapters of this thesis through the experimental study of the selected poly-lactic acid self-healing agent. A detailed description of the selected methods, including experimental setups and procedures, is provided in Chapters 4, 5, and 6, where the proposed framework is applied at the mortar, brick-mortar and masonry component level respectively.

The selection of methods for the experimental chapters was guided by a hierarchy of research objectives and by practical feasibility constraints. Priority was given to the recovery of performance, as the demonstration of measurable healing is a prerequisite for any further assessment. Accordingly, flexural tests (including three-point bending and bond wrench tests) were adopted across all material levels to induce damage and to

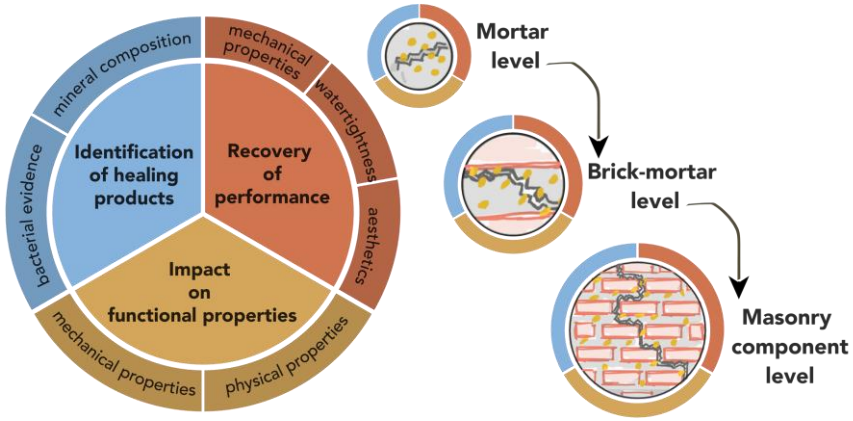


Figure 3-5 Overview of the framework proposed to assess the performance of self-healing mortars in masonry repair. The approach adheres to the three analytical dimensions defined for bio-concrete, namely recovery of performance, identification of healing products, and impact on functional properties, and translates them into the context of masonry through three corresponding material levels: mortar, brick–mortar, and component.

assess both mechanical and aesthetic recovery. These tests allow controlled crack initiation and propagation, which is essential for monitoring healing evolution in a reproducible manner. With respect to watertightness recovery, standardised methods such as the Karsten pipe method are available for assessing local water absorption in masonry. However, monitoring self-healing would require repeated attachment and removal of the pipe, potentially introducing variability in the sealing conditions. This motivated the adaptation of a water permeability test commonly used in self-healing concrete, which was applied at the brick–mortar. Although not pursued in this study, this approach could potentially be combined with subsequent shear testing to assess mechanical recovery. Due to time constraints, direct watertightness testing was not extended to the other levels; instead, crack-filling analysis was adopted as a non-destructive, indirect indicator of sealing progress. Due to time constraints, direct watertightness testing was not extended to the other levels; instead, crack-filling analysis was adopted as a non-destructive, indirect indicator of sealing progress. Future research should investigate the combined application of both methods at the brick–mortar level to cross-validate their results. Once the relationship between local water absorption and pressure-based permeability is established, the Karsten pipe method could provide a simple, non-destructive approach for larger-scale and in situ testing, used alongside visual crack-filling analysis to assess aesthetic recovery. For the identification of healing products, FTIR analysis was implemented where reaction products could be physically collected. This technique was prioritised over other analytical methods due to its relative speed and simplicity. FTIR was used in combination with reference samples to provide mineralogical evidence and to assist in discriminating between bacterial-induced healing and autogenous mechanisms. Finally, the impact of the self-healing agent on functional properties was investigated through a targeted selection of physical and mechanical tests, providing a preliminary understanding of its interaction with the host material.

While the combination of multiple and complementary analytical techniques is essential for drawing more robust conclusions, the experimental programme presented in the following chapters is intended to provide first insights into the applicability of the proposed agent. In this sense, the framework introduced in this chapter should be regarded as an initial structured draft rather than a definitive testing protocol. Each performance dimension and material level warrants further investigation in order to refine experimental methodologies and to establish stronger correlations between performance indicators. This underscores the need for the development of standardized and validated procedures specifically tailored to the assessment of self-healing technologies in masonry.

The following chapters build upon this framework, moving progressively from the mortar to the masonry component level. This implementation serves to demonstrate the

framework's practical application and to assess the potential of the selected PLA-based bacterial agent as a viable solution for masonry repair.

Table 3-1 Overview of the tests and main variables identified for each material level within the proposed framework. Variables reported in italic correspond to those investigated in the following chapters using the selected poly-lactic acid self-healing agent.

Material level		Mortar	Brick-mortar	Masonry component
Recovery of performance	Aesthetics	*Superficial filling of cracks (Optical microscope)*	*Superficial filling of cracks (Digital camera/ portable microscope)*	*Superficial filling of cracks (Digital camera/ portable microscope)*
	Mechanical properties	Depending on the induction method *If bending (three point bending test): flexural strength, bending stiffness,* fracture energy	Depending on the induction method *If bending (CMOD-controlled bond wrench test): flexural bond strength, bending stiffness,* fracture energy	Depending on the induction method *If bending (in-plane four-point bending test): flexural strength, bending stiffness,* fracture energy
	Watertightness recovery	Direct assessment: water permeability tests *Indirect assessment: aesthetic recovery (sealling)*	Direct assessment: *permeability tests*, Karsten pipe method Indirect assessment: aesthetic recovery *(sealling)*	Direct assessment: Karsten pipe method *Indirect assessment: aesthetic recovery (sealling)*
	Damage induction Method	*Mechanical: bending*, shear, tension Artificial: saw-cutting with spacers	*Mechanical: bending, shear*, tension Artificial: saw-cutting with spacers	*Mechanical: bending, shear*, tension
	Timing	*>28 days for cement-based or cement-lime mortars (with lime <30% of the binder).* >90 days for lime-pozzolana mortars >12 months for pure lime mortars.		
	Extent	>100 µm (visible limit), < healable limit (to be determined experimentally);		
	Healing conditions Environment	*Humid conditions (RH>95%)* *Wet-dry cycles* *80% RH*	*Most suitable conditions identified at the previous level*	*Most suitable condition identified at the previous level*
	Time	*Monitored through aesthetic recovery* *> 56 days for PLA healing agent*	*Monitored through aesthetic recovery* *> 56 days for PLA healing agent*	*Monitored through aesthetic recovery* *> 56 days for PLA healing agent*
Identification of healing products	Mineral composition	*FTIR*, XRD, Raman, ESEM-EDS on scraped products	*FTIR*, XRD, Raman, ESEM-EDS on scraped products	*FTIR*, XRD, Raman, ESEM-EDS on scraped products
	Bacterial activity	*Indirect assessment:* ESEM, *FTIR*, TGA on scraped products Oxygen sensors	*Indirect assessment:* ESEM, *FTIR*, TGA on scraped products	*Indirect assessment:* ESEM, *FTIR*, TGA on scraped products
Impact on functional properties	Mechanical properties	*Elastic modulus* *Compressive strength* *Flexural strength*	*Flexural bond strength* *Initial shear strength/cohesion* *Initial friction coefficient*	*Flexural strength, bending stiffness, fracture energy* *Compressive strength, Young's modulus*
	Physical properties	Workability *Bulk density* *Total water absorption at atmospheric pressure*	Total porosity, pore size distribution (MIP) Water absorpdion by capillarity, Vapour transport	-

Chapter 4

Mortar level performance of bacteria-based agent

Building on the framework introduced previously, this chapter evaluates the applicability of a bio-polymeric self-healing agent, originally developed for concrete, to lime–cement mortars relevant for (heritage) masonry repair. Four mortar compositions with increasing lime content were investigated under different healing environments to assess performance recovery, identify healing products, and evaluate material compatibility.

The results confirm that the agent is compatible with lime-based mortars. While mechanical recovery of fine cracks (≈0.07 mm) was largely driven by autogenous healing, the agent enhanced the reliability of the response. For larger cracks (≈0.5 mm), the agent significantly enhanced aesthetic recovery, promoting visible crack filling under both wet conditions and wet–dry cycles. Calcium carbonate was identified as the main healing product, confirming the activation of the agent and its compatibility with lime-based mortars. Regarding the agent's impact, only minor changes in physical properties were observed, while the effect on mechanical properties depended on the lime content. Notably, compressive strength increased by approximately 100% at high lime contents, underscoring the importance of composition-tailoring to ensure mechanical compatibility in repair applications.

While further investigation at the mortar level is still warranted, the outcomes of this chapter provide a sound basis and set the stage for investigating the healing agent at the brick–mortar interface in the next chapter.

The experimental results presented in this chapter are available via the 4TU.ResearchData repository at:

https://doi.org/10.4121/dc2c9975-468b-4422-ae62-945e48420c53

The data are distributed under the license type CC BY.

Part of this chapter was previously published by the author in:

Gaggero, M. B., Korswagen, P. A., Esposito, R., & Rots, J. G. (2024). **Bacteria-based self-healing agent for masonry repair: applicability to cement-lime mortars.** 78-79. Abstract from SUBLime Conference 2024, Funchal, Portugal

4.1 Introduction

In the context of initiating the study of self-healing strategies for cracked masonry repair, the use of an already established healing agent developed for concrete offers a pragmatic starting point. Among the solutions currently available, a self-healing agent based on a poly-lactic acid (PLA) carrier and bacteria appears particularly promising. As described in Chapter 2, this agent contains limestone-producing bacteria that are activated upon cracking when exposed to water, promoting crack filling through bacterial activity and the enhancement of carbonation. Indeed, the underlying mechanism is not only expected to be compatible with lime-based mortars but may even be more effective in such systems. Lime-rich mortars contain a higher amount of free lime, which favours carbonation processes promoted by the agent. In addition, the resulting healing product, calcium carbonate, corresponds to the binding phase of lime-based mortars, suggesting a high degree of chemical, physical, and mechanical compatibility. On this basis, a more complete recovery could be anticipated, in contrast to cement-based systems, where the healing product is mechanically weaker than the original binding phases and typically contributes primarily to the restoration of watertightness rather than strength.

Despite this promising rationale, the application of this agent to lime-based mortars has not been experimentally verified yet and therefore requires systematic investigation before implementation for masonry repair. Consequently, building on the framework introduced in Chapter 3, this chapter presents the first experimental implementation of the proposed agent to lime-based mortars. This first experimental step provides a controlled and manageable environment to evaluate the functioning of the healing agent, assess its compatibility with lime–cement mortars relevant for masonry repair, and identify favourable healing conditions, prior to implementing it to bricks.

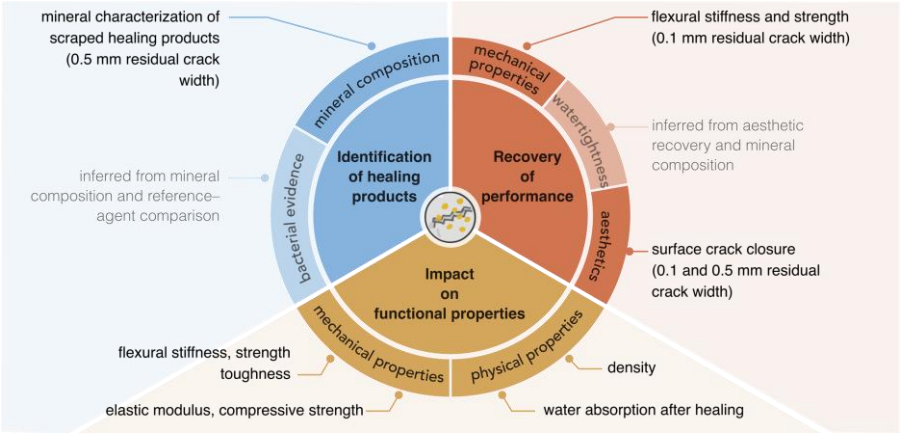


Figure 4-1 Schematic overview of the experimental approach adopted at the mortar level.

Following the framework, the agent's applicability is assessed through a combination of complementary indicators, including mechanical recovery, aesthetic recovery, identification of healing products, and the evaluation of its influence on relevant functional properties (Figure 2-2). To do so, four mortar compositions with increasing lime content are investigated under different healing environments to clarify the role of mortar composition and exposure conditions on healing behaviour. The following sections described the materials and methods used, and discuss the results obtained.

4.2 Materials and methods

4.2.1 Healing agent

The healing agent considered in this study consists of poly-lactic-acid (PLA) capsules containing bacterial spores, supplied as a granular additive (Figure 4-2) by Basilisk B.V. (Delft, the Netherlands). The agent was applied in the mortar mixtures as received, following the procedure exposed in the next section.

The capsules contain a PLA matrix that encloses bacterial spores from alkaliphilic (alkali-resistant) Bacillus cohnii-related strains, along with nutrients required for bacterial activation during spore germination (Figure 4-3). The PLA matrix serves a dual role: it protects the bacterial spores and, upon hydrolysis to calcium lactate, provides a precursor for calcium carbonate formation by active bacteria. Bacterial activation is triggered when external water infiltrates the material, causing the pH to drop below 11.5. Once activated, the bacteria can convert the precursor in the presence of oxygen (aerobic activity).

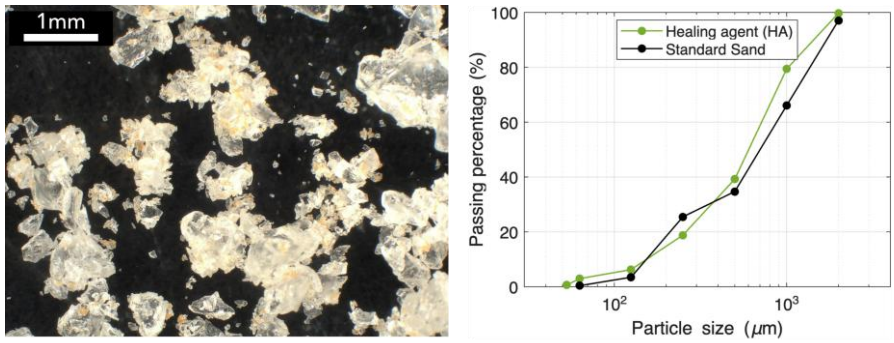


Figure 4-2 PLA-based bacterial agent: (a) optical microscopy image of the granules (Keyence VHX-6000 at ×50 magnification) and (b) cumulative particle size distribution.

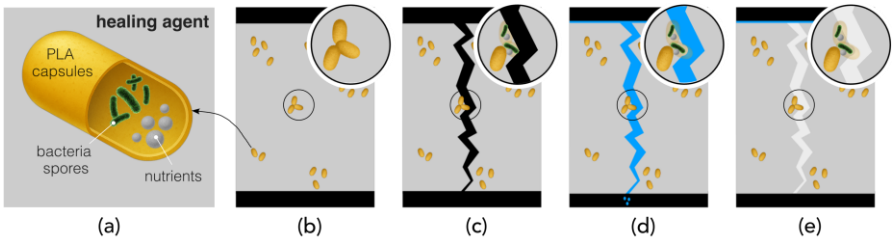


Figure 4-3 (a) PLA-based self-healing agent and (b-e) autonomous healing mechanism: undamaged state, crack formation with agent release, bacterial activation and crack filling.

4.2.2 Mortar mixtures

Four mortar compositions with and without the added-in healing agent were cast to investigate the applicability of the selected PLA-based self-healing agent at the mortar level. The mixtures featured increasing lime-to-cement ratios by volume (L/C) 0, 0.33, 1 and 3.33, respectively labelled C100L0, C80L20, C50L50, C20L80. The selection of mortar compositions was guided by a gradual transition from pure cement mortars to cement–lime formulations more suitable for heritage conservation practice in the Netherlands (personal communication with C. Groot). For each composition, two variants were prepared: a plain mortar without healing agent (labelled as Reference or R), and its self-healing counterpart containing the agent at a dosage of 10 kg/m^3 (labelled as Self-healing or B). Accordingly, eight mortar configurations were produced, covering the four compositions in both Reference (R) and Self-healing (B) form.

The binders used were Ordinary Portland Cement (CEM I 42.5 N) and commercial aerial lime (CL80S – EN 459-1) with an apparent density of 1.2 and 0.52 g/cm^3 respectively. Standard river sand, with a particle size distribution between 0.06 and 2 mm (Figure 4-2) and an apparent density of 1.7 g/cm^3, was used in a volumetric proportion of 1:2.5 (binder: sand). The water-to-binder (w/b) ratio was determined in accordance with EN 1015-2 (CEN 1998) on the reference mortar mixtures, to reach a flow of 175 ± 10 mm (CEN 1999a). The same w/b ratio was subsequently used with the self-healing mortar mixture. An overview of the mortar compositions considered is reported in Table 2-1.

All mixtures were prepared using a Hobart planetary mixer following the same procedure. First, all dry components were blended for 2 minutes at low speed. Subsequently, water was gradually added while the mixer was run for an additional minute. The mixer walls were then scraped to ensure full incorporation of the components, after which mixing proceeded for an additional minute at low speed. In the self-healing mixtures, the healing agent was incorporated during this additional minute, while the mixer was still running. Finally, all mixtures were mixed for one additional minute at medium speed.

Mortar bar specimens (40x40x160 mm^3) were cast in polystyrene moulds and cured in accordance with EN 1015-11 (CEN 1999b). Immediately after casting, the specimens were stored at 20 ± 2 °C and 95 ± 5 % RH for a total of 7 days. Specimens containing up to 50 % air lime in the binder (L/C 0, 0.33, and 1) were kept in the moulds for 2 days, whereas those with higher air-lime content (L/C 3.33) remained for 5 days. After demoulding, all specimens continued curing under the same conditions until day 7. Thereafter, they were stored at 21 ± 2 °C and 65 ± 5 % RH until testing. Temperature and relative humidity at the storage locations were continuously monitored using an EPD-TRH-INT sensor, with an accuracy of ±0.6 °C for temperature and ±2.5 %RH for relative humidity.

In total, five sets of three mortar bars were cast for each of the eight mortar configurations, resulting in 120 mortar bars. The experimental programme was structured to maximise the information obtained from the specimens, mainly addressing recovery of mechanical and aesthetic performance, identification of healing products, and the effect of the healing agent on the functional properties of the mortars. Figure 4-4 provides an overview of the tests performed on the five specimen sets cast for each mortar composition, together with the corresponding specimen ages at testing.. Set 1 was used for preliminary mechanical characterisation and to define the testing protocols subsequently applied to the remaining specimens. Set 2 was used to evaluate the effect of the healing agent on the mechanical properties investigated. After testing to failure, specimens from both sets were used to assess the aesthetic recovery of larger cracks

Table 4-1 Mix design of the investigated mortars.

binder composition	C100L0	C80L20	C50L50	C20L80
l/ c (lime/ cement ratio by volume)	0	0.33	1.0	3.33
c: l: s (cement: lime: sand by volume ratio)	1: 0: 2.5	5: 1.5: 16	1: 1: 5	1.5: 5: 16
b: s (binder: sand by volume ratio)	1: 2.5			
consistency (flow table)	175 ± 10 mm (w/ b ratio determined accordingly)			
w/ b (water/ binder by volume ratio)	0.68	0.69	0.72	0.78
l/ b (lime/ binder % by mass)	0	11	30	58
HA by total binder volume (% by vol)	10			
HA by total binder mass (% by mass)	5			

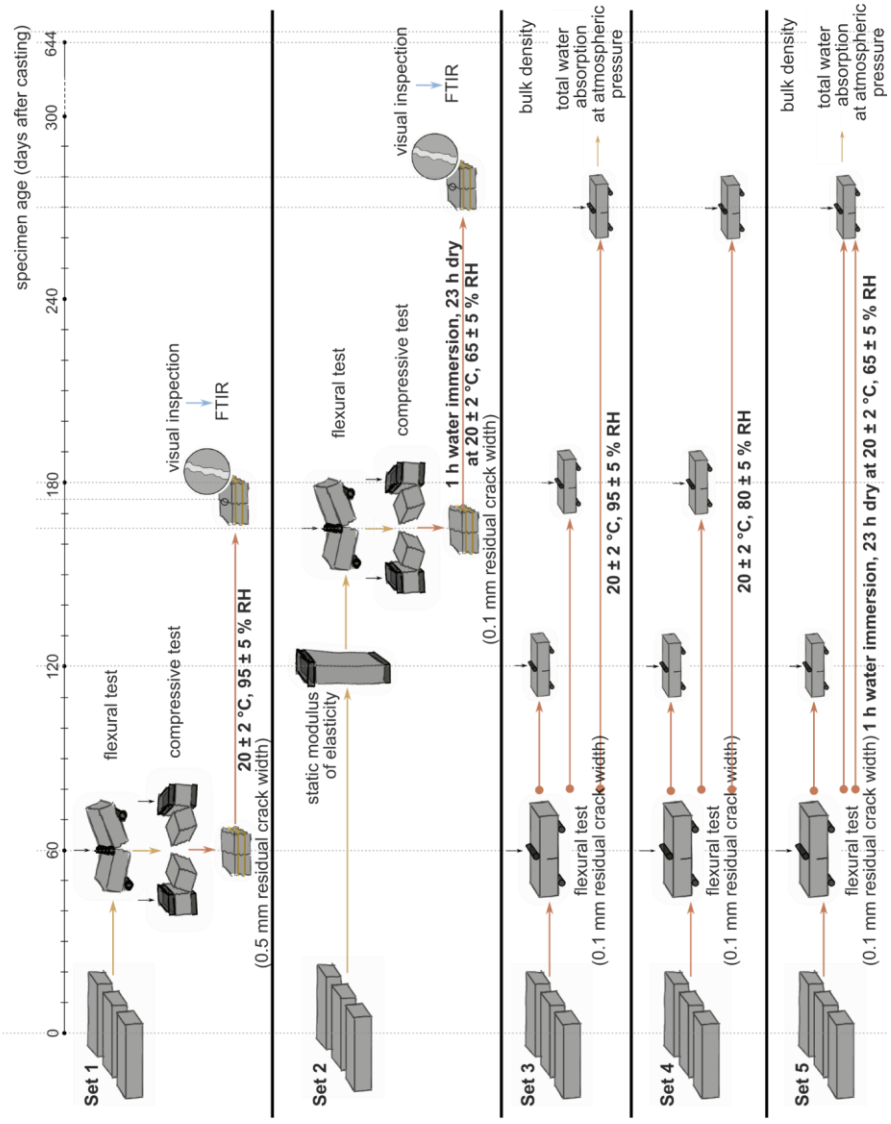


Figure 4-4 Experimental scheme and testing timeline for the five specimen sets cast for each mortar composition.

and analyse precipitate formation. The remaining three sets were used to evaluate mechanical and aesthetic recovery for finer cracks (≈0.07 mm) under different healing environments. In addition, the open porosity of healed specimens was assessed by water immersion tests (Section 1.2.3) to evaluate the effect of the agent on the pore structure. Details of the individual test setups are given in the following sections.

4.2.3 Bulk density and total water absorption at atmospheric pressure

Bulk density and total water absorption at atmospheric pressure were evaluated, in accordance with EN 1015-10 (CEN 1999c), at 644 days on specimens previously subjected to cracking, healing, and re-cracking. Specimens were air-dried to constant mass, after which their dry mass and volume were used to calculate the bulk density. They were subsequently immersed in water until a constant saturated mass was reached, and total water absorption at atmospheric pressure was calculated from the mass increase relative to the dry mass. Bulk density and water absorption were used as complementary indirect indicators of porosity, with bulk density providing an indication of total porosity and total water absorption at atmospheric pressure primarily reflecting the volume of water-accessible pores.

4.2.4 Static modulus of elasticity in compression

Cyclic compression tests were performed on 40×40×160 mm³ mortar prisms (Set 2) to evaluate the effect of the healing agent on the elastic modulus of different mortar compositions. Tests were conducted at 120 days using an adapted procedure for mortar prisms based on Mera Marques et al. (2020), which was itself developed from ISO 6784. A hydraulic jack with a maximum capacity of 250 kN was used. Depending on the mortar strength, either a 5 kN or 10 kN load cell was employed to maintain accuracy within the applied load range. Prior to testing, both loading faces were coated with a thin gypsum layer to restore planarity and ensure uniform load distribution (Figure 4-5 (a)). Four LVDTs (±1 mm range, ±0.001 mm accuracy) were attached at mid-height, one per face, to record vertical deformation (Figure 4-5 (b)(c)). Over the 60 mm measuring length, this corresponds to a strain-measurement accuracy of approximately ±17 μm/m.

A small preload (500 N for compositions with L/C ≤ 1 and 100 N for L/C = 3.33) was applied to ensure full contact between the specimen and the plates, followed by three

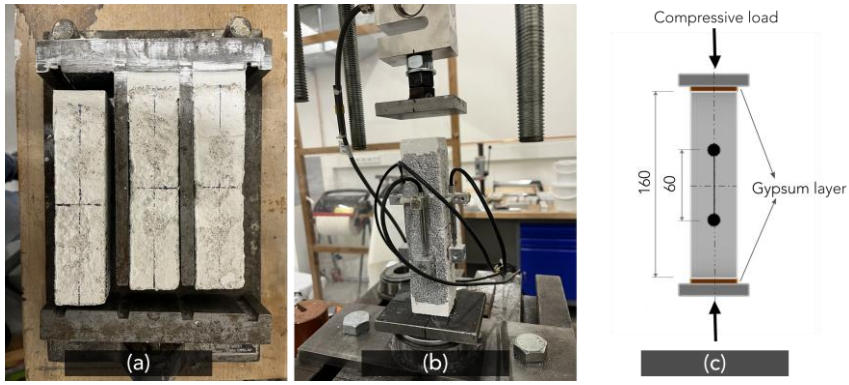


Figure 4-5 Experimental setup for the cyclic compression test used to determine the elastic modulus of mortars: (a) specimen preparation; (b) instrumented test specimen with four LVDTs recording axial deformation; and (c) schematic showing relevant dimensions.

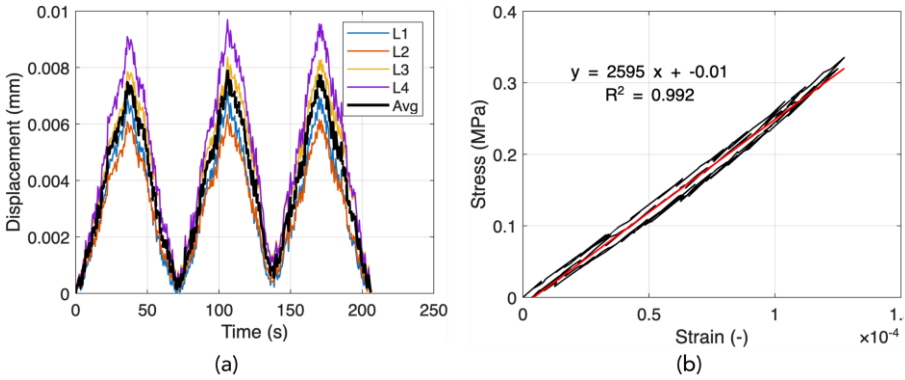


Figure 4-6 Example of a self-healing specimen with lime/ cement ratio of 3.33: (a) vertical displacement recorded by four LVDTs (L1-L4) during cyclic compression loading and (b) stress–strain relationship obtained from the last two cycles, including linear regression line.

loading–unloading cycles under displacement control at 0.001 mm/s, up to a load corresponding to 40% of the compressive strength. The compressive strength was determined using the mean compressive strength measured on the preliminary Set 1 specimens tested at approximately 60 days. The first loading is excluded from the analysis and performed only for the setting of the gauges as prescribed by the standard. Strain was calculated as the mean vertical deformation measured by the four LVDTs (Figure 4-6 (a)) divided by the initial gauge length (60 mm), and stress as the applied load divided by the loading area (40 × 40 mm²). A linear regression fitted to the stress–strain curve (Figure 4-6 (b)) provided the static elastic modulus of each specimen.

4.2.5 Flexural tests

Three-point bending tests were performed on mortar bars with three objectives: (i) to induce controlled cracking for the evaluation of healing performance, both aesthetic and mechanical; (ii) to quantify the mechanical restoration provided by the healing agent; and (iii) to assess its effect on the flexural properties of the different mortar compositions. The experimental set-up is reported in Figure 4-7.

Tests were performed in accordance with EN 1015-11 (CEN 1999b), with the specimens supported on two Ø10 mm rollers. To apply the load at mid-span, a metallic plate was glued to the top loading face using a two-component adhesive, forming a continuous contact line for the loading roller. This configuration compensated for the irregularity of the upper surface, corresponding to the casting face (i.e. the face not in contact with the mould), and ensured uniform load transfer during testing. Loading was applied with a 250 kN hydraulic jack and measured with a 5 kN load cell. The jack was operated in displacement control, using the average signal from two LVDTs (front L1 and back L2) monitoring the crack opening at the bottom face of the specimen. The load rate was 0.02 μm/s. Two additional vertical LVDTs (front L3 and back L4) measured the

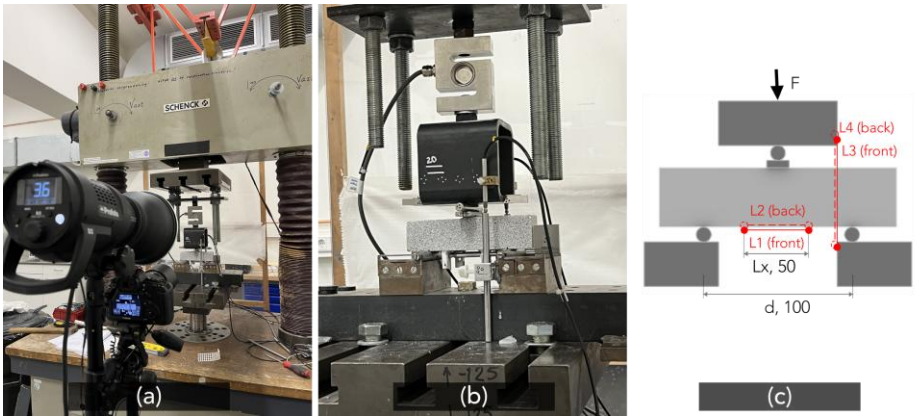


Figure 4-7 CMOD-controlled three-point bending test configuration adopted to evaluate the flexural behaviour of the mortars and to generate controlled cracking for subsequent recovery assessment: (a) overview of the test setup; (b) close-up of the specimen and LVDTs arrangement; and (c) schematic of the loading configuration and sensor positions.

relative displacement between the loading point and the supports. All LVDTs had a measuring range of ±1 mm and an accuracy of ±0.001 mm. Digital image correlation (DIC) was used on the front face to track crack initiation and propagation along the specimen height.

A first round of tests was performed using set No. 1 and 2. Set No. 1 was used to obtain preliminary information on flexural (and later compressive) strength, serving as an initial indication of the mechanical behaviour of the mixtures. Set No. 2 was employed to further characterise the material behaviour, including the determination of elastic modulus following the procedure described in Section 4.2.5. In this set, flexural tests were performed loading specimens until failure, with a single unloading–reloading cycle performed at a CMOD of 0.10 mm (Figure 4-8 (a)(b)). This unloading–reloading cycle enabled the evaluation of residual bending stiffness at the defined damage level and provided a reference benchmark for subsequent stiffness recovery assessment. Figure 4-8 provides a representative example of the measured response, in terms of the applied force versus the crack mouth opening displacement (CMOD) and the load-point deflection, both recorded by the front and back LVDTs on the specimen. The bending properties were obtained considering the averaged curve (black line in Figure 4-8) obtained considering the average LVDTs reading on front and back side of the specimen. The flexural strength (f_x), bending stiffness (E) and fracture energy (G) were determined as follows:

$$f_x = \frac{3}{2}\frac{F_{max}\,d}{b\,h^2} \tag{13}$$

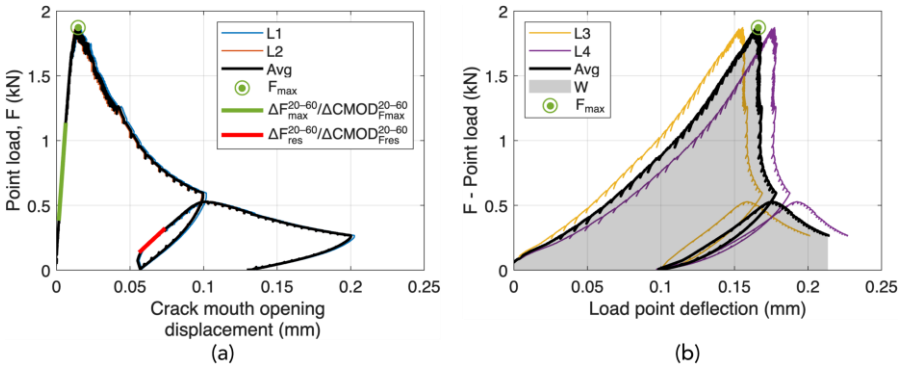


Figure 4-8 Flexural responses of the specimens used to characterise the mixtures and to determine the residual bending stiffness. (a) Load–CMOD curves from front and back LVDTs and their averaged response, highlighting the elastic and residual segments. (b) Corresponding load–deflection curves and averaged response used to determine fracture energy.

$$E = \frac{b\,L_x\left(2d - L_x\right)}{16\,I}\,\frac{\Delta F_{max}^{20-60}}{\Delta CMOD_{Fmax}^{20-60}} \tag{14}$$

$$G = \frac{W}{A} = \frac{W}{b\,h} \tag{15}$$

where F_{max} is the maximum load at failure, d is the distance between the bearing support, h is the height of the specimen, b is the thickness of the specimen, L_x is the measuring length of the CMOD sensors (L1 and L2) and I is the moment of inertia. ΔF_{max}^{20-60} and $\Delta CMOD_{Fmax}^{20-60}$ are the force and CMOD increments within the elastic stage (between 20% and 60% of the maximum load) used to assess the bending stiffness (E). W is the dissipated energy, computed as the area under the force–deflection curve (Figure 4-8 (b)) to derive the fracture energy (G), assuming as fracture surface (A) the fractured cross-sectional area. In addition to the aforementioned properties, the residual strength (f_{res}) and residual bending stiffness (E_{res}) were evaluated and later used as parameters to quantify the recovery after healing:

$$f_{res} = \frac{3}{2}\,\frac{F_{res}\,d}{b\,h^2} \tag{16}$$

$$E = \frac{b\,L_x\left(2d - L_x\right)}{16\,I}\,\frac{\Delta F_{res}^{20-60}}{\Delta CMOD_{Fres}^{20-60}} \tag{17}$$

The residual strength (f_{res}) was calculated from the residual force (F_{res}), i.e. the load at a CMOD of 0.10 mm. The residual stiffness (E_{res}) was evaluated in the range between 20% and 60% of the residual force (F_{res}), using the corresponding increments in force (ΔF_{res}^{20-60}) and CMOD ($\Delta CMOD_{Fres}^{20-60}$).

The second round of tests, performed on set No. 3-5, served to crack samples and assess the recovery in terms of aesthetics and mechanical behaviour. To this purpose, samples were loaded to a CMOD of 0.10, unloaded and left to heal under the conditions detailed in Section 4.2.7. A CMOD of 0.10 mm was selected as the target cracking level, as it represents the lower limit of just-visible damage (Korswagen 2024). Once the healing period was completed, the specimens were dried to constant mass at laboratory room temperature. Aesthetic recovery was first assessed through visual inspection (Section 4.2.8), after which the specimens were retested following the same loading procedure, enabling a direct comparison with their pre-healing behaviour.

As in the first round of tests, flexural strength and bending stiffness were calculated using Eq. (13) and (14). To distinguish properties assessed before and after healing, subscripts “0” and “1” denote values obtained before and after healing, respectively. Mean reference values for both strength and stiffness were calculated as the average of all tests conducted on undamaged specimens (sets 3-5) and are denoted as $f_x^{(avg)}$ and $E^{(avg)}$. From the pre-healing test, the residual strength (f_{res}^0) was also determined using formula (15). For the residual stiffness, the mean value measured during the first round of tests (sets 1-2) was considered and is denoted as ($E_{res}^{(avg)}$). Based on these parameters, the recovery of flexural strength (R_{fx}) and the recovery of bending stiffness (R_E) were evaluated using the following equations:

$$R_{fx} = \frac{f_x^1 - f_{res}^0}{f_x^{(avg)} - f_{res}^0} 100 \tag{18}$$

$$R_E = \frac{E^1 - E_{res}^{(avg)}}{E^{(avg)} - E_{res}^{(avg)}} 100 \tag{19}$$

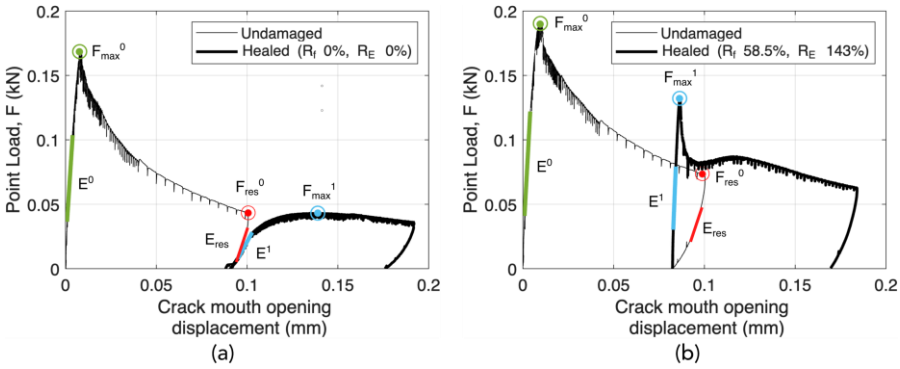


Figure 4-9 Example load–CMOD responses for two specimens with a lime/cement ratio of 3.33, illustrating the evaluation of mechanical recovery. (a) Specimen healed at 80% RH, showing no recovery in flexural strength or bending stiffness ($F^1_{max} \sim F^0_{res}$, $E^1 \sim E_{res}$). (b) Specimen healed under wet conditions, displaying marked recovery in both properties ($F^1_{max} > F^0_{res}$, $E^1 > E_{res}$). The curves highlight the parameters used to quantify recovery, including pre-healing and post-healing maximum load, residual strength, and the corresponding elastic stiffness.

Since cracked specimens still exhibit residual load-bearing capacity, recovery was assessed by considering both the undamaged and the residual properties. Using undamaged values as the sole reference neglects the contribution of residual post-cracking strength and stiffness and may therefore lead to an overestimation of recovery.

To illustrate the range of responses, Figure 4-9 shows two example specimens: (a) exhibiting no mechanical recovery and (b) displaying clear recovery after healing. In applying formulas (6)–(7), a recovery value of zero is assigned whenever the healed strength or stiffness falls below its corresponding residual value, ensuring that negative recovery values are not reported.

4.2.6 Compressive tests

To determine the effect of the healing agent on the compressive behaviour of the different mortar compositions, compressive tests were performed on Sets 1 and 2. While Set 1 provided preliminary strength values to define the loading protocol for the elastic modulus assessment, Set 2 was designated for a comprehensive mechanical evaluation. Accordingly, the compression tests on Set 2 were conducted at 170 days, on samples priorly tested for elastic modulus in compression and flexural tests until failure. As a result of the flexural tests, the mortar bars were split into two halves with dimensions of 40 × 40 × 80 mm³. Compression tests were performed on the portion of each half located away from the bending fracture plane.

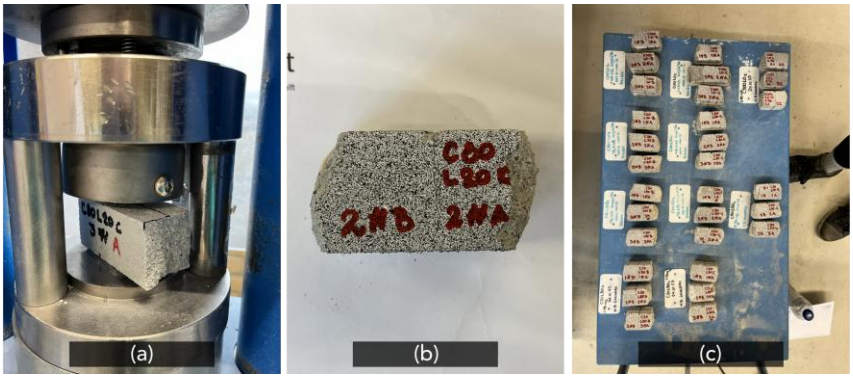


Figure 4-10 Compression testing and post-test handling of mortar specimens. (a) Setup of the uniaxial compression test performed on the 40 × 40 × 80 mm³ halves obtained after flexural and elastic modulus testing. (b)(c) Reassembled tested halves secured with elastic bands and prepared for the healing stage under humid conditions.

Test were performed using a force-controlled Instron Universal Testing Machine, with the specimens placed between two steel loading plates of 40 mm length (Figure 4-10 (a)). A monotonic load was applied at rates of 0.9, 0.7, 0.5, and 0.1 kN/s for L/C ratios of 0, 0.33, 1, and 3.33, respectively. The compressive strength (f_m) was calculated as the maximum load recorded during the test divided by the loaded cross-sectional area ($40x40mm^2$).

During compression tests, the 40×40×40 mm³ loaded portion (corresponding to half of the compression-tested specimen and one quarter of the original mortar bar) crumbled and detached. After testing, the remaining parts of the two specimen halves located close to the bending fracture plane were reattached using an elastic band and subsequently allowed to heal under wet conditions (20 ± 2 °C, 95 ± 5 % RH) and wet-dry cycles for 115 days (Figure 4-10 (b)(c)).

4.2.7 Healing environments

Three different environments were considered for healing of the mortar samples after three point bending tests: wet conditions (95 ± 5 % RH, 20 ± 2 °C), wet-dry cycles (1 h of water immersion followed by 23 h of drying at 20 ± 2 °C and 65 ± 5 % RH), and moderate-humidity conditions (80 ± 5 % RH, 20 ± 2 °C). All three environments were used to evaluate mechanical and aesthetic recovery of prismatic specimens pre-cracked to a CMOD of 0.1 mm. For larger cracks (>0.10 mm), the assessment was limited to aesthetic recovery under wet and wet–dry conditions.

For the evaluation of mechanical restoration, one specimen per composition was tested after 60 days of healing to provide an indication of the ongoing healing process at that stage. The remaining two specimens were tested at later ages, i.e. 120 and 210 days of healing. The allocation of the specimens across the different healing durations

and environments is summarised in Figure 4-4. After the designated healing period, all samples were dried to constant mass at laboratory room temperature, after which aesthetic recovery was assessed through visual observation and mechanical recovery was evaluated through retesting. For the evaluation of aesthetic restoration, crack healing was assessed after 115 days. Given the limited number of specimens available for each combination of mortar composition, healing environment and healing duration, the mechanical recovery trends presented and discussed in the following section should be regarded as exploratory.

4.2.8 Visual inspection

Visual inspection was used both to monitor the healing process over time and to qualitatively assess the aesthetic recovery before and after healing. Specimens were examined using a Keyence VHX-6000 digital microscope and a high-resolution (51 MP) photographic camera.

4.2.9 Fourier Transform Infrared Spectroscopy

Fourier Transform Infrared Spectroscopy (FTIR) spectra of the precipitate were recorded with a Nicolet iS5 Thermo Fisher Scientific instrument, equipped with an attenuated total reflection unit featuring a diamond crystal (400–4000 cm^{-1} spectral range; resolution of 4 cm^{1}).

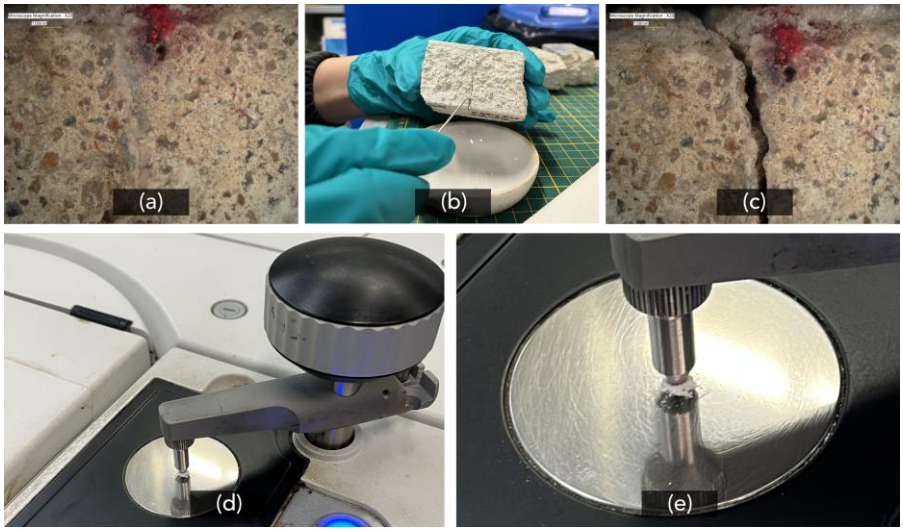


Figure 4-11 Procedure for FTIR sample preparation and analysis. (a) Crack area showing the precipitates to be collected. (b) Manual scraping of the precipitate using a Keyence VHX-6000 digital microscope to avoid collecting material from the surrounding mortar. (c) Detail of the cleaned crack after precipitate removal. (d) FTIR measurement using a Nicolet iS5 instrument equipped with a diamond ATR unit. (e) Zoom-in on the ground material used for testing.

Precipitates were collected from the specimens used for aesthetic restoration assessment, characterised by larger crack widths. This approach was adopted to ensure that the analysed material corresponded to healing products formed within the cracks, rather than to bulk mortar material. Mortar specimens were dried in an oven at 40 °C until constant mass prior to collection. Material was gently scraped from the crack areas using a microscope to avoid removing any of the surrounding mortar. The collected precipitate was then manually ground to obtain a fine powder. All samples were prepared immediately before testing. Figure 4-11 illustrates the procedure adopted for the collection of precipitates and subsequent characterisation.

4.3 Performance recovery

This section evaluates the viability of the proposed poly-lactic-acid (PLA) healing agent for the autonomous repair of lime-based mortars based on the experimental programme described in the previous section. The assessment focuses on the performance of the agent across the four mortar compositions (L/C ratios of 0, 0.33, 1, and 3.33) and under three distinct healing environments: wet conditions at 20 ± 2 °C and 95 ± 5 % RH; wet–dry cycles comprising 1 h of water immersion followed by 23 h of drying at 20 ± 2 °C and 65 ± 5 % RH, and a moderate-humid conditions at 20 ± 2 °C and 80 ± 5 % RH.

The following subsections present the results of the performance recovery evaluation, first providing an exploratory assessment of mechanical recovery based on flexural strength and bending stiffness, followed by an analysis of aesthetic recovery. The exploratory nature of the mechanical assessment reflects the limited number of specimens tested under each condition. Through this analysis, the applicability of the proposed poly-lactic acid–based healing agent to lime-based mortars commonly used in masonry repair is discussed.

4.3.1 Mechanical recovery

Mechanical recovery of the mortars was assessed by evaluating the recovery of bending stiffness (R_E) and flexural strength (R_{fx}) on prismatic specimens pre-cracked to a CMOD of 0.1 mm. Diff erent specimens from each mortar composition were tested after different healing durations; therefore, Figure 4-12 presents recovery results as a function of healing duration. To guide the reader, points within each configuration are connected with lines, using averaged values where multiple specimens were tested at a given healing duration. These lines are included only as visual guides and do not represent the

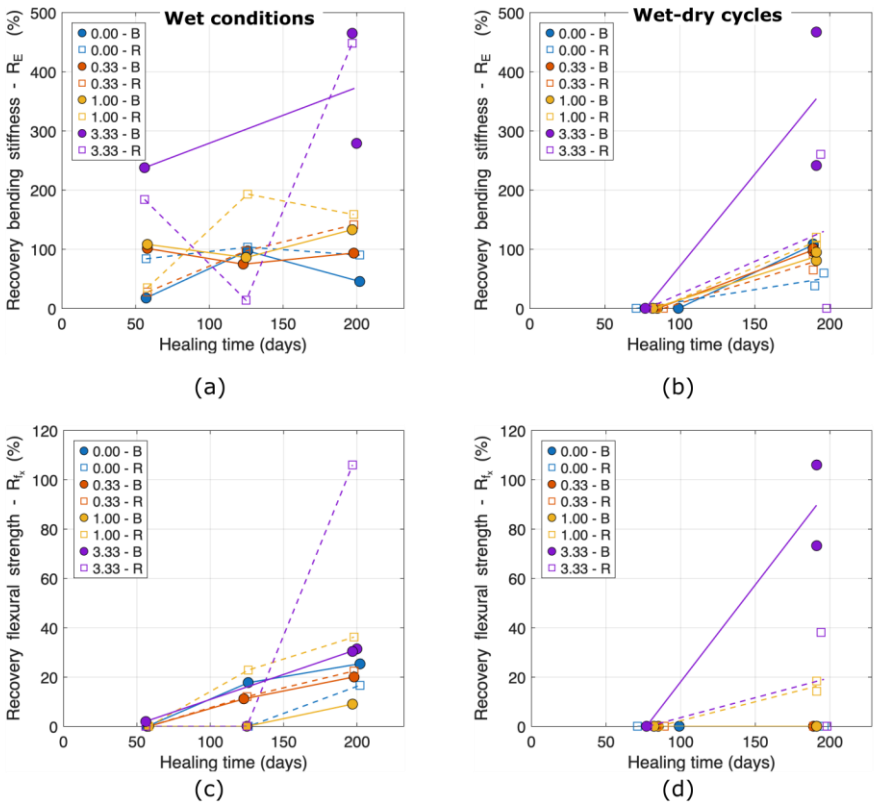


Figure 4-12 Mechanical recovery versus healing time for mortars with different L/C ratios, with bending stiffness recovery shown in (a,b) and flexural strength recovery in (c,d) under wet and wet–dry cycles conditions. Filled symbols indicate bacteria-based mortars and open symbols reference mortars; colours denote different L/C ratios. Lines connect data points belonging to the same mortar composition and, when multiple specimens were tested at the same healing time, connect the corresponding mean values. Lines are shown only as a guide to the reader.

time evolution of the same specimen or replicated measurements at successive healing durations. To complement this analysis and facilitate an indicative comparison across mortar compositions, Figure 4-13 presents the average recovery of each mortar composition a function of the lime-to-cement ratio (L/C). Because the specimens contributing to these averages were tested after different healing durations, the values represent descriptive summaries of the available results and not replicated measurements at a common healing duration. To account for differences in healing duration and avoid overestimating recovery, the averaged values are associated with the longest healing period, corresponding to 210 days. This approach is considered valid under the physically reasonable assumption of a non-decreasing recovery with healing time. In both figures, the performance of Reference specimens (R) and Bacteria-based

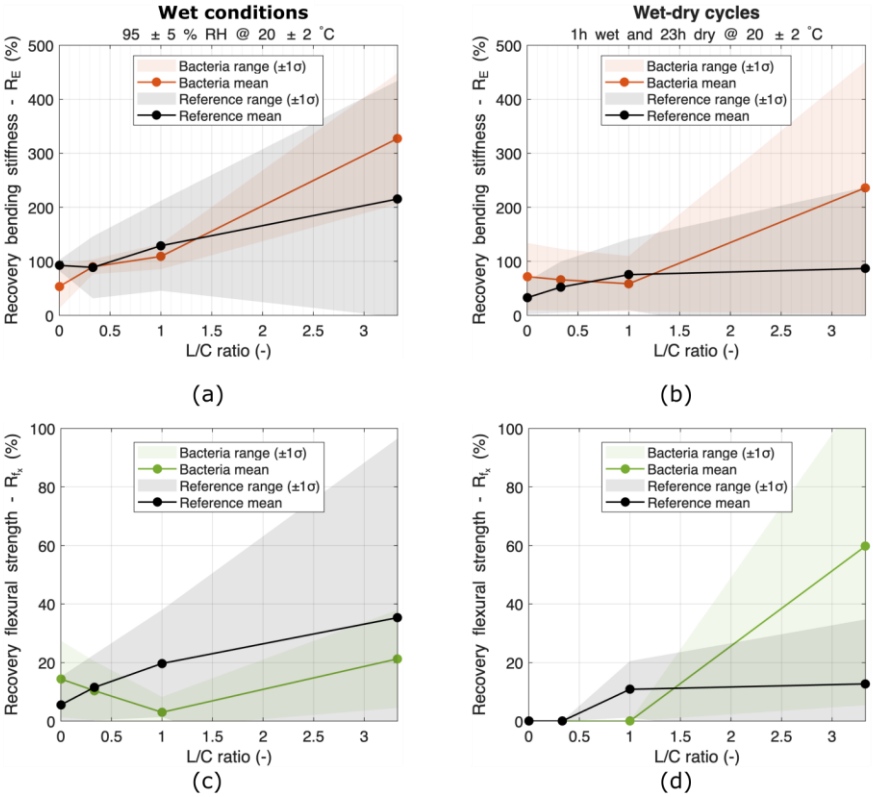


Figure 4-13 Mechanical recovery as a function of lime-to-cement (L/C) ratio after long-term healing (210 days) under wet conditions (95 ± 5% RH) and wet–dry cycles. Elastic modulus (bending stiffness) recovery is shown in (a,b) and flexural strength recovery in (c,d). Mean values are reported for reference and bacteria-based mortars, with shaded areas indicating the corresponding variability ranges (±1σ).

specimens (B) is compared under two curing environments: (I) wet conditions at 95 ± 5 % RH and 20 ± 2 °C, and (II) wet–dry cycles comprising 1 h of water immersion followed by 23 h of drying at 20 ± 2 °C and 65 ± 5 % RH. It should be noted that specimens exposed to moderate-humidity conditions at 80 ± 5 % RH and 20 ± 2 °C showed no measurable recovery for any composition; therefore, these results are not included. Overall, the experimental results show the occurrence of mechanical recovery in terms of bending stiffness and flexural strength in both reference and bacteria-based specimens with a mean residual crack width of approximately 0.07 mm. The observed differences in the onset and degree of recovery appeared to be associated with the lime-to-cement ratio, healing environment, and healing duration. These are discussed in the following paragraphs.

The tested specimens showed a general trend towards greater mechanical recovery at longer healing durations, with stiffness developing earlier than flexural strength due to

the progressive formation of healing products from the crack mouth towards the interior. However, because different specimens were tested at each duration, generally with only one specimen per condition, the connected data points do not represent repeated observations of the same specimen and cannot establish a statistically robust time-dependent evolution. Nevertheless, specimens tested after longer healing durations generally exhibited higher recovery values between approximately 60 and 210 days. At 60 days, no recovery was detected under wet–dry conditions, whereas under wet conditions partial or full stiffness recovery was already observed for all mortar compositions, in both reference and bacteria-based specimens. In contrast, flexural strength recovery developed more gradually in both environments and was not observed at early healing stages. For this reason, longer healing periods were considered for the remaining specimens. After approximately 210 days, all specimens exhibited stiffness recovery under both wet conditions and wet–dry cycles; strength recovery was consistently observed for all specimens healed under wet conditions and remained limited to lime-rich compositions under wet–dry conditions. This earlier and more prevalent recovery of stiffness is consistent with the physical sequence of the healing process, whereby healing initiates at the crack mouth and progresses inward. Early surface sealing restores geometric continuity and bending stiffness, whereas the recovery of tensile load-bearing capacity requires more extensive crack filling across the crack depth. Furthermore, the initial precipitation may consist of a relatively porous or poorly consolidated matrix, which provides sufficient contact to restore stiffness but lacks the cohesive strength necessary to withstand significant tensile stresses. While limited information is available on the time scales associated with autogenous healing, observations reported for bacterial systems similar to the one considered in this study indicate that visible crack healing at the surface may initiate after approximately 14 days under humid conditions, whereas healing products extending several millimetres into the crack are only detected after longer periods, on the order of 56 days or more (He 2025). In this context, the present results are consistent with these observations: healing periods of around 60 days appear sufficient to promote surface crack sealing and the associated recovery of stiffness, whereas healing durations of approximately 200 days result in only partial recovery of flexural strength. This suggests that even longer healing times may be required to assess the potential for full restoration of strength. To substantiate this interpretation, future studies should combine extended healing periods with microstructural analyses, such as thin-section observations, to directly verify the depth and continuity of healing products within the crack.

In addition to developing earlier than flexural strength, bending stiffness recovery consistently exhibited higher values and frequently exceeded 100% across both reference and bacteria-based specimens. This behaviour can be attributed to a combination of crack-related healing and continued stiffening of the bulk mortar matrix

during the prolonged curing period. Ongoing hydration and carbonation processes likely contributed to an increase in intrinsic material rigidity, which, when combined with partial crack closure, resulted in stiffness values surpassing those measured prior to cracking. From a methodological perspective, this observation highlights the relevance of including undamaged specimens subjected to the same curing history in order to decouple stiffness gains associated with matrix ageing from those directly attributable to crack healing.

Following the discussion of the observed healing-duration trends, it becomes evident that the recovery response was not uniform across **mortar compositions** or **curing environments**. Given the limited number of specimens tested at individual healing times, averaged values are used to facilitate an indicative comparison comparison across mortar compositions. Accordingly, the averaged results shown in Figure 4-13 are interpreted as indicative of recovery at the longest healing duration investigated in this study (up to approximately 210 days), while acknowledging that this approach may underestimate the maximum achievable recovery. Distinct recovery trends can be observed for reference and bacteria-based mortars depending on the curing environment. These differences are addressed in the following sections by separately analysing autogenous healing and the contribution of the bacterial healing agent.

Focusing on the Reference specimens (black curves), autogenous healing was clearly observed and generally increased with rising lime content; however, the large scatter associated with the results hampers the identification of a clear trend. Although the mean values suggest higher flexural strength recovery at increasing L/C ratios, the overlap between the variability ranges of consecutive compositions prevents a definitive assessment of a monotonic increase. Nevertheless, a comparison between the two extreme compositions investigated (L/C 0 and 3.33) highlights a clear contrast, as the mean recovery at a lime/cement ratio of 3.33 exceeds the variability range of the cement-rich reference (lime/cement ratio of 0), suggesting a markedly higher autogenous healing potential at high lime contents. This behaviour can be attributed to several concurrent factors. First, the increased availability of free lime at higher lime/cement ratios favours carbonation-driven crack filling. Second, since the resulting carbonation products are mechanically weaker than the original cementitious phases and resemble the binding phases typical of lime-based mortars, strength recovery in cement-rich mortars remains limited and is largely associated with crack sealing. Finally, the higher porosity typically associated with lime-rich mortars likely facilitates the ingress of water and carbon dioxide into the crack, enhancing crystallisation processes compared to denser, cement-rich matrices. The curing environment significantly modulated these trends. Under wet conditions, even low-lime compositions showed measurable strength recovery, which can be probably attributed to delayed hydration. Conversely, under wet–dry cycles, strength recovery was restricted to high-lime mortars, indicating that moisture availability

was insufficient to activate delayed hydration and that carbonation became the dominant healing mechanism. Notably, for the highest lime content (L/C = 3.33), comparable mean strength recovery was observed under both healing regimes, with differences falling within the experimental scatter. Regardless of composition, stiffness recovery was generally observed under both environments, either partially or fully. Although correlations between composition, curing conditions, and recovery are apparent, the present dataset is insufficient to define a robust empirical law. Future studies based on expanded datasets could explore predictive relationships incorporating L/C ratio, curing environment, crack width, and healing time.

When considering specimens incorporating the bacterial healing agent (green curves), a different response was observed compared to the reference system. Under wet conditions, no clear increase in mean flexural strength or stiffness recovery was detected across the investigated compositions. Instead, a more consistent recovery response was observed across the tested specimens containing the agent. This effect was particularly evident at high lime contents (L/C = 3.33), where all specimens exhibited measurable strength recovery, in contrast to the reference mortars, which showed a highly heterogeneous response, with only one out of the three samples showing recovery. These observations suggest that, under continuous moisture exposure and for small crack widths, where autogenous healing is already effective, the agent might enhances the reliability and robustness of the healing process rather than increasing its average magnitude. Under wet–dry cycles, the influence of the bacterial agent became more pronounced in terms of mean performance. Strength recovery values approaching 60% were achieved, exceeding those observed in the corresponding Reference specimens. However, this increase in average recovery was accompanied by substantial variability.

It should be emphasised that the conclusions drawn in this section are based on a limited experimental dataset. Consequently, further testing with a larger number of specimens and controlled healing durations is required to confirm the observed trends and to quantitatively assess the relative contributions of autogenous healing and the bacterial agent considered in this thesis. While the agent is expected to promote a more reliable, faster, and more effective recovery, particularly for larger crack widths, the present results only show a more consistent response across the tested specimens under some conditions. Replicated testing at matched healing durations is required to confirm this trend. In addition, although both wet conditions and wet–dry cycles were identified as favourable healing environments, a systematic investigation of healing time and initial crack width is required to fully characterise their combined influence on mechanical recovery.

4.3.2 Aesthetic recovery

Aesthetic recovery was qualitatively assessed through visual inspection of cracked specimens using high-resolution photography and optical microscopy. Two groups of specimens were considered, representative of different crack width regimes. The first group comprised the prisms discussed in the mechanical recovery section (section 4.3.1), which were pre-cracked to a mean residual crack width of approximately 0.07 mm; examples of these fine cracks are presented in Figure 4-14. The second group consisted of specimens fractured to failure and subsequently reassembled using elastic bands, resulting in substantially wider cracks. Immediately after reassembly, the initial surface crack width was estimated by optical microscopy from multiple local measurements, typically five per specimen, taken at randomly selected locations along the visible crack path. The reported value of approximately 0.5 mm represents an indicative mean of these local measurements. Because of the irregular crack geometry and the restraint imposed by the elastic bands, whose tension was not controlled, the apparent crack width may have been influenced by the reassembly procedure. These specimens were used to investigate the visual effectiveness of the bacterial healing agent, with representative images presented separately for wet–dry cycles (1 h wet, 23 h dry at 20 ± 2 °C) (Figure 4-17) and wet conditions (95 ± 5 % RH, 20 ± 2 °C) (Figure 4-18). Consequently, the observations should be interpreted as qualitative evidence of precipitation and surface sealing under restrained conditions rather than as a quantitative measurement of crack-width recovery.

Very fine cracks exhibited rapid visual closure during healing, which influenced their suitability for aesthetic assessment. The specimens pre-cracked to approximately 0.07 mm often showed cracks that were difficult to clearly identify after healing, even when using optical microscopy at relatively high magnification, particularly in lime-rich mortars. In several cases, cracks became visually indistinguishable after approximately 60 days

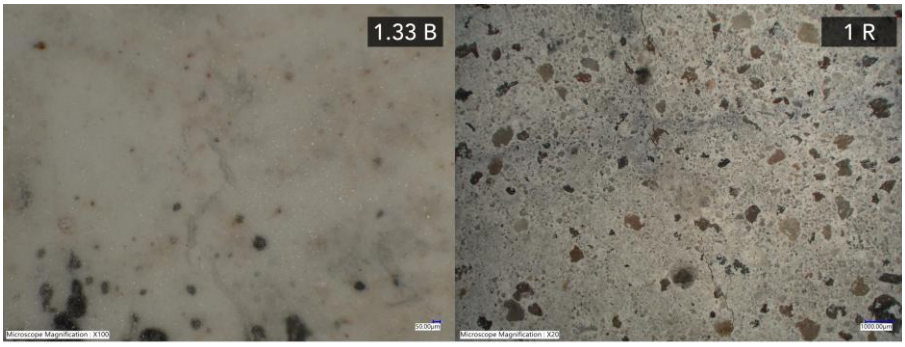


Figure 4-14 Example optical images of fine cracks (mean residual crack width ≈ 0.07 mm) in mortar specimens after 60 days of healing under wet conditions: (a) 3.33 L/C with healing agent; (b) 1 L/C without healing agent.

of healing, especially for compositions with higher lime content, where surface sealing appeared to occur rapidly. While this behaviour is consistent with the mechanical evidence of early stiffness recovery, it limits the use of such fine cracks as a reliable tool to monitor and compare aesthetic healing across different compositions and curing conditions.

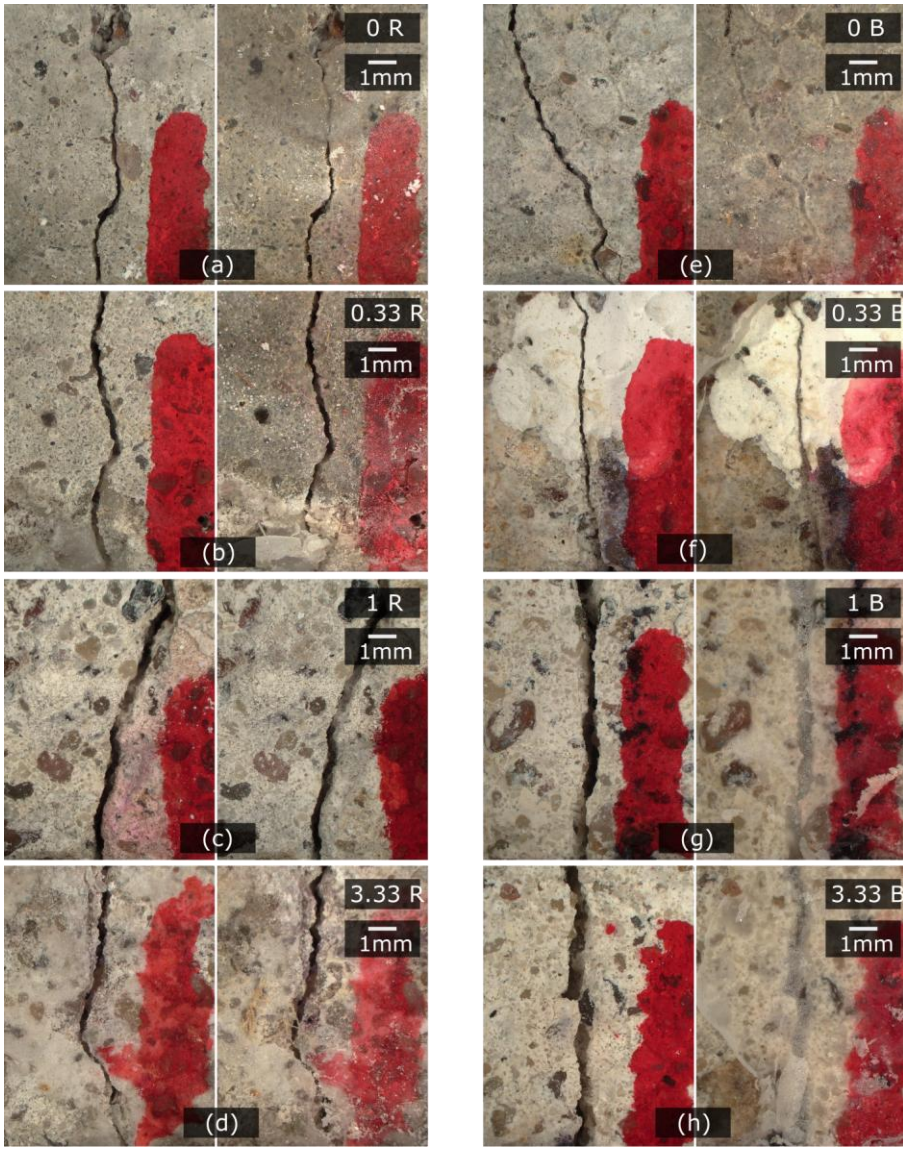


Figure 4-15 Example images showing the pre- and post-healing crack appearance in mortar specimens with large cracks (≈0.5 mm) subjected to wet–dry cycles for 115 days of healing. (a–d) show reference mortar (R) specimens, while (e–h) show bacteria-based mortar (B) specimens, for increasing lime-to-cement (L/C) ratios.

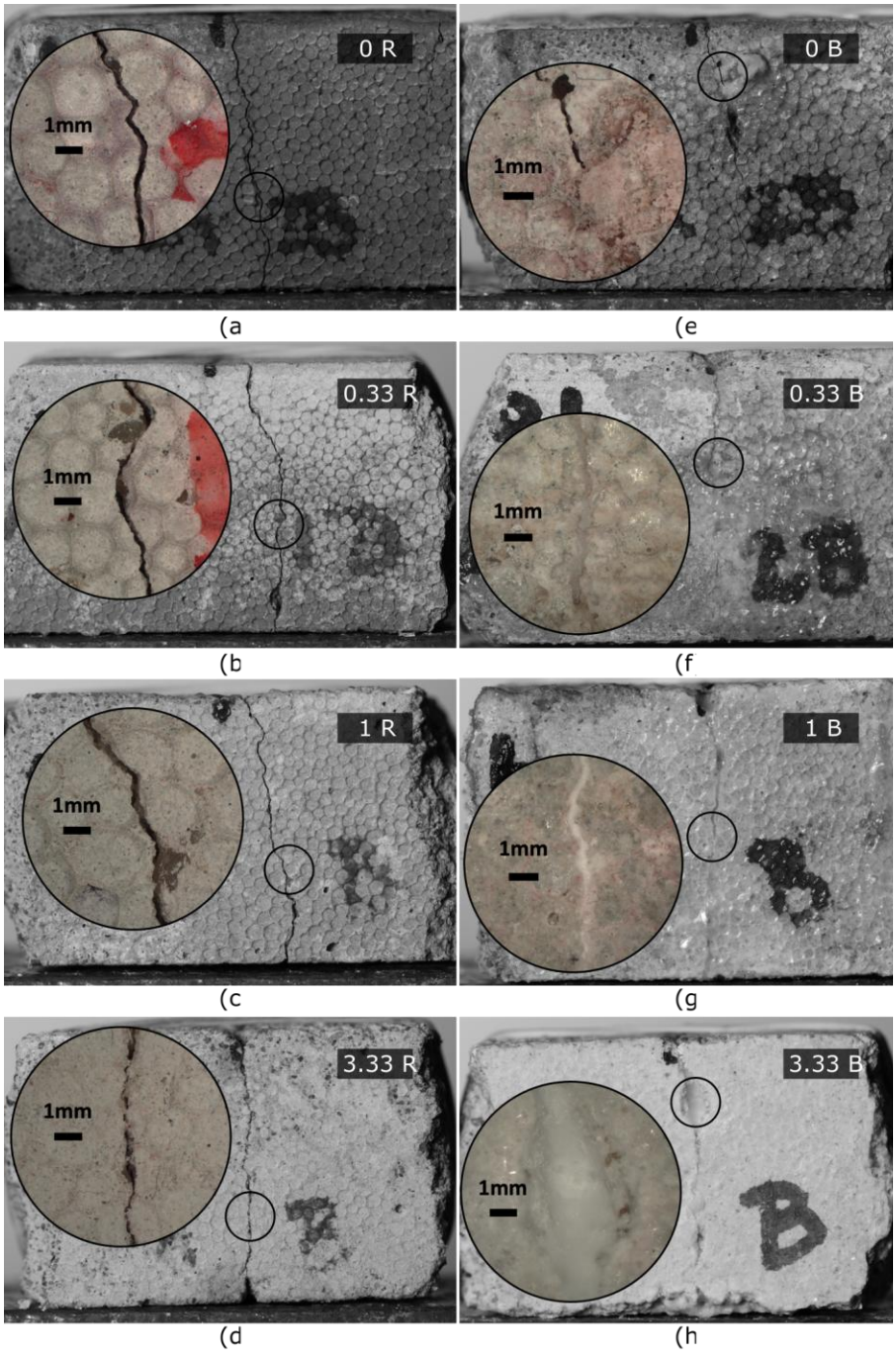


Figure 4-16 Post-healing crack appearance for reference (a–d) and bacteria-based (e–h) mortar specimens with large cracks (≈0.5 mm), after 115 days of healing under wet conditions. Insets provide 30x magnified crack views.

Larger cracks enabled a clearer visualisation of aesthetic healing and highlighted the superior performance of bacteria-based mortars compared to reference ones. For specimens with crack widths of approximately 0.5 mm, a pronounced difference was observed between reference mortars and bacteria-based mortars. After approximately 115 days of healing, specimens containing the bacterial agent exhibited visible crack closure along its length under both wet conditions and wet–dry curing conditions. This effect was particularly evident in lime-rich compositions, which tended to exhibit slightly wider cracks and showed more pronounced precipitation within the crack. In contrast, reference specimens without the healing agent showed little to no visually appreciable crack closure over the same healing period. These visual observations indicate that the aesthetic effectiveness of the bacterial healing agent becomes more apparent at larger crack widths, particularly in lime-rich mortars.

4.4 Identification of healing products

The identification of healing products was carried out using Fourier Transform Infrared Spectroscopy (FTIR). The analysis was performed exclusively on specimens containing large cracks (≈0.5 mm), which allowed material to be selectively sampled from within the crack volume. This approach was adopted to minimise contributions from the surrounding bulk mortar and to focus specifically on the products formed as a result of the healing process. Accordingly, FTIR spectra were acquired from bacteria-based mortars with high lime contents (L/C = 1.0 and 3.33) after 115 days of healing under wet

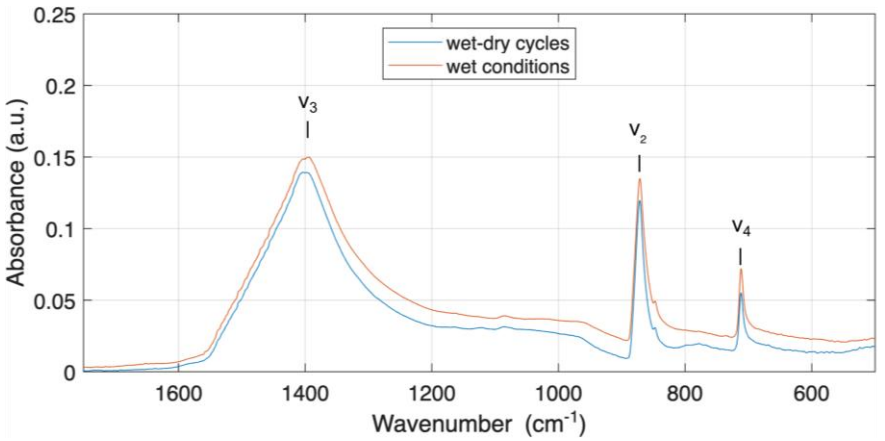


Figure 4-19 FTIR spectra of bacteria-based mortar specimens with high lime content (lime-to-cement ratios of 1.0 and 3.33) after 115 days of healing, cured under wet conditions and wet–dry cycles.

conditions (95 ± 5 % RH, 20 ± 2 °C) and wet–dry cycles (1 h wet, 23 h dry at 20 ± 2 °C). The corresponding spectra are presented in Figure 4-19.

The FTIR spectra exhibit characteristic absorption bands associated with calcium carbonate phases, including the prominent ν_3 asymmetric stretching band around 1400–1450 cm^{-1} and the ν_2 and ν_4 bending vibrations near 870 cm^{-1} and 710 cm^{-1}, respectively, which are commonly attributed to calcite (Wiktor and Jonkers 2011). These features were consistently observed for both curing environments. No distinct absorption bands that could be unambiguously attributed to bacterial cell components or organic compounds were detected. This suggests that the bacteria primarily act as a catalyst or nucleation source for mineral precipitation rather than contributing detectable organic residues to the healed crack. Similar observations have been reported in the literature for bacteria-based self-healing systems, where the healing products are predominantly mineral in nature.

4.5 Impact on functional properties

The impact of the bacterial healing agent on the physical and mechanical properties of the mortar was assessed by comparing bacteria-based mortars with reference mixes of identical composition. Physical properties (bulk density and total water absorption at atmospheric pressure) and mechanical properties (strength, stiffness, and fracture-related parameters) were evaluated across different lime-to-cement (L/C) ratios. The corresponding results are presented in Figure 4-20 and Figure 4-21.

Regarding physical properties, the results indicate that mortar composition remains the dominant factor governing density and total water absorption at atmospheric pressure , with both reference and bacteria-based mortars exhibiting decreasing density

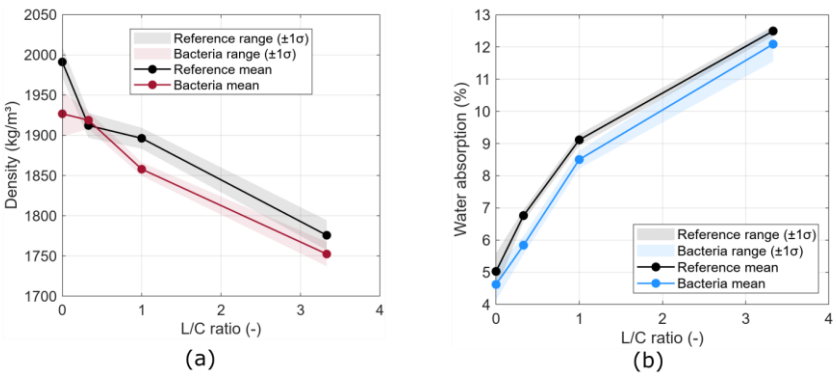


Figure 4-20 Bulk density (a) and water absorption (b) of reference and bacteria-based mortars as a function of the lime-to-cement (L/C) ratio. Mean values and variability ranges (±1σ) are shown.

and increasing total water absorption at atmospheric pressure with increasing lime-to-cement (L/C) ratio (Figure 4-20). The incorporation of the bacterial agent generally resulted in slightly lower values for both parameters. However, these differences were small relative to the experimental variability, limiting the evidence for a systematic influence of the agent. The simultaneous slight decreases in bulk density and total water absorption at atmospheric pressure are not necessarily inconsistent, as the two parameters reflect different characteristics of the mortar. Bulk density depends on both solid-phase density and total void volume, whereas total water absorption at atmospheric pressure primarily reflects water-accessible pores. The observed trend may therefore reflect the combined influence of the lower-density PLA carrier and changes in pore accessibility, potentially involving isolated voids or a local filler effect. However, the present results do not allow these mechanisms to be distinguished, and further characterization of solid-phase density, air content, and pore-size distribution and water absorption kinetics would be required. Overall, the small differences indicate that the bacterial agent had a limited influence on the measured bulk density and total water absorption at atmospheric pressure. Nevertheless, these measurements do not directly characterize moisture transport, and physical compatibility with historical masonry cannot be established from these results alone.

For most mechanical properties, the influence of the bacterial healing agent was found to be composition-dependent rather than uniform across the investigated mixes (Figure 4-21). At low to intermediate lime contents (L/C < 1.0), bacteria-based mortars generally exhibited slightly lower mechanical properties than the corresponding reference mortars. At the highest lime content (L/C = 3.33), however, the mean compressive strength increased from 0.88 ± 0.26 MPa for the reference mortar to 1.69 ± 0.16 MPa for the bacteria-based mortar, corresponding to an increase of approximately 92%. From a practical perspective, the magnitude and composition-dependent nature of these changes demonstrate that the healing agent cannot be treated as a mechanically neutral addition. A mortar formulation selected to be compatible with existing masonry may no longer retain the intended properties after incorporation of the agent. Therefore, compatibility should be assessed using the final bacteria-based formulation, and its composition should be adjusted to achieve the intended mechanical compatibility with the original mortar, brick units, and brick–mortar interface. This approach allows the repair mortar to be designed to preferentially accommodate future damage while preserving the original masonry.

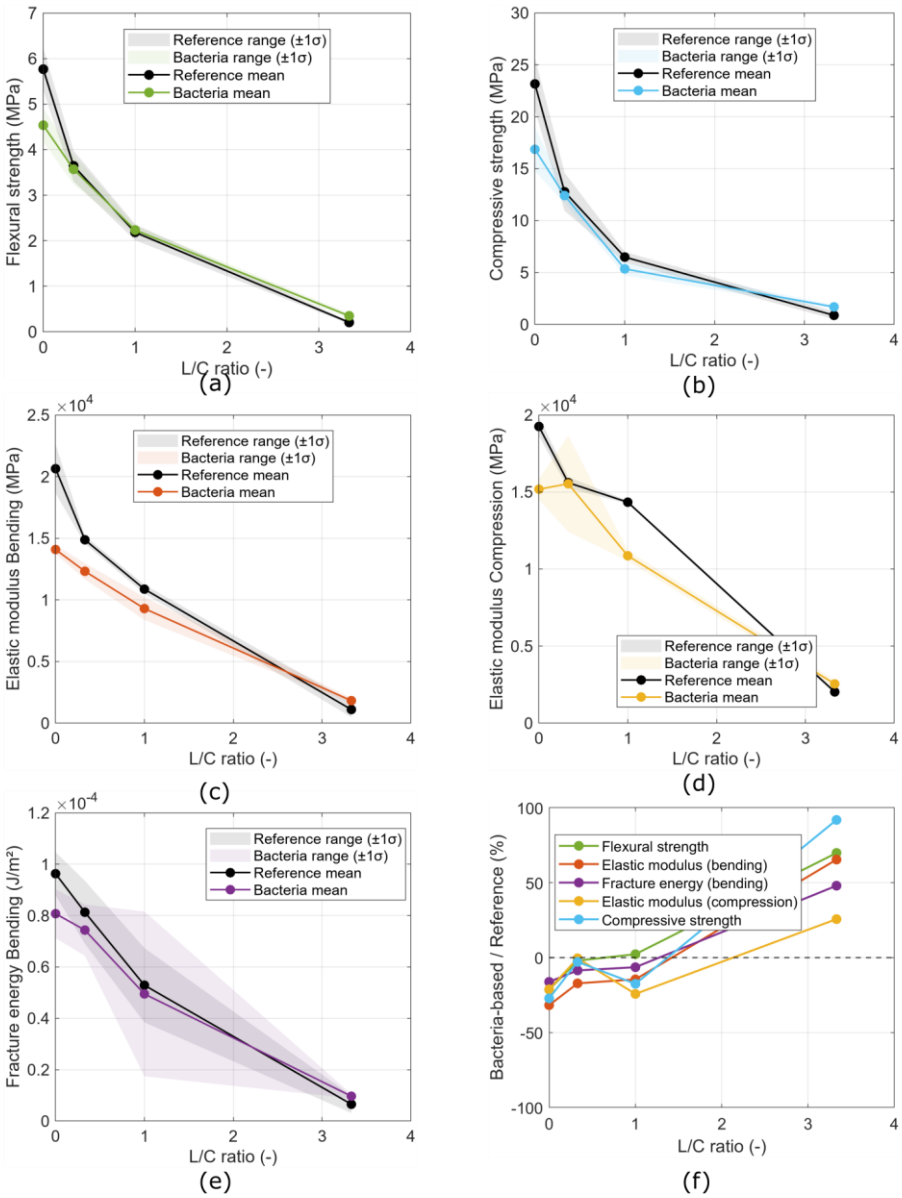


Figure 4-19 Effect of the healing agent on mortar properties: (a–e) strength, stiffness, and fracture energy; (f) mean relative variation of bacteria-based mortars with respect to the reference. Shaded areas indicate ±1 σ.

4.6 Conclusions

This chapter investigated the applicability of the poly-lactic-acid healing agent, originally developed for cementitious systems, to lime–cement mortars relevant for masonry repair. To this end, four mortar compositions were considered, ranging from pure cement to a cement–lime composition suitable for masonry repair in the Netherlands, and three different healing environments, wet conditions (95 ± 5 % RH, 20 ± 2 °C), wet-dry cycles (1 h wet, 23 h dry at 20 ± 2 °C), and moderate-humidity conditions (80 ± 5 % RH, 20 ± 2 °C). The agent's applicability was assessed through a combination of complementary indicators (Chapter 3), including mechanical recovery, aesthetic recovery, identification of healing products, and the evaluation of its influence on relevant functional properties.

Mechanical recovery in lime–cement mortars was confirmed to be a time-dependent process resulting from autogenous mechanisms and agent-related effects. As expected, autogenous healing played a dominant role in lime-rich mortars, particularly in terms of bending stiffness recovery, which developed relatively early due to surface crack sealing. In contrast, flexural strength recovery remained limited and developed more slowly, requiring extended healing periods and remaining partial within the investigated timeframe. Importantly, although the incorporation of the bacterial agent did not systematically increase the average mechanical recovery, it led to a more reliable and consistent response, especially for the lime-rich composition (L/C = 3.33). This reduction in scatter indicates that the agent enhanced the robustness of the autogenous healing process rather than its peak mechanical performance.

The influence of the healing environment was found to be crucial. Continuous wet conditions (20 ± 2 °C, 95 ± 5 % RH) and wet–dry cycles (1 h wet, 23 h dry) both enabled mechanical recovery, whereas moderate-humidity conditions (80 ± 5 % RH, 20 ± 2 °C) did not activate either autogenous or bacterial healing processes. For lime-rich mortars, the bacterial agent contributed to a more uniform recovery response under wet conditions, while under wet–dry cycles it promoted higher average recovery values, albeit with increased variability.

Aesthetic recovery provided additional insight into the role of crack width. Very fine cracks (≈0.07 mm) were found to seal rapidly, limiting their suitability for visual monitoring, whereas larger cracks (≈0.5 mm) enabled a clearer assessment of healing. For these larger cracks, mortars containing the agent consistently outperformed reference mortars, showing pronounced crack filling under both wet conditions and wet–dry conditions. This confirms that the contribution of the agent becomes increasingly relevant as crack width increases, where autogenous healing alone is insufficient to achieve visible crack closure. While cement-based mortars have been reported to heal cracks up to approximately 0.8 mm (Wiktor and Jonkers 2011; Mors and Jonkers 2017), the present results suggest that this threshold may be higher for lime-based systems.

This expectation is linked to the higher availability of calcium hydroxide in lime-based mortars and to the carbonation-enhancing healing mechanism of the bacterial agent. Further research is warranted to establish the maximum crack width that can be effectively healed in such materials.

The identification of healing products by FTIR revealed calcium carbonate as the dominant phase formed within healed cracks, with no distinct bacterial fingerprint detected. Although this phase may also originate from autogenous healing, the absence of visible precipitation in the reference samples indicates that the bacterial agent likely contributed to the observed healing. Accordingly, the results are consistent with the expected carbonation-promoting action of the agent.

The fact that cracks of up to 0.5 mm were found to be completely filled with calcium carbonate precipitates allows for the hypothesis that the agent also restores the watertightness of the mortar. Given the low solubility of calcium carbonate in water, the formation of a continuous mineral phase within the crack is expected to hinder water ingress, which would represent a significant advantage in terms of masonry durability. However, this functional improvement remains an assumption and should be verified at mortar level through dedicated permeability or capillary absorption tests.

Finally, the assessment of physical and mechanical properties showed that the incorporation of the agent does influence the material properties but does not introduce major compatibility concerns. Physical properties were largely governed by mortar composition, with only minor differences between reference and bacteria-based mortars. The effect on mechanical properties was composition-dependent: at low to intermediate lime contents, bacteria-based mortars generally exhibited slightly reduced baseline properties, whereas at high lime content (L/C = 3.33) the agent led to a marked improvement, particularly in compressive strength. These findings underline the importance of considering mortar composition when implementing bacteria-based healing mortars in practice.

Overall, this chapter demonstrates that the PLA-based self-healing agent can be successfully applied to lime-rich mortars, enhancing the healing response without compromising material compatibility criteria for masonry repair in historical construction. While there is still much to be explored at this level, the current findings provide a robust validation of the agent's applicability to lime-based mortars and allow to explore the impact at brick-mortar level in the next chapter.

Chapter 5

Brick-mortal level performance of bacteria-based agent

Building on the mortar-level investigation of the poly-lactic-acid (PLA) bacteria-based healing agent, this chapter evaluates its applicability at the brick–mortar level as defined in Chapter 3. Performance was assessed in terms of mechanical, watertightness, and aesthetic recovery, as well as its effect on relevant functional properties.

Mechanical recovery was explored through flexural bond strength recovery in brick–mortar couplets. The results showed autogenous and autonomous mechanisms, with an inverse relationship between crack width and recovery. Autogenous healing promoted partial recovery for fine cracks, becoming ineffective above 0.1 mm. Conversely, specimens containing the bacterial agent exhibited recovery, averaging ~27% and reaching up to 65%, for crack widths up to ~0.16 mm after 180 days under wet conditions (20±2°C and 95±5% RH).

Watertightness recovery was investigated by measuring water permeability of masonry cores. Recovery remained partial and variable due to large, irregular cracks, highlighting the influence of crack geometry, healing time and the need for controlled crack induction.

Aesthetic recovery was assessed through visual inspection, confirming agent activation and stable precipitation under wet conditions, without evidence of leaching. Characterisation of healing products is required.

Overall, the results confirm the applicability of the PLA-based agent at the brick–mortar level and provide a basis for further investigating at the masonry component level in the next chapter.

The experimental results presented in this chapter are available via the 4TU.ResearchData repository at:

https://doi.org/10.4121/44992ce3-1496-4832-ad42-89eaa28cef5e

The data are distributed under the license type CC BY.

5.1 Introduction

Advancing the study of self-healing strategies for masonry repair, the poly-lactic-acid (PLA)–based healing agent considered in this study has been shown in Chapter 4 to be compatible with cement–lime mortars commonly used in masonry restoration. The results demonstrated that the agent did not introduce adverse effects on mortar properties and successfully activated under wet–dry cycles (1 h wet, 23 h dry at 20 ± 2 °C) and wet conditions (95 ± 5 % RH, 20 ± 2 °C), promoting calcium carbonate precipitation within cracks and leading to crack filling, aesthetic recovery, and partial mechanical restoration. Although the results obtained at the mortar scale are promising, they represent only a first step towards a practical repair solution. To validate the suitability of the agent for masonry restoration, it is therefore essential to extend the investigation to the brick–mortar level, where the interaction between the self-healing material and the brick can be explicitly evaluated.

As explained in Chapter 3, the presence of the brick modifies the porosity of the overall system, potentially changing how the healing agent responds to the healing environment. In this phase, the use of small-scale masonry specimens allows for validation of the healing environment using samples that are still easily handled in a laboratory setting, while being representative for masonry joints actual constructions built with real-size bricks. This step is fundamental to avoid the limitations encountered in previous pilot studies, where wet–dry cycles combined with more porous masonry (as the one built with solid clay bricks and lime-cement mortars) led either to leaching phenomena due to abrupt moisture fluctuations or to a lack of activation caused by excessive water availability (Gaggero et al. 2025). Therefore, this manageable scale provides the necessary flexibility to explore a broader range of environmental conditions if required, ensuring the most effective triggers are identified before moving to larger assemblies.

Following the framework introduced in Chapter 3, the effectiveness of the healing agent at this scale is assessed through a combination of complementary indicators, including mechanical recovery, watertightness, aesthetic restoration, and the evaluation of its influence on relevant functional properties (Figure 5-1). To this end, small-scale masonry specimens were constructed using the cement–lime mortar with the highest lime content investigated in Chapter 4, combined with solid clay bricks representative of those found in historical masonry in the Netherlands. Building on the successful outcomes at the mortar level, wet conditions at 95 ± 5 % RH at 20 ± 2 °C were chosen for this stage. This environment ensures a stable and faster activation of the healing agent, compatible with the experimental setting, while mitigating the risks of leaching and

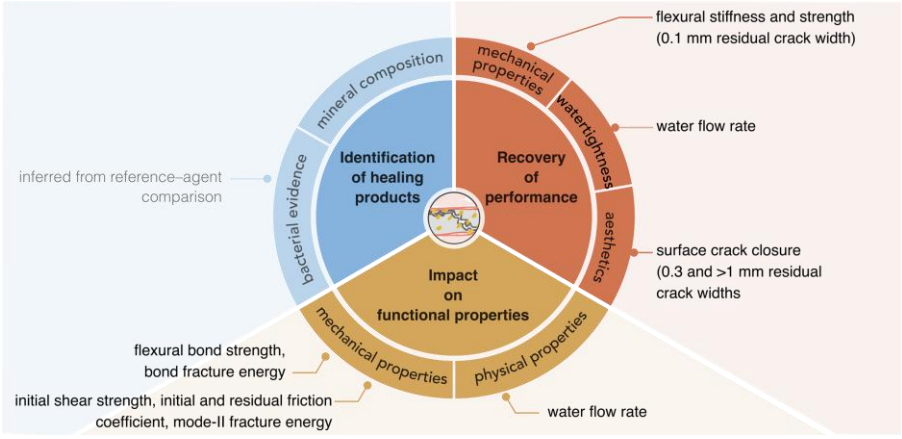


Figure 5-1 Schematic overview of the experimental approach adopted at the brick-mortar level.

inconsistent moisture availability. The following sections describe the materials and methods adopted and discuss the results obtained.

5.2 Materials and methods

5.2.1 Masonry mortars

The cement–lime mortar with a lime-to-cement ratio of 3.33, investigated at the mortar level in Chapter 4, was selected to further investigate the applicability of the healing agent at the brick–mortar interface level. This specific composition was chosen due to its suitability for historical masonry repair in the Netherlands (C. Groot, personal communication). The mortar consisted of Ordinary Portland Cement, commercial hydrated lime, and standard sand, with a cement:lime:sand volumetric ratio of 1.5:5:16 and a water-to-binder ratio of 0.78. The binder–sand proportion and water content were kept identical to those adopted at the mortar level described in Chapter 4, ensuring comparable fresh and hardened properties. Details on the raw materials and mix proportions are reported in Section 4.2.2.

Based on this composition, two mortar types were produced: a reference mortar (labelled as Reference) and a bacteria-based mortar (labelled as Bacteria). The bacteria-based mortar was obtained by incorporating the PLA-based bacteria-containing healing agent (Section 4.2.1) at a dosage of 10% by binder volume. The reference mortar had the same composition but did not contain the healing agent. Apart from the addition of the agent, no changes were introduced with respect to the reference mixture, allowing the effect of the healing agent to be isolated.

All mortar mixtures were prepared by a professional bricklayer in the Netherlands using a handheld mechanical mixer. For both mortar types, the mortar was mixed until a

Table 5-1 Fresh and hardened properties of the investigated mortars. Values are reported as mean ± standard deviation.

mortar	No.	Reference	Bacteria-based
flow (mm)	3	181 ± 11	175 ± 7
compressive strength (MPa)	6	1.74 ± 0.10	2.29 ± 0.19
flexural strength (MPa)	3	0.28 ± 0.02	0.29 ± 0.01

homogeneous and workable consistency was achieved. In the case of the bacteria-based mortar, the PLA-based bacteria-containing healing agent was added once a homogeneous mortar had been obtained, and mixing was subsequently continued for approximately one minute to promote uniform dispersion of the agent.

Three batches were produced to manufacture all specimens. The fresh and hardened properties of the mortars, determined through flow table tests (CEN 1999a) and flexural and compressive tests (CEN 1999b), are reported in Table 5-1. Flow was measured immediately after mixing, while flexural and compressive strengths were determined at 90 days.

5.2.2 Bricks

Solid clay bricks with nominal dimensions of 175 × 40 × 85 mm³ (length × height × thickness) were used to cast the masonry specimens (Figure 5-2(a)). The bricks exhibited a compressive strength of 16.4 MPa, an MIP-accessible porosity of 30.8%, and a median pore-entry diameter of 4.2 µm (corresponding to a pore-entry radius of 2.1 µm). Compressive strength was determined according to EN 772-1 (CEN 2011), while the MIP-accessible porosity and pore-entry size distribution were determined by mercury intrusion porosimetry (MIP) performed on fractured brick samples. The results are presented in Figure 5-2(b) as cumulative intruded pore volume versus pore-entry radius.

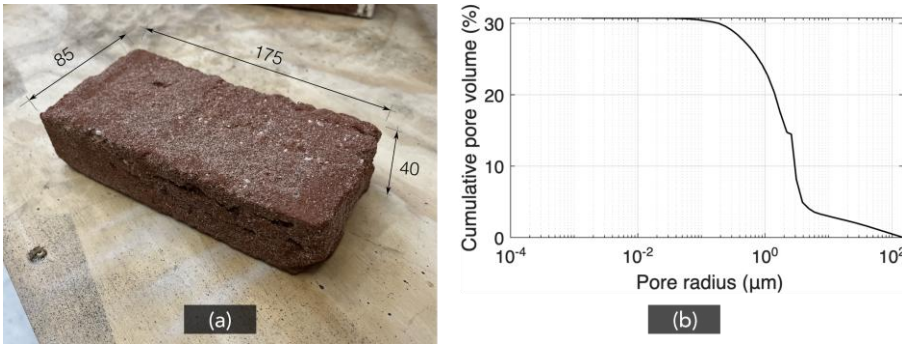


Figure 5-2 Solid clay bricks used in the experimental programme: (a) dimensions in mm; (b) cumulative pore volume versus pore radius determined by mercury intrusion porosimetry (MIP).

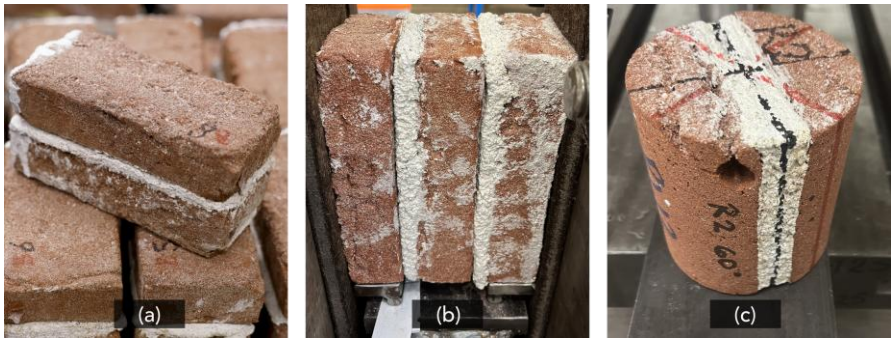


Figure 5-3 Masonry specimen used in the experimental programme: (a) couplets, (b) triplets, and (c) cores extracted from stack prisms.

This brick type was selected to replicate the absorption characteristics of historical clay bricks in the Netherlands, typically characterized by high MIP-accessible porosity (above 25%) and median pore-entry diameters of approximately 5 μm (B. Lubelli, personal communication).

5.2.3 Masonry specimens

Reference and bacteria-based masonry specimens were cast to explore the applicability of the healing agent at the brick–mortar interface level. Three specimen configurations were prepared to address the different experimental tests. Couplets were produced for bond wrench tests to determine both functional properties, healing and aesthetic recovery (Figure 5-3(a)), triplets were cast for shear triplet tests to evaluate functional properties (Figure 5-3(b)), and stack-prism specimens were constructed to extract cylindrical cores for permeability tests (Figure 5-3(c)). From the stack prisms, cores with a diameter of 75 mm were diamond-drilled, ensuring that the brick–mortar interface was included within the extracted specimen.

All masonry specimens were constructed by a professional mason with a nominal mortar joint thickness of 10 mm. After construction, the specimens were covered with plastic sheets to limit rapid water evaporation and to promote uniform curing conditions. Specimens were cured under laboratory conditions and tested after a minimum age of 70 days. Core extraction from the stack prisms was performed at an age of 117 days using a water-cooled drilling system; cores were tested after 100 days after extraction.

5.2.4 Bond wrench tests

Bond wrench tests were performed to evaluate the effect of the agent on masonry's bond behaviour and its performance recovery after cracking. Tests were carried out using a computer-controlled bond wrench set-up, allowing accurate control of the crack opening (Gaggero and Esposito 2023). The experimental set-up is reported in Figure 5-4.

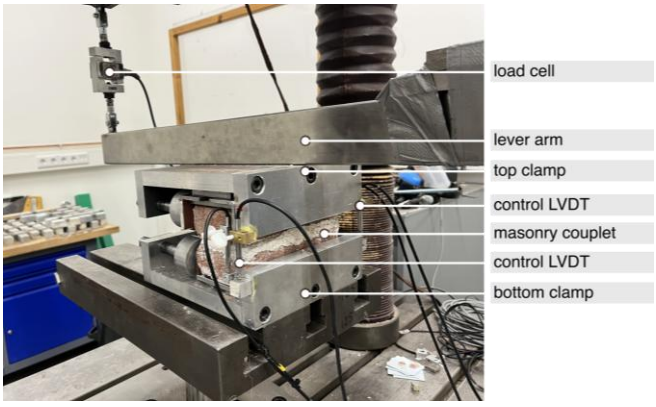


Figure 5-4 CMOD-controlled bond wrench test set-up adopted to evaluate the flexural behaviour of masonry and to generate controlled cracking for subsequent recovery assessment.

The test configuration applies a bending moment to a single brick–mortar interface by means of a lever arm clamped to the top brick while the bottom brick is restrained. Loading was applied under crack mouth opening displacement (CMOD) control, defined as the average displacement measured between the top and bottom clamps using two Linear Variable Differential Transformers (LVDTs). The load was applied using a hydraulic jack with a capacity of 250 kN and measured by a 5 kN load cell. The load was applied at a rate of 0.002 mm/s and data was recorded every 0.1 s. In addition, two LVDTs were mounted on the tension face of the specimen to directly measure the opening of the induced crack, allowing the residual crack width after unloading to be determined and used as the initial crack width for healing. All LVDTs had a measuring range of ± 1 mm and accuracy of ± 0.001 mm.

Two sets of 10 couplets per specimen type were tested to characterise both types of masonries and assess the effect of the healing agent on the flexural bond behaviour. The first set was tested until failure after 70 days of hardening, while the second set was tested after 200 days of hardening. Within this second set, half of the specimens were loaded up to a target CMOD of 0.1 mm, while the remaining half were loaded up to a target CMOD of 0.3 mm. After testing, the specimens were left to heal under the conditions detailed in Section 5.2.7 and, after completion of the healing period, retested under the same configuration to assess mechanical recovery. Figure 5-5 shows a representative example of a couplet tested up to a target CMOD of 0.1 mm, including the response measured during the first test and the subsequent re-test after healing, reported in terms of CMOD measured by LVDTs attached to the couplet and vertical displacement of the jack.

To evaluate the effect of the healing agent, flexural bond strength and the associated fracture energy were calculated from bond wrench tests. Flexural bond strength was

determined for undamaged specimens in both test series. Fracture energy, however, was calculated only for the first series, since only those specimens were loaded up to complete failure. The following equations were used to compute both parameters:

$$f_w = \frac{F_{max}\, e_1 + F_a\, e_a - \frac{2}{3} d \left(F_{max} + F_a + \frac{P}{4} \right)}{\frac{b\, d^2}{6}} \tag{20}$$

$$G_{f_w} = \frac{W}{A} \tag{21}$$

where F_{max} is the maximum force registered during the test by the load cell, F_a is the normal force as a result of the weight of the bond wrench apparatus, P is the weight of the masonry brick pulled off the specimen and any adherent mortar, e_1 is the distance from the applied load to the tension face of the specimen, e_a is the distance from the centre of gravity of the clamp to the tension face of the specimen, b and d is the mean length of the bed joint and the mean width of the bed joint respectively, W is the area underneath the force versus vertical displacement of the jack is considered and A is the fracture surface, i.e. the cross-section of the tested interface.

For the evaluation of mechanical recovery, flexural bond force was used as the reference parameter, since the specimens were not loaded to complete failure during the pre-cracking stage. A recovery parameter was therefore defined based on the flexural bond force, accounting for the residual capacity of the cracked specimens before healing. recovery was assessed by considering both the undamaged and residual properties. Using undamaged values as the sole reference would neglect the

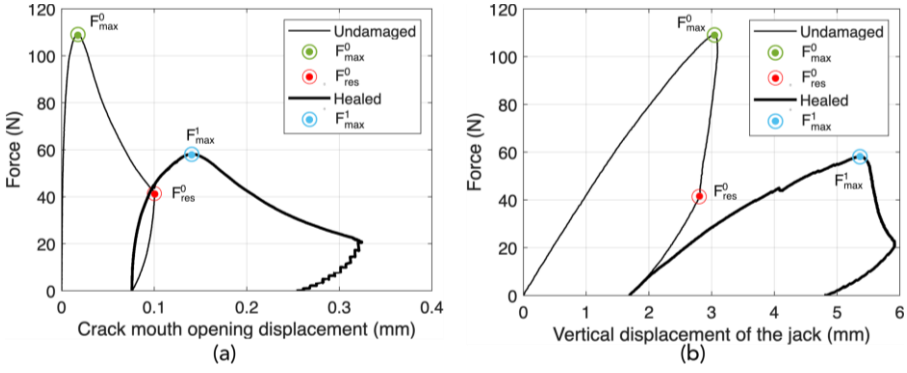


Figure 5-5 Bond wrench test response of a couplet loaded up to a target CMOD of 0.1 mm: comparison between the initial test and the re-test after healing. The response is reported in terms of (a) crack mouth opening displacement (CMOD), measured by LVDTs attached to the couplet, and (b) vertical displacement of the loading jack.

contribution of residual post-cracking strength and may therefore lead to an overestimation of recovery. Accordingly, a recovery parameter was defined as follows:

$$R_{Fw} = \frac{F^{1}_{max} - F^{0}_{res}}{F_{max}{}^{(avg)} - F^{0}_{res}} 100 \quad (22)$$

where F^{1}_{max} is the maximum flexural bond force measured after healing, F^{0}_{res} is the residual flexural bond force measured at the end of the pre-cracking stage prior to healing and $F_{max}{}^{(avg)}$ is the mean of the peak flexural bond force recorded during the first loading cycle (F^{0}_{max}). The average peak force was preferred over the single F^{0}_{max} because the brittle response of the couplets leads to large scatter in the peak load, and averaging limits the risk of artificially inflated recovery values (e.g., apparent recoveries exceeding 100%).

5.2.5 Water permeability test

Water permeability tests were performed on masonry cores to evaluate the effect of the agent on permeability properties of masonry, and its healing capacity in restoring permeability. As no standardised water permeability test is available for masonry, the test procedure was adapted from constant-head permeability tests commonly used in self-healing concrete research. The experimental set-up is reported in Figure 5-6.

A constant hydraulic pressure corresponding to a 1 m water column, equivalent to approximately 0.1 bar, was applied to the specimens, while the water flow through the specimens was continuously measured over time. The specimens consisted of cylindrical cores with a diameter of 75 mm, containing a single brick–mortar interface. Each specimen was fixed at the bottom of the water column and placed inside a rigid PVC pipe. A rubber sheet and adjustable couplings were used to seal the specimens and prevent lateral leakage, ensuring that water flow occurred exclusively through the

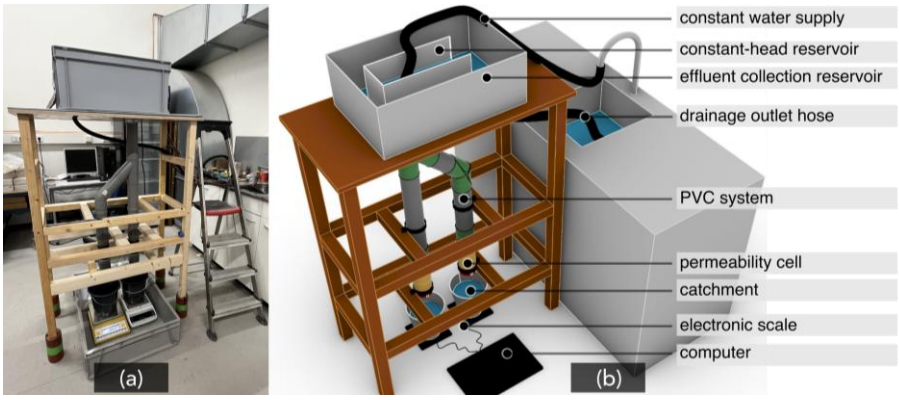


Figure 5-6 Experimental set-up for water permeability testing: (a) overall view of the test rig; (b) schematic illustration highlighting the main components.

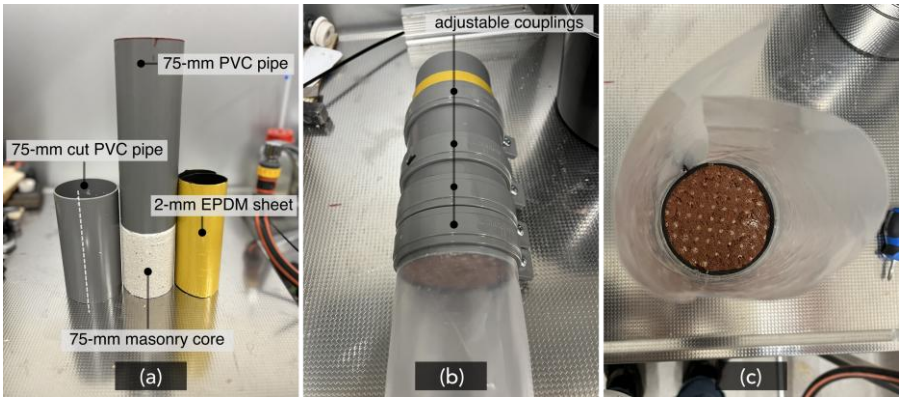


Figure 5-7 Permeability cell: (a) main components; (b) assembled configuration using adjustable couplings; (c) bottom view showing the EPDM-wrapped core inside the pipe.

exposed cross-sectional area (Figure 5-7). The effectiveness of the sealing system was verified by testing fully sealed specimens, for which no measurable water flow was detected. Water was supplied from a constant-head reservoir and applied vertically to the top surface of the specimen. During testing, the water level in the column was kept constant to ensure stable hydraulic pressure. The discharged water was collected at the bottom in a container placed on an electronic scale connected to a computer.

During the test, the cumulative discharged water was recorded as a function of time, and the flow rate was calculated for each specimen and used as an indicator of permeability. The corresponding flow rate was subsequently calculated for each specimen as the derivative of the cumulative discharge curve with respect to time and used as an indicator of permeability. Figure 5-8 illustrates an example of measured cumulative discharged water and the derived flow rate.

Tests were performed on undamaged specimens, cracked specimens, and cracked specimens subjected to healing conditions. To avoid potential activation or wash-out of the healing agent due to repeated water exposure, different specimen sets were used for each condition, with eight specimens per condition. For cracked and healed specimens, a shear-sliding crack was generated at brick-mortar interface by performing splitting tests on core with different joint orientations with respect to the loading direction, e.g. (Sassoni and Mazzotti 2013; Jafari et al. 2020). This approach was originally conceived to allow the evaluation of shear behaviour and, where possible, the subsequent assessment of both watertightness and mechanical restoration on the same specimens. However, due to the limited number of specimens available, this combined assessment could not be fully implemented, and core specimens were used to evaluate solely watertightness recovery, while conventional triplet tests were performed to assess shear functional properties at brick-mortar interface. In this context, watertightness recovery was quantified using the following formula:

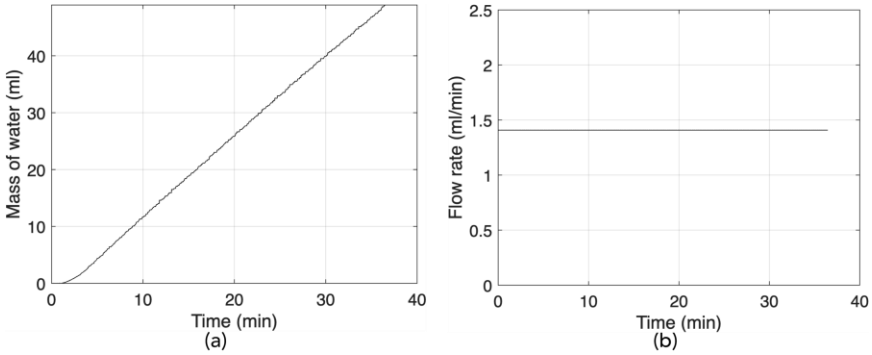


Figure 5-8 Example of water permeability test result: (a) cumulative discharged water versus time and (b) flow rate derived from (a).

$$R_{WT} = \frac{Q_{cracked}^{(avg)} - Q_{healed}}{Q_{cracked}^{(avg)}} \tag{23}$$

where $Q_{cracked}^{(avg)}$ is the average flow rate measured on cracked specimens and Q_{healed} is the flow rate measured after healing.

5.2.6 Shear triplet tests

Shear triplet tests were performed to evaluate the effect of the healing agent on the shear behaviour of masonry. Test were performed in accordance with EN 1052-3 (CEN 2002) using the set-up shown in Figure 5-9.

The specimens were tested under constant transverse pre-compression, while a shear load was applied to the central masonry unit. Three pre-compression levels were investigated (0.2, 0.6, and 1.0 N/mm²), with three specimens tested per level. Transverse pre-compression was applied perpendicular to the bed joints using a manual

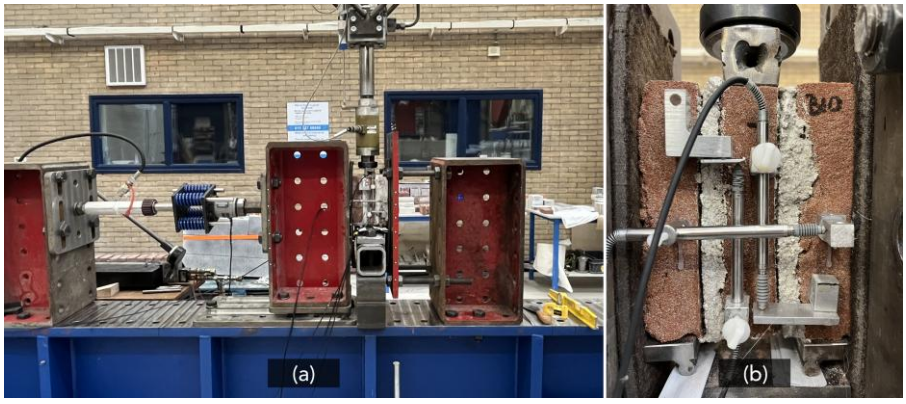


Figure 5-9 Shear triplet test set-up adopted to evaluate the effect of the self-healing agent on shear properties of masonry.

hydraulic jack and kept constant (±2%) throughout the test by means of a spring system. Springs with stiffnesses of 15, 60, and 115 N/mm were used for pre-compression levels of 0.2, 0.6, and 1.0 N/mm², respectively. Shear loading was applied under displacement control using a 100 kN hydraulic jack. Relative displacements were monitored with LVDTs mounted on both faces of the specimen to characterise peak and residual shear behaviour. On each face, two vertical LVDTs and one horizontal LVDT were installed to measure, respectively, the relative sliding of the central brick with respect to the two lateral bricks and the normal deformation of the specimen (Figure 5-9 (b)). All LVDTs had a 10 mm measuring range and an accuracy of ±0.001 mm. The displacement rate was 0.005 mm/s, and data were recorded at 1 s intervals.

Shear strength and pre-compressive stress were calculated from the applied loads and the cross-sectional area of the specimen. The mode-II fracture energy was evaluated by excluding the contribution of frictional sliding and was therefore computed as the area under the shear force–sliding curve up to the onset of the residual plateau (U). Once a friction-dominated sliding regime had developed, residual shear properties were quantified. At this stage, the transverse pre-compression was increased stepwise and maintained constant at each level, allowing the residual shear strength to be determined at multiple pre-compression levels on the same specimen. The relationships between shear strength and pre-compressive stress were then used to derive both peak and residual shear parameters by means of a linear Coulomb-type formulation.

In most tests, the shear response exhibited two distinct peak loads, reflecting the non-simultaneous failure of the two brick–mortar interfaces within the triplet specimen (Figure 5-10). The first peak (F_v^I) corresponded to the mobilisation of shear resistance along a single interface, whereas the second peak (F_v^{II}) was associated with the mobilisation of both interfaces. Accordingly, the shear strength corresponding to the first

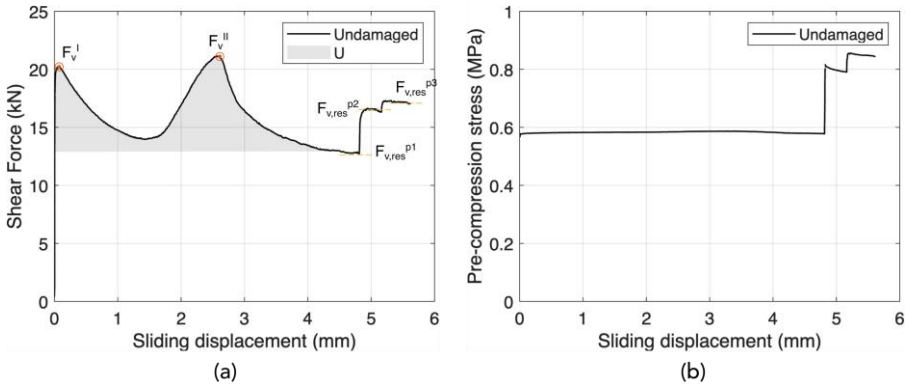


Figure 5-10 Example of shear triplet test result: (a) shear force and (b) pre-compression stress against the sliding displacement.

peak was calculated using the cross-sectional area of a single interface, while the second peak was evaluated considering the combined area of both interfaces.

5.2.7 Healing environment

After cracking, masonry specimens were stored under wet conditions in a moist room at 20 ± 2 °C and 95 ± 5 % relative humidity for 180 days to promote healing. Although both wet conditions and wet–dry cycles proved effective at the mortar level (Chapter 4), only continuous wet conditions were adopted here. Pilot investigations at the brick–mortar scale showed that wet–dry cycles may result in leaching of healing products or inactivation of the healing agent when used in solid clay brick masonry built with cement–lime mortars.

After the designated healing period, specimens were removed from the healing environment and allowed to dry to constant mass under laboratory conditions prior to re-testing. Mechanical and watertightness recovery was subsequently evaluated through retesting, following the same procedures adopted for the initial mechanical characterisation.

5.2.8 Visual inspection

Visual inspection was used both to monitor the healing process over time and to qualitatively assess the aesthetic recovery after healing. Immediately prior to (re)testing, the healed state was documented using a portable digital USB microscope (50–1600× magnification, 8× LED illumination).

5.3 Performance recovery

5.3.1 Mechanical recovery

The mechanical recovery of couplets was assessed by evaluating the restoration of flexural bond force after 180 days of healing under wet conditions at 20 ± 2 °C and 95 ± 5 % relative humidity. The 180-day healing period was selected as a compromise between consistency with the tests performed at the mortar level (tested after 60, 120 and 210 days of healing, showing increasing recovery with time) and the constraints of the experimental schedule. Couplets were pre-cracked through CMOD-controlled bond wrench tests to target crack openings of 0.1 mm and 0.3 mm, which resulted in residual crack widths to be healed of approximately 0.065 mm and 0.16 mm, respectively. Residual crack widths were measured using the LVDTs attached on the tension face of the specimen. Both reference specimens and specimens containing the PLA-based healing agent were considered. Specimens loaded until complete failure were not included in the recovery analysis, as no mechanical recovery was observed for either reference or bacteria-based specimens. In these cases, cracking was characterised by very large and highly irregular openings, which prevented any measurable restoration.

Figure 5-11 summarises the recovery results, expressed as the percentage of recovered flexural bond force with respect to the pre-cracking reference value. The results are presented as a function of the initial crack width (Figure 5-11(a)) and grouped into two representative crack-width ranges (Figure 5-11(b)). The dashed lines shown in Figure 5-11(a) are included to provide a qualitative indication of the overall trends.

Before delving into the results, it should be noted that, for the masonry investigated, cracking developed predominantly within the mortar joint rather than at the brick–mortar interface (the reader is referred to section 5.5). This condition can be regarded as favourable for self-healing, as both sides of the crack consist of mortar with inherent autogenous healing capacity and, in the case of bacteria-based specimens, also with autonomous healing potential provided by the bacterial agent. This should not be interpreted as implying that effective healing is restricted to this configuration, as pilot studies (Gaggero et al. 2024) have demonstrated that the healing agent can also be activated for cracks located at the brick–mortar interface. However, due to the different material properties across the crack, healing in such configurations may be expected to develop more slowly and to be potentially less effective. Consequently, the results discussed below are representative of cracks developing within a mortar joint.

An inverse relationship between initial crack width and mechanical recovery can be observed for both materials in Figure 5-11(a). As crack width increases, the recovered bond force decreases, reflecting the increasing difficulty of restoring mechanical continuity within wider cracks for a fixed healing period. In addition, a clear difference of performance between reference and bacteria-based specimens can be observed. The reference specimens exhibit a steep decay in recovery with increasing crack width: for cracks exceeding approximately 0.1 mm, recovery rapidly drops to negligible values, indicating that autogenous healing alone becomes ineffective. In contrast, specimens containing the bacterial healing agent show a lower rate of decay. With the exception of a single specimen, all bacteria-based specimens display measurable recovery across the investigated crack-width range. In particular, for cracks approaching 0.16 mm, recovery values between 10% and 65% are observed, demonstrating that the agent effectively extends the healable crack-width range beyond that achievable by autogenous mechanisms alone. This behaviour is consistent with observations from the preliminary experimental study carried out prior to this thesis on a commercialised cement-based mortar containing the same healing agent, where recovery decreased with increasing crack width but remained systematically higher than that of the reference specimens (Gaggero et al. 2024).

The boxplot representation in Figure 5-11(b) further highlights the effect of the healing agent by grouping the results into the two crack widths explored. For fine cracks (≈0.065 mm), reference and bacteria-based specimens exhibit comparable behaviour. Mean recovery values are nearly identical, averaging approximately 45% for the reference

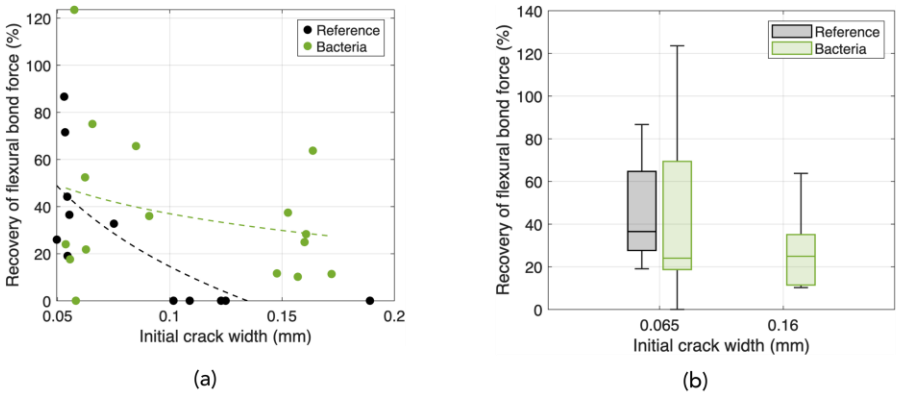


Figure 5-11 Mechanical recovery of flexural bond force after 180 days of healing under wet conditions. (a) Recovery percentage as a function of initial crack width. (b) Boxplot comparison of recovery grouped by crack width range, highlighting the enhanced performance of the self-healing mortar in cracks larger than 0.1 mm.

mortar and 46% for the bacteria-based mortar. This indicates that, for very narrow cracks, autogenous healing mechanisms are sufficient to promote partial bond recovery. For wider cracks (≈0.16 mm), the difference becomes pronounced. The reference specimens showed no recovery, confirming the limited capacity of autogenous healing for cracks beyond 0.1 mm. In contrast, the bacteria-based specimens consistently exhibit recovery, with a mean value of approximately 27%, despite some scatter. This demonstrates that the bacterial agent becomes particularly effective in the crack-width range where autogenous healing fails.

Regardless of the healing agent performance, these results underline the role of the targeted crack width and healing duration in experimental design. While autogenous healing in masonry specimens remains largely unexplored and warrants further investigation, the present results indicate that larger crack widths exceeding the range where autogenous healing is active are needed when the aim is to isolate and quantify the contribution of the healing agent. Otherwise, the measured recovery may be largely governed by autogenous mechanisms, masking potential agent-related effects. Given that autogenous healing depends on the material composition, identifying the crack-width range governed by autogenous mechanisms is a necessary step to define the lower bound for crack selection, while systematic exploration of the upper crack-width limit is required to determine the damage threshold beyond which neither autogenous nor autonomous healing can provide mechanical recovery. Finally, the present results are based on a single healing duration of 180 days. While this timeframe was sufficient to reveal clear differences between reference and bacteria-based specimens, extending the experimental programme to multiple healing intervals would be valuable to characterise healing kinetics at the brick–mortar interface and to assess whether higher,

or potentially complete, mechanical recovery can be achieved with longer healing periods and perhaps even for wider crack widths.

5.3.2 Watertightness recovery

The recovery of watertightness was assessed by measuring the water permeability of masonry cores in the undamaged, cracked, and healed conditions. Separate specimen groups were tested in the cracked and healed conditions. For each healed specimen, watertightness recovery was estimated by comparing its flow rate with the mean flow rate of the corresponding independently tested cracked group. Figure 5-12 summarises the main quantitative results, illustrating the flow-rate distributions of the cracked and healed groups and the corresponding estimated watertightness recovery grouped by specimen type. The undamaged values, which exhibited median flow rates of about 0.08 mL/min, are reported in Section 5.5 and were omitted from Figure 5-12(a) because their substantially lower magnitude prevents their clear visualisation on the adopted scale.

Crack induction led to a pronounced increase in water permeability for both reference and bacteria-based specimens. On average, the water flow increased by approximately one order of magnitude, rising from about 0.8 mL/min in the undamaged condition to around 4 mL/min in the cracked state. In addition, a significant dispersion of results was observed, probably attributed to the process for crack induction: cores were tested until failure and subsequently manually reassembled, resulting in relatively large and irregular crack openings. Crack widths varied considerably, ranging approximately from 0.1 mm up to 1.3 mm, making it difficult to define a representative average value. Notably, the bacteria-based group exhibited a slightly higher median water flow in the cracked state compared to the reference group, suggesting that the induced cracks in these specimens may have been more severe or hydraulically more conductive. Nevertheless, comparable overall ranges indicate that similar damage levels were generally achieved in both groups.

After the healing period, the group-level distributions did not show a systematic reduction in water flow: the median remained approximately unchanged for bacteria-based specimens and increased for reference specimens (Figure 5-12(a)). However, when each healed specimen was compared with the mean flow rate of the corresponding cracked group, partial watertightness recovery was estimated for both specimen types, albeit with substantial scatter. The bacteria-based specimens exhibited an extremely wide variability in recovery, ranging from negligible values up to nearly 90%. In this context, it should be emphasised that only about half of the healed specimens in each group exhibited a flow rate below the corresponding cracked-group mean, making it difficult to draw definitive conclusions regarding the effectiveness and consistency of the recovery process. This interpretation is further limited by the variability in the induced

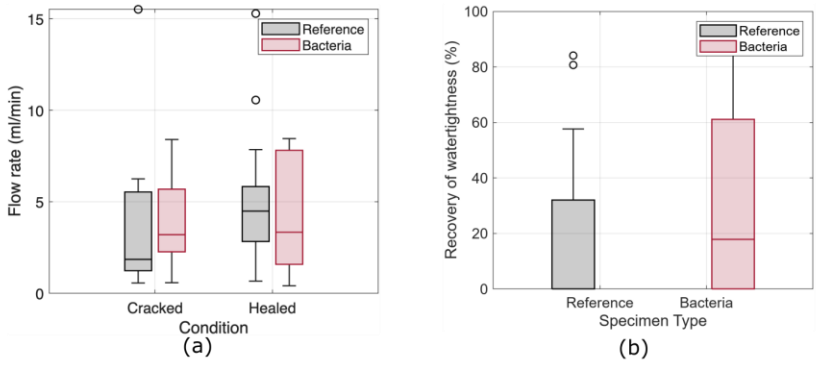


Figure 5-12 Water permeability test results in terms of: (a) water flow rates measured in the independently tested cracked and healed specimen groups; and (b) estimated watertightness recovery of each healed specimen, calculated relative to the mean flow rate of the corresponding cracked group. Undamaged flow rates are reported in Section 5.5 and omitted from (a) because of their substantially lower magnitude. Open circles indicate outliers.

crack geometries, as the cracked and healed groups comprised different specimens and cannot be assumed to have experienced equivalent initial damage.

These results are consistent with the visual inspection presented in the following section, which shows that healing was localised rather than uniform along the crack path. This localisation explains the absence of full recovery of water tightness: local sealing of preferential flow paths can reduce permeability to some extent, but incomplete crack filling limits the overall effectiveness of the recovery, particularly for large and irregular crack openings.

To enhance the effectiveness and consistency of healing, future investigations should consider inducing damage without cutting the specimens to complete failure and repeating the permeability tests under more controlled crack-opening conditions. Nevertheless, the adopted test configuration proved suitable for assessing water tightness recovery in bacteria-based masonry systems. Despite the inherent variability associated with irregular crack geometries, the experimental set-up is simple and allows for a clear comparison between reference and bacteria-based specimens, making it a practical tool for evaluating healing performance.

5.3.3 Aesthetic recovery

Aesthetic restoration at the brick–mortar interface was qualitatively assessed through visual inspection using a portable digital microscope. Two crack-width regimes were considered: (i) fine cracks generated during bond wrench tests, with residual widths of approximately 0.16 mm or smaller, and (ii) larger cracks obtained from fully broken and manually reassembled masonry cores, originally prepared for watertightness restoration tests.

For small cracks (≤ 0.16 mm), the assessment of aesthetic recovery proved challenging. As illustrated in Figure 5-13, cracks in this range were often difficult to clearly identify after healing, irrespective of the presence of the healing agent. This limitation is primarily related to the combination of small crack widths and the use of a portable microscope, which, while suitable for in situ observations, provides limited depth of field and contrast compared to laboratory-based optical systems. In addition, due to the inherent surface roughness and irregularity of the masonry specimens, cracks were frequently located slightly below the exposed surface, further complicating focusing and visual interpretation. Similar limitations were also observed at the mortar scale (Chapter 4), where fine cracks became difficult to visually assess after healing. Taken together, these observations reinforce the conclusions drawn from the mechanical recovery results, indicating that the use of larger crack widths is more appropriate when the objective is to clearly evaluate the contribution of the healing agent.

For larger cracks, obtained from fully fractured cores that were manually reassembled prior to healing, visual inspection revealed localised precipitation within the crack region (Figure 5-14). These cracks were characterised by a highly irregular geometry, with strongly variable apertures along their length and local crack widths often above 1 mm. Under these conditions, neither reference specimens nor specimens containing the bacterial healing agent exhibited complete crack closure. Instead, precipitation was observed only in discrete zones. The lack of continuous crack filling qualitatively explains why full restoration of watertightness was not achieved in these specimens and the large scatter of results.

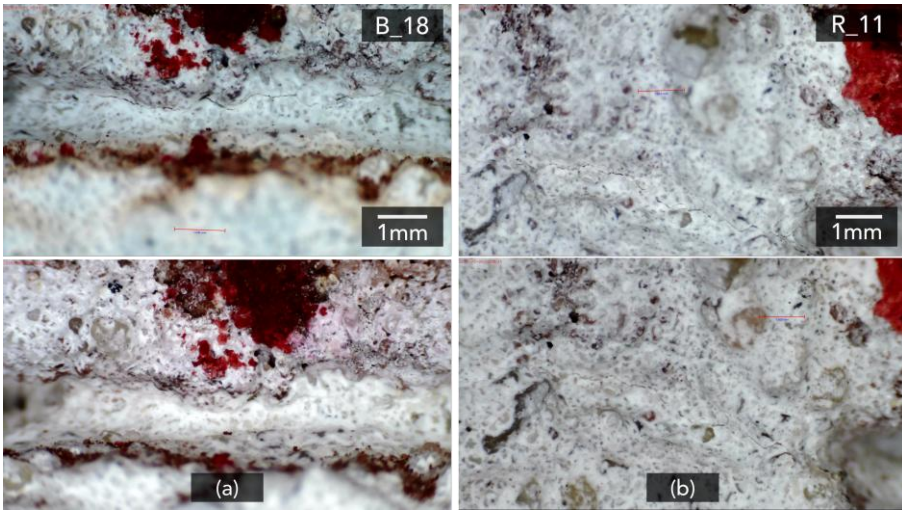


Figure 5-13 Portable microscope images of fine cracks in masonry couplets before (top) and after (bottom) healing under wet conditions: (a) bacteria-based specimen (B_18) and (b) reference specimen (R_11).

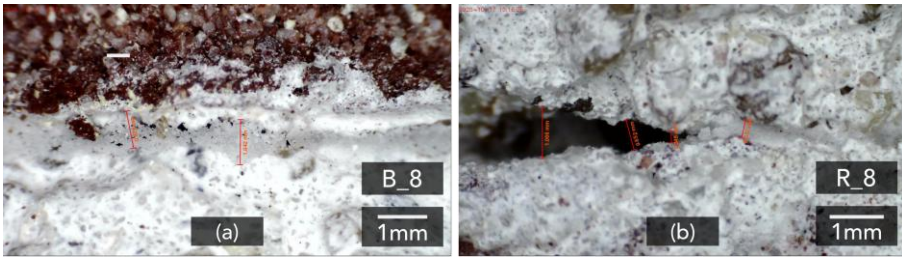


Figure 5-14 Portable microscope images of large, irregular cracks in fully broken and manually reassembled masonry cores after healing: (a) bacteria-based specimen (B_8) and (b) reference specimen (R_8).

Although full aesthetic restoration was not achieved for these large and irregular cracks, no evidence of leaching or surface wash-out of the precipitated material was observed during visual inspection. This indicates that the healing agent was effectively activated and that the formed products remained stable under the selected healing environment. In this respect, healing under continuous wet conditions (95 ± 5 % RH, 20 ± 2 °C) appears to represent a suitable alternative to wet–dry cycles for masonry made of porous solid clay bricks and lime-based mortar, differently than previous studies where leaching phenomena were reported. (Gaggero et al. 2024).

These results highlight the importance of adopting controlled cracking strategies for laboratory studies, rather than fully fractured and manually reassembled specimens, when evaluating performance recovery. In addition, given the surface irregularity of masonry specimens, residual crack widths larger than 0.1 mm are preferable, as they allow a more reliable visual assessment of aesthetic restoration. This threshold (~0.1 mm) also represents the practical lower limit for reliable visual crack detection on the tested surfaces (Korswagen 2024). The role of healing time also warrants further investigation, as longer exposure periods may influence the extent and continuity of precipitation.

5.4 Identification of healing products

The identification of healing products at the brick–mortar level was considered as part of the performance assessment; however, practical limitations related to crack geometry and material availability constrained detailed characterisation. For masonry cores containing large cracks, obtained from fully fractured and manually reassembled specimens, the amount of precipitated material observed within the crack was limited and spatially discontinuous (Figure 5-14). As a result, it was not possible to collect a sufficient quantity of precipitate for reliable chemical characterisation. For couplets containing fine cracks, sampling of healing products was also not feasible due to the following. Due to the very small crack widths involved, selective collection of material

from within the crack without simultaneously removing surrounding mortar was not possible. Any attempt to sample material from these cracks would therefore have resulted in a mixed sample dominated by bulk mortar, rather than the actual healing products of interest, preventing meaningful interpretation.

Despite these limitations, visual inspection did not reveal any evidence of leaching, suggesting proper activation of the healing agent under the applied healing conditions. In addition, healing performance was consistently assessed through direct comparison with reference specimens, thereby excluding the contribution of autogenous healing. On this basis, it can be hypothesised that the observed effects are attributable to the proper activation of the healing agent.

Nevertheless, direct experimental verification of the nature of the healing products remains necessary. Future studies would benefit from adopting testing configurations that enable the formation and controlled sampling of larger, more accessible cracks, allowing selective characterisation of precipitated material. Such analyses would provide direct confirmation of the chemical composition of the healing products.

5.5 Impact on functional properties

The effect of the bacterial healing agent on the functional performance of brick–mortar specimens was investigated by comparing reference and bacteria-based specimens with respect to shear behaviour, flexural behaviour, and permeability. For the masonry configuration adopted in this study, no systematic differences in failure mode were observed between reference and bacteria-based specimens. For both, failure was predominantly observed to occur within the mortar for triplets and couplets, indicating a cohesive failure mechanism, whereas cores more frequently exhibited failure along the brick–mortar interface. Overall, these observations indicate that the selected materials and construction procedure achieved a high-quality brick-mortar interface. Figure 5-15 illustrates representative failure patterns observed for the different specimen types. Figure 5-16 and Figure 5-17 summarise the main quantitative results, which are discussed below.

The shear test results show that the presence of the bacterial healing agent does not lead to significant changes in the shear response. As shown in Figure 5-16(a) and (c), the residual shear strength and the fracture energy associated with shear behaviour remain essentially unchanged for reference and bacteria-based specimens across the investigated pre-compression levels (0.2, 0.6 and 1 MPa). The friction coefficient and

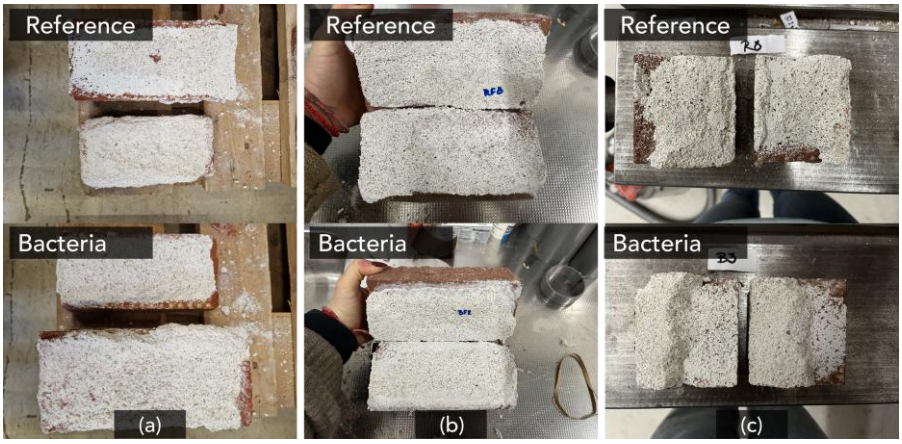


Figure 5-15 Representative failure modes observed in (a) triplets, (b) couplets, and (c) cores for both reference and bacteria-based specimens.

cohesion show some variation between reference and bacteria-based specimens, with differences below 20%. This variation, however, remains within the inherent scatter typically associated with masonry materials; in the present study, the coefficient of variation of the shear-related parameters ranges between 6% and 32%, depending on the parameter considered and the applied pre-compression level. Accordingly, the shear results show that the bacterial healing agent does not introduce changes in shear properties.

In contrast to the shear behaviour, the flexural response of couplets shows a clear increase for those containing the bacterial healing agent. As shown in Figure 5-16 (b) and (d), the flexural bond strength and the associated fracture energy are consistently higher for bacteria-based specimens compared to the reference. It should be noted that failure occurred predominantly within the mortar rather than at the brick–mortar interface for both types of couplets, indicating a cohesive failure mechanism. This suggests that the addition of the agent significantly enhances the mechanical performance of the mortar itself, rather than affecting the brick-mortar bond. This observation is consistent with the characterisation at the mortar level presented in Chapter 4, where mortars containing the bacterial agent exhibited higher flexural strength and fracture energy (Figure 4-21 (a), (e)) compared to the reference.

The observed increase in the flexural bond properties of the mortar, and consequently in the flexural behaviour of the couplets, may be attributed to a combination of factors, as discussed below. Although the same water content was used for both reference and bacteria-based mortars, slight differences were observed in fresh-state properties, such as flow (Table 5-1). However, considering the inherent variability of flow measurements, these differences cannot be conclusively attributed to the presence of

the healing agent. Previous studies investigating the same healing agent in cement-based materials have reported its potential influence on air content (Tziviloglou 2018), which could in turn affect bond strength. This is consistent with the lower bulk density observed in mortar specimens built with the bacteria-based mortar (Figure 4-20(a)). At the same time, the healing agent is introduced as a fine granular material without direct

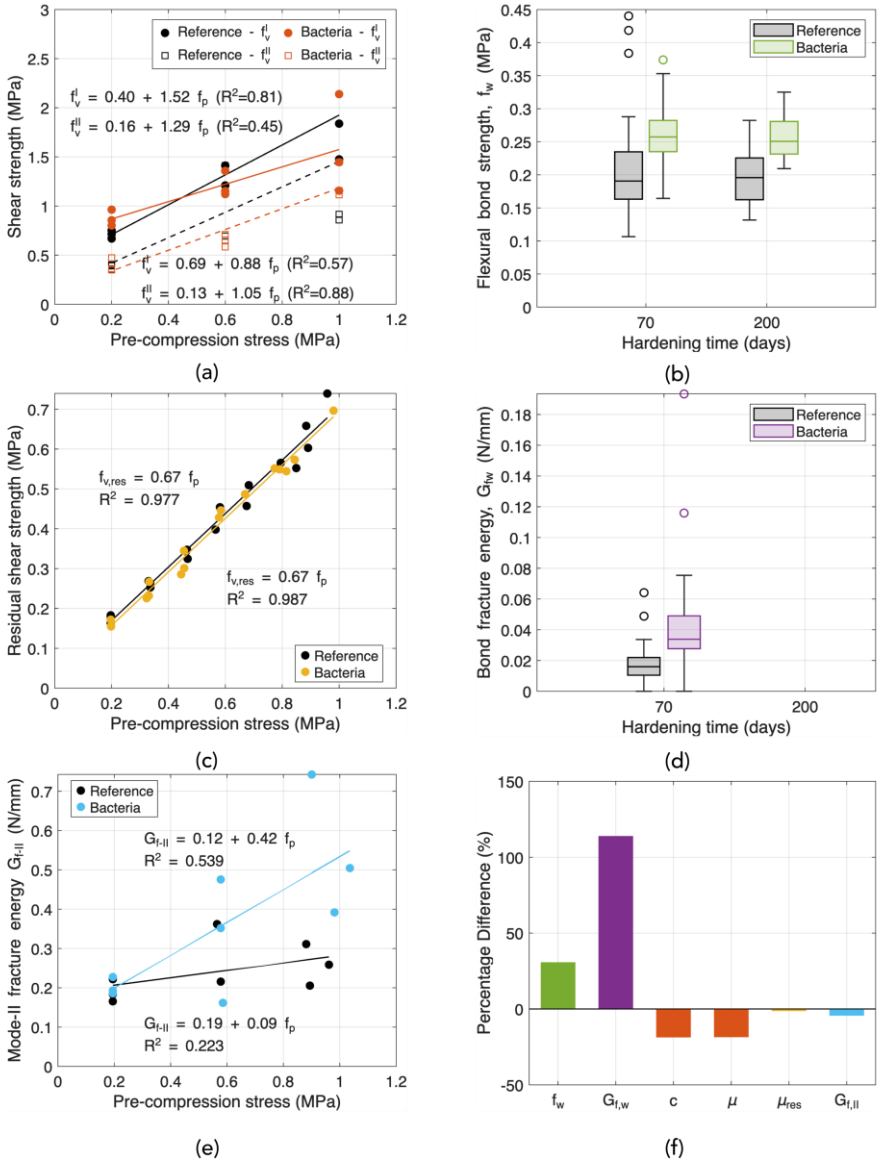


Figure 5-16 Effect of the healing agent on functional properties of brick-mortar interface behaviour: (a,c,e) shear behaviour; (b,d) flexural bond behaviour; (f) mean relative variation of bacteria-based specimens with respect to reference specimens.

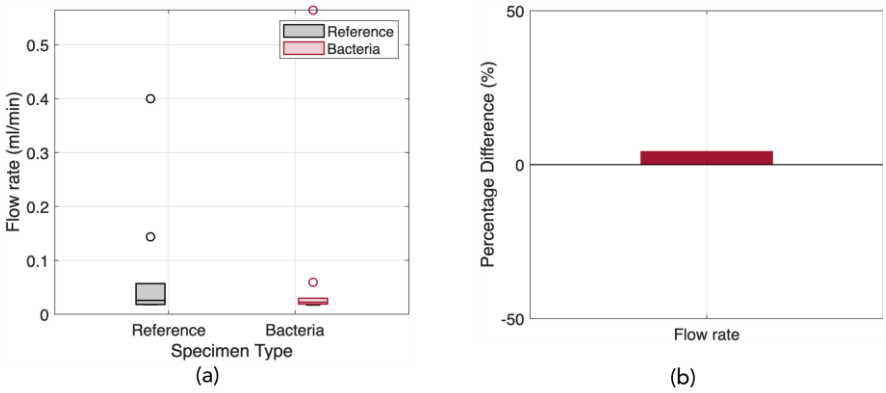


Figure 5-17 Effect of the healing agent on masonry permeability: (a) flow rate values obtained on undamaged specimens; (b) mean relative difference of bacteria-based specimens with respect to the reference.

substitution of sand and may therefore locally act as a filler. This is evidenced by the reduction in open porosity observed in water absorption tests (Figure 4-20(b)), suggesting a more refined pore structure. Regardless of the specific contribution of these mechanisms, the observed increase in flexural bond strength of 31% does not raise concerns in terms of applicability, with failure remaining predominantly within the mortar. By acting on the mortar composition, properties can be tuned to achieve the desired performance while maintaining mechanical compatibility with existing masonry materials, which is a key requirement for repointing applications.

The comparison between different hardening ages indicates that, for the masonry configuration considered, a curing period of approximately 70 days is sufficient to reach a stable flexural bond strength. No systematic increase is observed at later ages, suggesting a limited sensitivity of the interface bond strength to further material ageing within the investigated timeframe. This observation implies that the mechanical recovery measured through bond wrench tests is unlikely to be affected by ongoing material curing beyond this period. Nevertheless, the inclusion of undamaged specimens tested at corresponding ages remains advisable to explicitly account for potential ageing effects.

Despite the observed enhancement in flexural bond behaviour, this improvement does not translate into a reduction in water permeability. As shown in Figure 5-17, differences in water flow between reference and bacteria-based specimens remain below 5%. Since permeability is governed by the interconnectivity of the pore network, these results suggest that the capillary structure of the mortar and the brick-mortar interface is not affected by the inclusion of the agent.

To further assess the effect of the healing agent, additional characterisation would be beneficial. Future research could incorporate Mercury Intrusion Porosimetry (MIP) to verify if the agent promotes a refinement of the microstructure without altering the critical

pore diameter responsible for hydraulic transport. Furthermore, sorptivity and water vapor permeability tests could provide additional evidence regarding the impact of the agent on capillary suction and moisture breathing capacity, to ensure hygrothermal compatibility when repointing.

5.6 Conclusions

This chapter investigated the applicability of a poly-lactic-acid (PLA) healing agent at the brick–mortar level, moving beyond the mortar scale addressed in the previous chapter and towards a more representative masonry configuration. Following the framework presented in Chapter 3, the performance of the agent was assessed through mechanical, watertightness, and aesthetic recovery, as well as its impact on relevant functional properties of the interface.

Mechanical restoration was addressed as a first performance indicator, allowing the respective contributions of autogenous and autonomous healing mechanisms to be distinguished. The results clearly demonstrate that mechanical recovery of couplets is strongly governed by crack width, with a pronounced inverse relationship between the initial crack opening and the degree of recovery. For very fine cracks (≈0.065 mm), autogenous healing mechanisms alone proved sufficient to restore approximately 45% of the flexural bond force, resulting in comparable recovery levels for reference and bacteria-based specimens. However, once crack widths exceeded approximately 0.1 mm, autogenous healing became ineffective and mechanical recovery in reference specimens rapidly dropped to negligible values. In contrast, specimens containing the bacterial healing agent consistently exhibited measurable mechanical recovery within this wider crack-width range. For cracks approaching 0.16 mm, recovery values averaged approximately 27% and reached up to 65%, demonstrating that the autonomous healing system effectively extends the healable crack-width range beyond the limits of autogenous mechanisms. While recovery remained partial and exhibited some scatter, these results provide clear experimental evidence that the agent enables mechanical restoration at damage levels where conventional masonry mortars are no longer able to self-repair.

The assessment of watertightness and aesthetic recovery provided further insights into the effectiveness and limitations of the healing process. Although the bacterial agent was successfully activated, as indicated by localised precipitation within the crack region and a reduction in water flow observed in approximately half of the tested specimens, complete sealing was not achieved for large and highly irregular cracks exceeding 1 mm. The wide variability in permeability recovery, ranging from negligible values up to approximately 90%, highlights that recovery of watertightness is currently constrained by crack geometry and by the discontinuous nature of precipitation along the crack path.

Nevertheless, visual inspection confirmed that wet conditions promote healing without leaching, suggesting that the selected healing environment is suitable for solid clay masonry built with lime-based mortars.

Analysis of the functional properties indicated that the incorporation of the bacterial healing agent does influence the mechanical behaviour of the brick–mortar system, but without introducing adverse effects. The inclusion of the agent did not alter the initial water permeability of undamaged specimens, as reflected by comparable water flow values between reference and bacteria-based samples. However, while the shear response remained largely unchanged, the flexural bond strength and fracture energy showed a significant increase in bacteria-based specimens. These effects should therefore be regarded as parameters to be considered when studying the agent in the context of repointing applications, where mortar composition is typically tailored to achieve mechanical properties compatible with those of the existing masonry. In this sense, the observed influence of the agent highlights the need to account for its contribution when designing bacteria-based repointing mortars, rather than representing a limitation.

Finally, this research highlights critical methodological considerations for future studies on bacteria-based self-healing masonry mortar. The results indicate that experimental designs aiming to isolate the contribution of a healing agent must target crack widths larger than 0.1 mm to surpass the threshold governed by autogenous healing. Accordingly, undamaged specimens cured and stored under the same conditions should be included as parallel controls to quantify time-dependent effects alone, given the relatively short curing period adopted for the laboratory specimens. In addition, the permeability test configuration adopted in this study proved suitable for detecting changes in watertightness and for comparing reference and bacteria-based specimens. However, the large scatter observed in the results clearly indicates that crack induction must be more tightly controlled when the objective is to understand, within a limited healing period, how crack geometry governs permeability and its recovery. Although irregular and discontinuous cracks are representative of field conditions, using more controlled crack geometries in laboratory studies facilitates interpretation by reducing geometric variability and enabling cause–effect relationships to be identified. With longer healing periods, the influence of crack irregularity on the measured recovery may become less critical, as precipitation and sealing may progressively develop along a larger portion of the flow paths. Furthermore, while the 180-day healing period successfully revealed differences in performance, additional investigation into healing kinetics and the chemical characterisation of precipitates is required to fully substantiate the long-term mechanical and hydraulic restoration of the brick–mortar interface.

Chapter 6

Masonry component level performance of bacteria-based agent

Building on the investigation of the poly-lactic-acid (PLA)-based healing agent at the mortar and brick-mortar levels, this chapter evaluates its applicability at the masonry component level, following the framework introduced in Chapter 3. The agent's performance was assessed through qualitative indicators of recovery (aesthetics), identification of precipitated products, and evaluation of its influence on mechanical and in-plane flexural properties.

To this end, masonry spandrels and compression wallettes were constructed using the materials and protocol from Chapter 5. The experimental programme showed that specimens containing the healing agent exhibited leaching after curing, which became more pronounced after the healing and drying phases. The identified precipitates confirmed the agent's migration and incorrect functioning, while the extensive leaching impaired the masonry's functional properties, specifically its aesthetics. Without meeting these two framework criteria, assessing mechanical recovery was deemed unjustifiable.

The observed migration does not imply that the agent is inherently unsuitable for masonry applications. Rather, it indicates that the adopted curing procedure was inadequate to retain the soluble compounds within the mortar at this larger scale. While this issue emerged during laboratory investigation, it may also be relevant for real applications, where moisture gradients and drying conditions could similarly promote migration. The results therefore underline the need for adapted curing and healing protocols that ensure retention of the healing agent within the mortar, both for laboratory and practical implementation.

The experimental results presented in this chapter are available via the 4TU.ResearchData repository at:

https://doi.org/ 10.4121/0c988fd2-5d18-4e4f-9d65-3a3a2c7fff6a

The data are distributed under the license type CC BY.

6.1 Introduction

In view of demonstrating the applicability of autonomous self-healing mortars for masonry repair, the poly-lactic-acid (PLA)–based healing agent investigated in this thesis has shown promising performance at the first investigation levels defined by the framework in Chapter 3. At the mortar level (Chapter 4), the agent activated under wet conditions (95 ± 5 % RH, 20 ± 2 °C) and wet–dry conditions (1 h wet, 23 h dry at 20 ± 2 °C), promoting calcium carbonate precipitation and leading to crack filling and aesthetic recovery without compromising compatibility with cement–lime mortars. Subsequently, at the brick–mortar level (Chapter 5), the agent enabled measurable recovery in terms of flexural bond strength and watertightness under wet conditions, providing a sound basis for further validation in more representative masonry configurations.

As explained in chapter 3, placing multiple bricks in a certain bond pattern brings the system closer to real composite masonry and may alter the interaction with the healing environment by changing exposed surfaces and transport paths. In addition, component-level testing allows to study cracking patterns that are more representative of those in actual masonry elements, while still maintaining a manageable experimental setup that allows controlled damage, monitored healing, and repeatable testing. In this way, this level provides an intermediate validation step that helps bridge smaller-level evidence and the requirements of more representative applications.

In this chapter, the applicability of the PLA-based healing agent is investigated at the masonry component level, i.e. in larger-scale composite brick-joint assemblies arranged in a specific bond pattern. Following the framework proposed in Chapter 3, recovery was

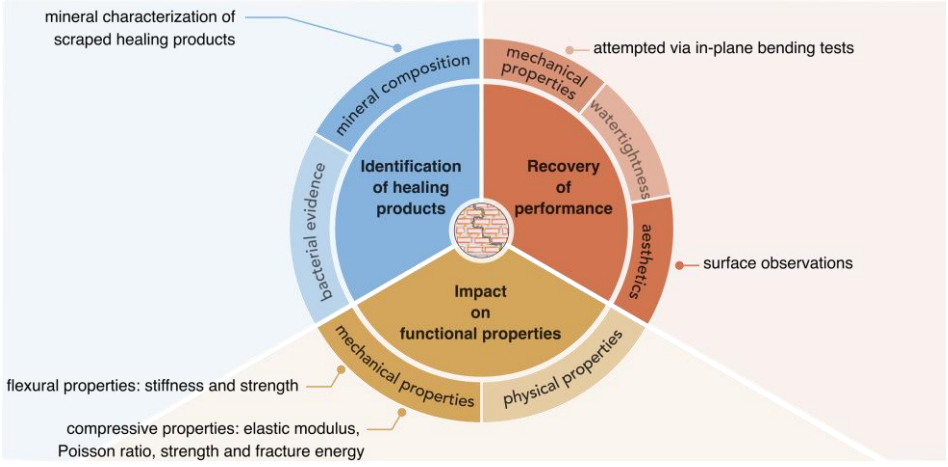


Figure 6-1 Schematic overview of the experimental approach adopted at the masonry component level.

assessed qualitatively in terms of aesthetics, complemented by characterisation of precipitates and evaluation of the agent's influence on functional properties (Figure 2-1). To this end, masonry spandrels and compression wallettes were built using the same materials and workmanship adopted in Chapter 5. Building on the outcomes obtained at the previous level, wet conditions were selected for this stage. The following sections describe the materials and methods adopted and discuss the results obtained.

6.2 Materials and methods

6.2.1 Masonry materials and specimens

To ensure comparability across the different levels of investigation, the materials used in this chapter are identical to those investigated at the brick–mortar level in Chapter 5. Detailed specifications for the solid clay bricks (175×40×85 mm^3) and the cement–lime mortar (lime/ cement ratio of 3.33) can be found therein. Consistent with previous chapters, two mortar types were produced: a reference mixture and a bacteria-based mixture incorporating 10% by binder mass of the poly-lactic-acid (PLA) healing agent, described in 4.2.1.

The specimens were built by the same professional mason and during the same construction period as those presented in Chapter 5, using materials from the same production batch and identical construction procedures, ensuring consistent workmanship and material properties. The construction procedure followed the same protocol, featuring 10 mm thick mortar joints. The experimental programme involved the construction of three compression wallettes and five spandrels per mortar composition (totalling six compression wallettes and ten spandrels) in running bond. The geometry and dimensions of the specimens are detailed in Figure 6-2(b) and (c), respectively. The

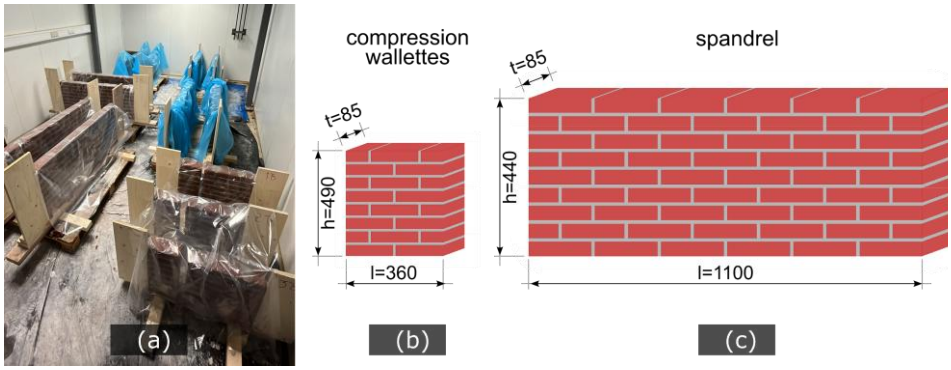


Figure 6-2 Specimen construction: (a) view of the masonry specimens covered with plastic foils during the curing stage; geometry and dimensions of (b) the compression wallettes and (c) of the spandrels (dimensions in mm). The masonry thickness (t = 85 mm) is dictated by the selected brick, which was chosen to replicate the porosity of historic buildings in the Netherlands.

Table 6-1 Mix design of the investigated mortars.

Mortar	Reference	Bacteria-based
flow (mm)	174 ± 5	174 ± 6
compressive strength (MPa)	1.41 ± 0.22	2.49 ± 0.24
flexural strength (MPa)	0.12 ± 0.01	0.26 ± 0.02

resulting masonry thickness of 85 mm was dictated by the dimensions of the selected brick. As described in Section 5.2.2., the brick type was selected as the closest available match to the porosity characteristics of historical clay bricks in the Netherlands. To manufacture all specimens, the mortar was mixed in seven separate batches. The fresh and hardened properties of the mortars, determined through flow table tests (CEN 1999a) and flexural and compressive tests (CEN 1999b), are reported in Table 2-1.

Immediately after construction, all specimens were covered with plastic foil to prevent rapid moisture loss and stored until testing in their as-built vertical orientation in an enclosed laboratory space (Figure 6-2(a)). Spot measurements during the storage period indicated ambient conditions of approximately 22 °C and 45% RH. Surface deposits were first observed upon removal of the foil immediately before testing, although their exact time of formation could not be determined.

Compression wallettes were tested at 50 days in accordance with the procedure described in Section 1.2.2., to characterise the functional compressive properties once the mortar had reached sufficient maturity. Spandrels were tested at 240 days following the procedure described in Section 1.2.3., as the bending programme was scheduled after completion of the brick–mortar level investigation reported in Chapter 5. The difference in testing age therefore reflects the experimental programme sequence.

6.2.2 Compression tests on wallettes

Compression tests were performed to evaluate the effect of the healing agent on the compressive properties of masonry. Test were performed in accordance with EN 1052-1 (CEN 1998) and ASTM E111(2017), using the set-up shown in Figure 6-3. Before testing, a thin gypsum capping layer was applied to the loading faces to ensure a uniform distribution of the compressive load.

Tests were performed using a 300 kN hydraulic jack in displacement control. The jack applied the load by lifting a steel loading plate (active side), while a passive steel plate was located at the top of the specimen. A hinge placed between the load cell and the top plate was used to reduce potential eccentricities during loading. The load was applied at a rate of 0.005 mm/s to ensure reaching the maximum stress within 15 to 30 minutes, and data were recorded every 0.5 s. To determine the modulus of elasticity, the compressive load was applied in three equal increments until half of the probable maximum load was reached. After each increment, the load was held constant for 2 min

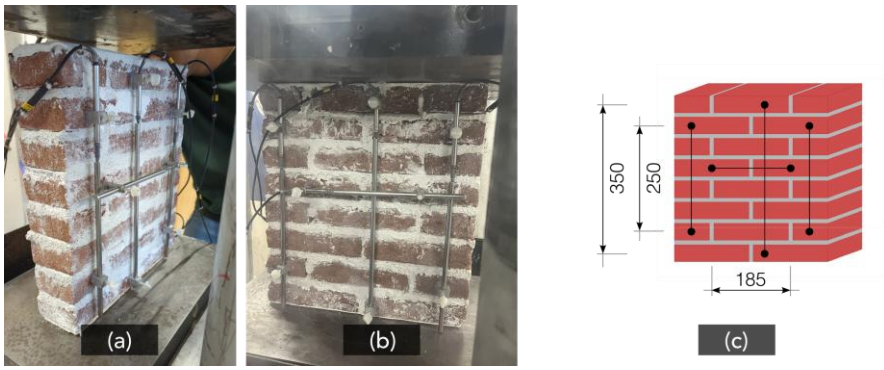


Figure 6-3 Experimental setup for compression tests: (a) back view and (b) front view; (c) sensor layout (dimensions in mm).

± 1 min. After completion of the last step, loading continued up to failure. Figure 6-4(a) and (b) shows an example of the applied loading rate (jack displacement) and the corresponding force–time response, respectively.

Each specimen was instrumented with vertical and horizontal Linear Variable Differential Transformers (LVDTs) to record axial and transverse deformations. The sensor layout and length are reported in Figure 6-4(c). The same layout was used on the front and back faces of the specimen, resulting in a total of eight LVDTs (four per face). On each face, three vertical LVDTs were used to measure axial deformation: two (10 mm range) were mounted near the left and right edges of the specimen, and a third one (2 mm range) was positioned at the centre of the face. In addition, one horizontal LVDT (2 mm range) was placed at mid-height to record transversal deformation. The accuracy of the LVDTs was ±1 μ m.

Compressive strength (f'_m), elastic modulus (E_3) and compression fracture energy ($G_{f\text{-}c}$) were derived from the experimental results. Compressive stress was calculated from the measured load and the specimen cross-sectional area, while axial strain was computed from the vertical LVDT readings by dividing each measured displacement by its corresponding sensor's initial length (Figure 6-4(c)). For strain evaluation, the readings from the four LVDTs with identical gauge length (two per face, positioned near the specimen edges) were averaged. An example of stress–strain curve is shown in Figure 6-4(c). Accordingly, the compressive strength was calculated as:

$$f'_m = \frac{F_{max}}{t\,l} \tag{24}$$

where F_{max} is the maximum force recorded during the test, t and l are the specimen thickness and length, respectively. The elastic modulus was evaluated as the chord modulus between 1/10 and 1/3 of f'_m on the stress-strain curve following the prescriptions

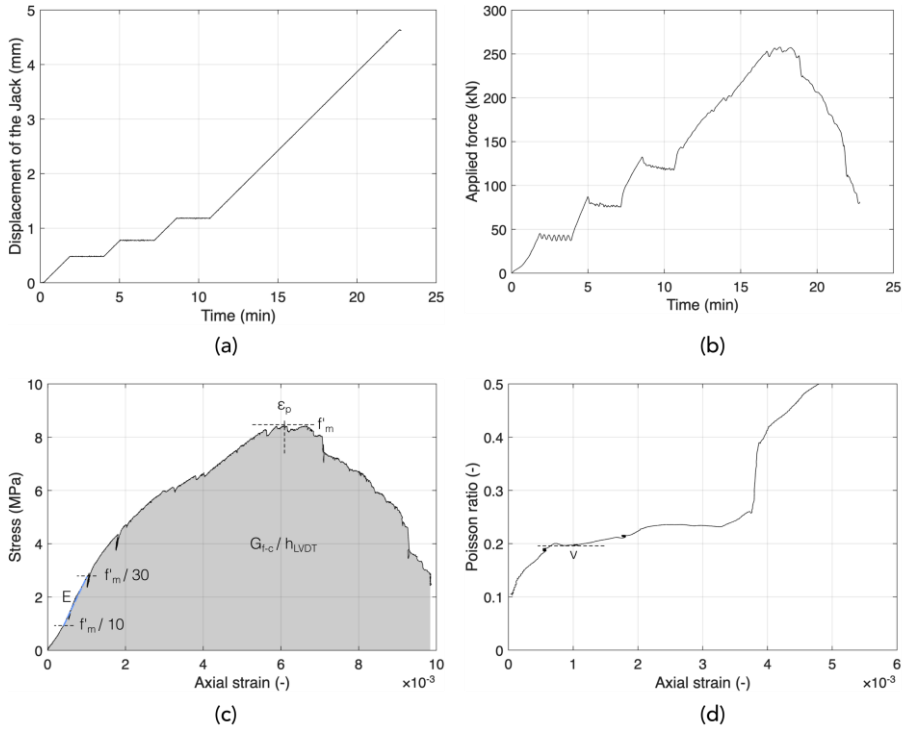


Figure 6-4 Example results from compression tests: (a) imposed loading rate expressed as jack displacement (mm) versus time; (b) applied force versus time; (c) stress–strain response used to determine compressive strength, elastic modulus, and compressive fracture energy; and (d) Poisson's ratio as a function of axial strain used for Poisson's ratio evaluation.

of ASTM E111(2017). In addition, the compressive fracture energy was determined as the area underneath the stress-displacement curve, using the averaged displacement from the vertical LVDTs (average of sensors with identical gauge length, as defined above), calculated up to a 30% of the peak strength. Finally, the Poisson ratio v was determined within the elastic range (between 1/10 and 1/3 of the maximum force), as the ratio between the lateral strain (measured with the horizontal LVDTs) and the axial strain (from the averaged vertical LVDTs). An example is reported in Figure 6-4(d).

6.2.3 In-plane four-point bending tests on spandrels

In-plane four-point bending tests were performed to assess the effect of the healing agent on the bending response of masonry components and induce controlled cracking to enable the evaluation of post-healing recovery in terms of aesthetics. A modified four-point bending configuration was adopted, based on the procedure proposed by Korswagen (Korswagen et al. 2018), which aims to mimic ground-floor spandrels subject to cyclic load-induced propagation of settlement and shrinkage cracks (e.g., vibrations or thermal fluctuations). The set-up used (Figure 6-5) differs from the standard

configuration EN 1052-2 (CEN 1999c) by inducing tensile stresses at the top of the specimen (applying the load outside the supports) and incorporating counterweights to ensure testing under cyclic loading without sudden failure.

The specimen rested on two bottom rollers (40 mm diameter), while the vertical load was applied at the top via two coupled hydraulic jacks (100 kN capacity each) equipped with load cells (100 kN capacity each). The load was transferred to the specimen surface through two 20 mm diameter rollers. A 64 kg counterweight was applied at the bottom, vertically aligned with the top jacks, to compensate for self-weight and allow for cyclic unloading. Loading was applied under Crack Mouth Opening Displacement (CMOD) control, using the displacement at the tension side of the spandrel spanning three head joints as control variable. The displacement was measured by a potentiometer featuring a ±10 mm range and 0.01% accuracy. Additional potentiometers were placed on the back of the specimen to capture the specimen deformation. Four vertical and three horizontal potentiometers (all ±10 mm range) were placed to measure vertical displacement and head joint crack opening, respectively. Furthermore, three vertical potentiometers (±30 mm range) on an external fixed beam were used to verify verticality. All potentiometers used had an accuracy of 0.01%. Simultaneously, the front face was monitored using Digital Image Correlation (DIC) to monitor crack propagation for the full duration of the loading protocol.

One specimen per configuration was tested monotonically to provide a baseline for the cyclic protocol. The remaining four specimens underwent cyclic testing (15 repetitions per step), with amplitude increments of 0.025 mm starting from an initial 0.025 mm (Figure 6-6(a)). A preload of 2 kN (1 kN/jack) was initially applied to activate the control system and maintained as the minimum load during unloading to prevent contact loss (Figure 6-6(b)). Because unloading was limited by a constant minimum force, the minimum displacement reached in each cycle was not constant (Figure 6-6(a)). The test was programmed to stop upon reaching the peak load, intentionally

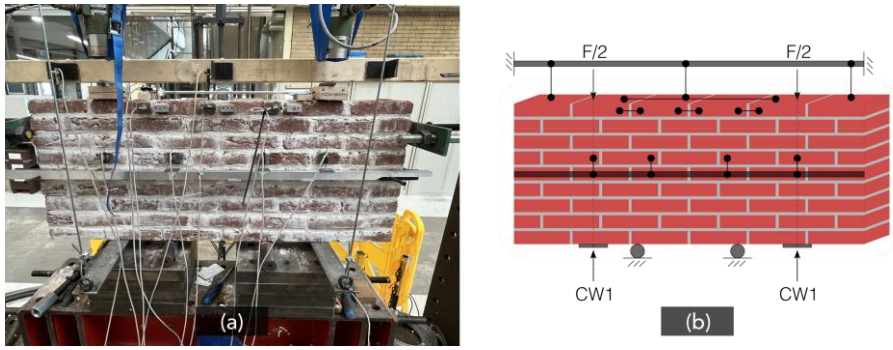


Figure 6-5 CMOD-controlled four-point bending configuration adopted to evaluate flexural behaviour of spandrels and generate controlled cracking for recovery assessment: (a) overview of the test setup and (b) sensor layout.

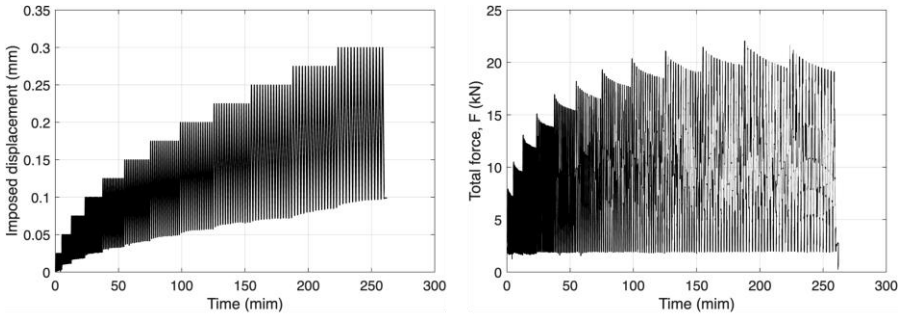


Figure 6-6 Loading protocol applied during bending tests: (a) imposed displacement of the jack versus time and (b) corresponding applied force versus time.

avoiding the post-peak softening phase to guarantee specimen removal and future healing. Thus, upon reaching the maximum force, the ongoing step was fully completed before terminating the test. Once terminated, the specimen was secured with horizontal bands to enable its removal without inducing further damage and ensure proper transportation to the healing environment as detailed in section 1.2.4.

To evaluate the agent's effect on the flexural performance of masonry components, the flexural strength (f_{x3}) and elastic modulus (E_{fx3}) were assessed using the following formulations:

$$f_{x3} = \frac{M_{max}}{W} = \frac{F_{max} d_3 / 2 + p d_1^2 / 8}{W} \quad (25)$$

$$E_{fx3} = \frac{M_{el}}{\chi_{el} I} \quad (26)$$

where, M_{max} is the maximum bending moment, W is the section modulus, F_{max} is the maximum force, d_3 is the distance between the loading and the bearing supports, d_1 is the distance between the bearing supports and p is the masonry self-weight uniform load (calculated based on an experimentally measured total mass of 80 kg). The elastic modulus was computed from the bending moment–curvature curve, using the slope in the linear elastic range between 10% and 30% of the maximum bending moment together with the specimen's moment of inertia (I), adopting the approach by (Jafari 2021). Accordingly, M_{el} and χ_{el} denote the bending moments within this interval and the corresponding curvatures.

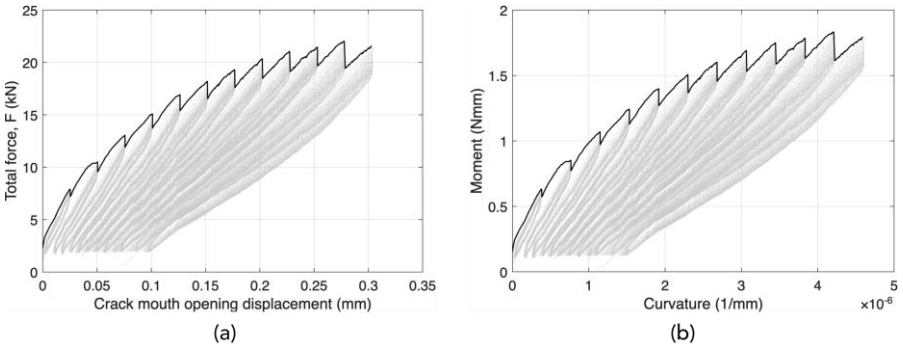


Figure 6-7 Example bending response used for flexural characterisation: (a) total force–CMOD curve and (b) corresponding moment–curvature curve.

6.2.4 Healing environment

After cracking, masonry specimens were stored under wet conditions in a fog room at 20 ± 2 °C and 95 ± 5 % relative humidity for 110 days to promote healing. To transport the specimens to the healing environment without inducing additional damage, a pallet with a vertical support structure was employed (Figure 6-8). After the designated healing period, the specimens were removed from the controlled environment and left to dry under laboratory conditions prior to visual inspection and precipitate characterisation.

6.2.5 Visual inspection

Visual inspection was used to monitor the specimens throughout the testing period, both before and after healing. Specimens were examined with the naked eye and documented using a 12 MP digital camera.



Figure 6-8 Transport and storage arrangement for healing in wet conditions: (a) pallet with a wooden supporting frame to keep specimens vertical and prevent horizontal movement during transport; and (b) specimens positioned on the pallet and protected with plastic foil during healing.

6.2.6 Fourier Transform Infrared Spectroscopy

Fourier Transform Infrared Spectroscopy (FTIR) spectra of the precipitate were recorded with a Nicolet iS5 Thermo Fisher Scientific instrument, equipped with an attenuated total reflection unit featuring a diamond crystal (400–4000 cm–1 spectral range; resolution of 4 cm1). Precipitates were collected from the spandrels after healing. Before collecting, specimens were left to dry in laboratory conditions. Material was gently scraped from the surface and manually ground to obtain a fine powder.

6.3 Performance recovery

The specimens were inspected with the naked eye and documented via a 12 MP digital camera; Figure 6-9 illustrates the surface condition before and after healing. Before the healing phase (Figure 6-9(a) and (b)), the specimens already exhibited a slight leaching effect, exclusively localised at the mortar joints. After 110 days in wet conditions, this phenomenon became much more pronounced, with precipitates spreading to the adjacent brick surfaces, as detailed in Figure 6-9(c). Since this effect was exclusively observed in specimens containing the healing agent, it can be attributed to the migration of its soluble compounds (presumably calcium lactate resulting from the poly-lactic substrate hydrolysis), a process that likely commenced during the hardening period of the masonry specimens.



Figure 6-9 Visual inspection of bacteria-based specimens: (a) spandrel and (b) compression wallette prior to healing; (c) spandrel after the healing period. In each column, the top images show an overview of the specimen surface, while the bottom images provide corresponding close-up views.

While absent in smaller brick-mortar specimens from the previous chapter, this phenomenon was only evident in larger masonry assemblies (wallettes and spandrels). This scale effect can probably be attributed to the fact that larger assemblies have a much lower exposed (drying) joint surface-to-volume ratio (0.04 mm^{-1} vs 0.24 mm^{-1} for spandrels), which establishes a **steeper internal moisture gradient during drying**. When coupled with the significant lime content of the mortar, which results in a **highly porous matrix** with high water retention capacity, this gradient induces a strong capillary flow toward the drying surfaces of the joints. This mechanism is further facilitated by the **high solubility of calcium lactate**, providing a steady supply of dissolved compounds to be transported.

This process might be exacerbated by the **heat produced during early cement hydration** (Zou et al. 2012). The reduced exposed joint surface area restricts thermal dissipation, leading to a thermal buildup that simultaneously increases the solubility of the healing agent (Kubantseva and Hartel 2002), and amplifies the driving force of the moisture transport towards the exterior. Although lime carbonation is also highly exothermic, its rate is typically slow (Rodriguez-Navarro et al. 2023), rendering its thermal contribution likely negligible compared to that of the cement. Although cement-based mortars typically generate higher hydration heat, this leaching phenomenon is generally not observed in such systems. This is likely due to the significantly lower and less connected porosity of such mortars, which probably restricts the capillary pathways necessary for agent migration.

Due to this widespread efflorescence, it became evident that the healing agent did not function as intended. Instead of achieving an aesthetic recovery, the surface condition was severely compromised, affecting the material's functionality. According to the proposed framework, the successful validation of the agent relies on all performance criteria being equally fulfilled. Since functional requirements were clearly unmet, evaluating the mechanical recovery was deemed unjustifiable.

6.4 Identification of healing products

The identification of healing products was carried out using Fourier Transform Infrared Spectroscopy (FTIR). Samples were exclusively scraped from bacteria specimens, with the aim of collecting only the observed leaching products. The resulting spectrum is reported in Figure 6-10.

The analysis suggests that the main component of the surface sample is calcium lactate. This is supported by the strong absorption band at 1600 cm^{-1} (carboxylate group) and the sharp peak at 1130 cm^{-1} (C-O bond), which are typical "fingerprints" of this compound. Secondary peaks associated with calcium carbonate (calcite) are also visible, primarily identified by the peak at 870 cm^{-1}, indicating limited surface carbonation

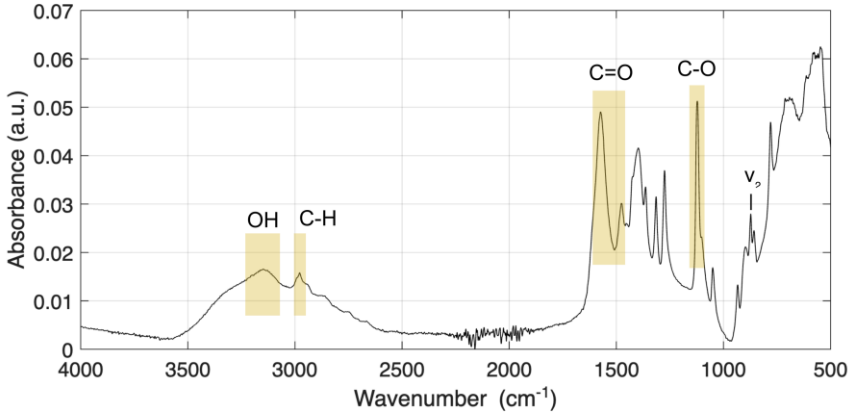


Figure 6-10 FTIR spectrum of material scraped from the masonry surface after healing.

or early-stage agent activity. However, the intensity of these peaks is significantly lower than that of the lactate signals, suggesting that calcite is a minor constituent.

Consequently, the FTIR results support the hypothesis that the healing agent leached to the surface due to moisture transport. This highlights the necessity of adjusting the curing and healing protocols for laboratory investigations to retain the substrate within the mortar.

6.5 Impact on functional properties

The effect of the healing agent on the functional performance of masonry components was investigated by comparing reference (R) and bacteria-based (B) specimens, in terms of compressive and flexural performance. The results obtained are reported in Figure 6-11 and Figure 6-12.

Overall, the incorporation of the healing agent did not lead to a substantial change in the measured properties. For both vertical compression and in-plane bending, strength and elastic modulus exhibit only limited differences between the two series, with percentage differences below 15%. In the compressive response, a difference of approximately 30% is observed in peak strain and fracture energy, suggesting a slightly reduced ductility in compression. A similar magnitude of change is observed for Poisson's ratio. However, for fracture energy and Poisson's ratio, the comparison is less conclusive, as both parameters display higher variability, which limits the significance of the observed shifts. The marked differences observed at the mortar level (compressive strength: +77%; flexural strength: +117%; Section 6.2.1) did not translate into comparable differences at the masonry component level, consistent with the role played by the brick in the overall behaviour of masonry. Consistently, both series exhibited comparable failure modes, predominantly characterized by vertical cracking and splitting

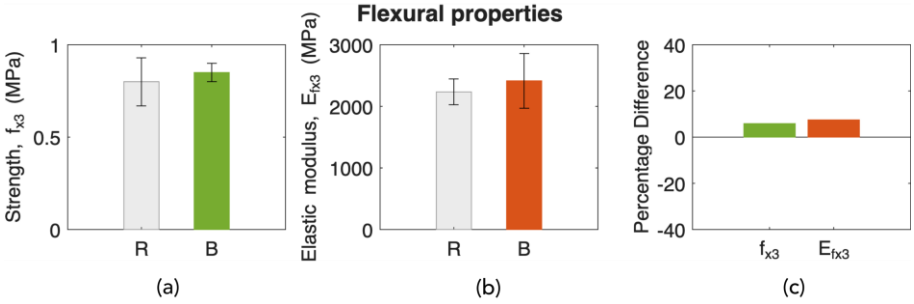


Figure 6-11 Mean flexural properties of masonry for the reference (R) and bacteria-based (B) series (error bar indicates standard deviation): (a) flexural strength and (b) elastic modulus. (f) Percentage differences between R and B are reported for each parameter.

of the brick units. In the compression wallettes, vertical cracks developed in the central region and extended through the specimen thickness. In the spandrels, cracks consistently initiated at the middle head joint and propagated through the height, predominantly as vertical cracks splitting the bricks. Examples are reported in Figure 6-13, while the failure modes for all individual specimens are available in the digital repository provided in the data availability statement.

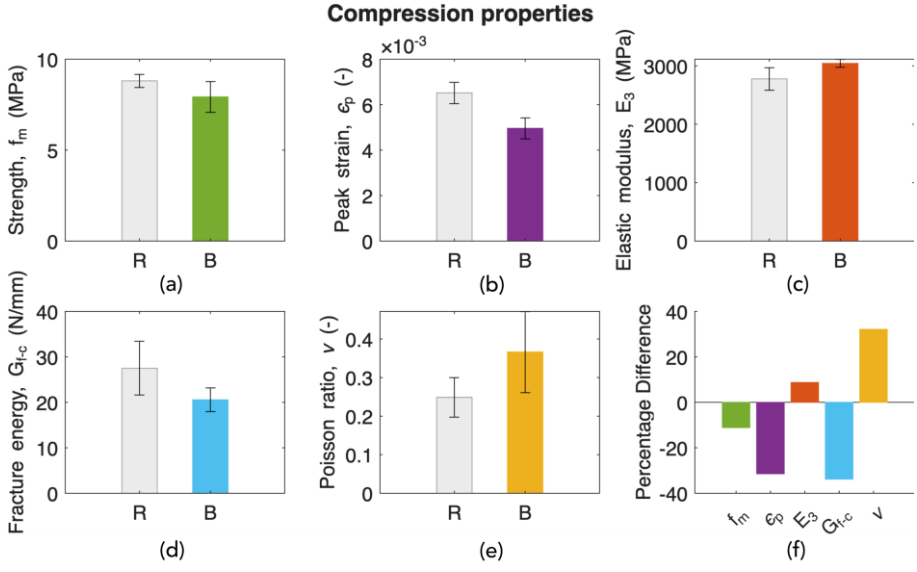
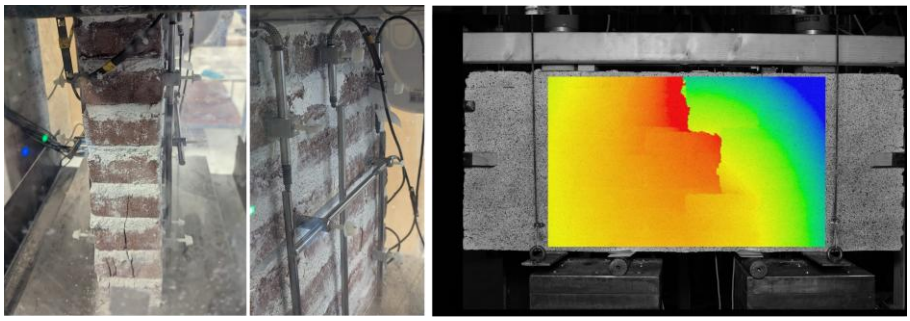


Figure 6-12 Mean compressive properties of masonry for the reference (R) and bacteria-based (B) series (error bar indicates standard deviation): (a) compressive strength, (b) peak compressive strain, (c) elastic modulus, (d) compressive fracture energy and (e) Poisson's ratio. (f) Percentage differences between R and B are reported for each parameter.



(a) (b) (c)

Figure 6-13 Crack pattern obtained in (a)(b) compression tests on wallets and (b) in-plane four point bending tests on spandrels.

However, these findings should be considered a lower-bound estimate, as the extensive leaching described previously may have partially masked the agent's full impact. A meaningful assessment should therefore be repeated once a curing that effectively retains the agent within the specimens has been established. Besides this limitation, the data presented in this chapter can be used to evaluate the representativeness of the studied masonry in replicating the mechanical properties of historical Dutch buildings. It should be noted that the initial material selection was primarily based on porosity considerations. Using the NEN-NPR 9998+C1:2020 guidelines as a benchmark, the reference series shows a compressive strength of 9.4 MPa and a fracture energy of 27 N/mm, which are 10.6% and 35% higher, respectively, than the thresholds reported for clay brick masonry built before 1945 ($f'_{m,NPR9998}$ = 8.5 MPa, $G_{f\text{-}c,NPR9998}$ = 20 N/mm). Given the newly built condition of the laboratory specimens, the measured properties are consistent with the normative benchmarks. Nevertheless, a full understanding of representativeness is left for future research. This should involve the mechanical properties and failure modes identified at previous levels to provide a complete validation of the replicated masonry.

6.6 Conclusions

This chapter investigated the applicability of a poly-lactic-acid (PLA)–based healing agent at the masonry component level, moving beyond the mortar and brick–mortar levels addressed in the previous chapters and towards larger-scale composite brick-joint assemblies. Following the framework presented in Chapter 3, the agent was assessed through qualitative recovery (aesthetics), identification of precipitated products, and evaluation of its impact on functional properties. For this purpose, masonry spandrels and compression wallettes were used.

The outcomes at the masonry component level highlight a critical upscaling challenge for autonomous self-healing solutions: the retention of soluble healing agent compounds

within the mortar. Unlike the brick-mortar specimens investigated in Chapter 5, larger masonry assemblies (both spandrels and compression wallettes) exhibited severe leaching of calcium lactate (confirmed via FTIR analysis), already visible after the curing phase. This scale effect can likely be attributed to a different moisture transport dynamic of larger assemblies. The smaller exposed (drying) joint surface likely creates a high internal moisture gradient during drying. When coupled with the high open porosity of the lime-rich mortar and the inherent solubility of the agent substrate, this gradient presumably forces the outward migration of the dissolved compounds, leading to the leaching observed. This process might be further exacerbated by the exothermic heat of cement hydration, enhancing both the solubility of the agent and the driving force of the moisture transport towards the drying surfaces. In less porous materials, such as pure cement-based mortars, the refined pore structure would likely prevent the escape of dissolved compounds despite this thermal buildup. These observations demonstrate that, at the component scale, moisture-driven migration can critically compromise the intended retention of the healing substrate within the mortar.

Future work should therefore focus on developing a curing/healing protocol for laboratory investigations on masonry component level that effectively prevents leaching, and on repeating the component-level programme to meaningfully evaluate the agent's performance and validate its practical applicability for masonry repair. Beyond the laboratory implications, these observations indicate that retention of soluble agent-related compounds must also be considered for on-site application to existing structures. In real applications, moisture gradients, intermittent wetting and uncontrolled drying may drive comparable transport processes, potentially affecting both effectiveness and surface appearance, and should therefore be investigated.

Chapter 7

Conclusions and Outlook

This final chapter consolidates the findings of this research on applying bacteria-based self-healing mortars for cracked masonry repair. This topic's relevance is underscored by the inevitable ageing of masonry and widespread cracking in the Netherlands caused by gas-extraction induced seismicity and land subsidence.

Given the field's emerging nature, the research began with an extensive literature review and preparatory studies to establish a conceptual foundation. Building on this, a framework was designed to systematically study bacteria-based self-healing mortars across mortar, brick-mortar, and masonry component levels. Using this framework, the thesis investigates a commercial poly-lactic-acid (PLA)–based healing agent originally developed for concrete. At each level, the agent's effect was evaluated in terms of performance recovery, healing products, and functional properties, using materials representative of historical construction in the Netherlands.

The following conclusions are structured around the main phases of the research and directly linked to the questions formulated in Chapter 1. Beyond summarising main findings, this chapter reflects on the research's contribution to both the scientific community and society. Finally, directions for future research are proposed, outlining key challenges that must be addressed to advance the development of autonomous self-healing strategies specifically tailored to masonry applications.

7.1 Summary of main research findings

The main objective of this work is to assess the technical viability of self-healing mortars for masonry repair, with a specific emphasis on the conservation of heritage constructions. To this end, the research integrated an extensive literature review with the design of a dedicated methodological framework, enabling the systematic evaluation of a bacteria-based poly-lactic acid (PLA) healing agent across three masonry levels: mortar, brick-mortar and masonry component.

The key findings are synthesised below.

7.1.1 Formulation of the conceptual starting point and hypothesis for autonomous self-healing in masonry

Cracking is an unavoidable and durability-governing factor in traditional unreinforced masonry, making these structures a prime target for autonomous repair. Joints inevitably suffer from damage due to weathering, settlement, vibrations; actions that are expected to intensify with climate change. Engineered self-healing mortars can offer an effective mitigation strategy, particularly for heritage conservation where minimal intervention is paramount.

Implementing autonomous self-healing mortars in masonry has a high probability of success, as the technology is inherently inspired by the autogenous (intrinsic) mechanisms of traditional lime-based masonry mortars. The full realisation of this potential requires targeted masonry research into both autogenous healing, i.e., the material's innate ability to repair microcracks mainly through carbonation, and autonomous strategies, which employ engineered additions to enhance this recovery. Characterising the limits of this intrinsic capacity is critical for designing autonomous triggers that intervene precisely when autogenous self-healing reaches its limit.

The extensive body of research on (cement-based) self-healing concrete reveals a critical opportunity for masonry: the implementation of established agents targeting calcium carbonate precipitation. In traditional lime-based masonry mortars, these agents would produce a compatible healing product that potentially goes beyond mere surface sealing. This potential could allow masonry to surpass the performance benchmarks typically observed in cement-based systems, which often face mechanical limitations.

Preparatory studies conducted on a commercially available agent show potential, concluding that masonry's porosity and healing environments are primary regulators of healing success. A mismatch between the healing environment and the porosity of bricks and mortar can lead to premature leaching of the agent's carrier, emphasising the crucial role of material selection and healing environment.

From a practical implementation perspective, repointing is proposed as a viable entry point for autonomous self-healing mortars, as it offers a non-invasive solution that adapts seamlessly to the conservation requirements of historical masonry. As a standard maintenance practice, it provides a procedure to introduce healing agents directly into the structure's most vulnerable areas, provided that compatibility is maintained between the repair mortar and the existing materials (brick and mortar). This focus on repointing does not preclude future integration into new constructions or other delivery methods.

7.1.2 Design of an experimental framework for exploring autonomous repair in masonry

To systematically study autonomous self-healing agents for masonry applications, this research designed and implemented a dedicated experimental framework. Addressing the novelty of the field and the complexity of masonry as a composite of bricks and mortar joints, the adopted approach moved beyond individual experiments, providing a coherent multi-level structure for investigation.

To ensure practical viability, the evaluation integrated three interdependent dimensions: the recovery of performance, specifically mechanical properties, watertightness and aesthetics; the characterisation of healing products; and the assessment of the agent's effect on functional properties. Although measurable recovery of damaged properties is the essential first step, the technology cannot be justified for real applications without proving that the healing stems from the designed mechanism and confirming that the agent does not detrimentally affect the material's functional properties.

Due to the composite nature of masonry, the assessment of self-healing performance was structured to progress systematically from the mortar level to the brick-mortar level up to the masonry component level. While self-healing agents are conventionally developed and initially screened at the mortar level to verify their activation and performance, evaluating their applicability in masonry requires expanding the scope to include the brick, the brick-mortar interaction, and the integrated assembly of these components in a certain bond pattern.

To address mechanical and aesthetic recovery, CMOD-controlled bending tests were successfully implemented to induce precise and controlled damage at the mortar, brick-mortar, and masonry component levels. To this end, a CMOD-controlled bond wrench test setup, developed by the author in previous research, proved instrumental in systematically exploring the healing performance at the brick-mortar level.

To address watertightness restoration, this research addressed open methodological gaps by adapting pressure-based permeability tests, originally

developed for concrete, to masonry cores. This provided a refined testing strategy for the brick-mortar level, offering a distinct advantage over standard wall-scale protocols by facilitating iterative screening through smaller specimens and faster test durations.

Initial efforts on identifying governing parameters, such as healing conditions and duration, allowed for the definition of preliminary criteria. This approach provides a foundation for future research to refine these parameters into a comprehensive testing procedure.

An extensive test program was designed and conducted to validate the repair strategy through the proposed framework, covering diverse performance aspects across all three masonry levels. Involving over 240 specimens and 420 individual tests, the program progressed from mortar bars to couplets, triplets, and extracted cores, culminating in wallettes and spandrels. Each stage compared the autonomous, bacteria-based healing agent against reference mortars under varying healing environments.

7.1.3 Experimental validation of the effectiveness of a bacteria-based self-healing agent in historical masonry

The investigation at the **mortar level** confirms the suitability of the PLA-based healing agent for lime-cement mortars, demonstrating effective activation under favourable conditions, without compromising functional properties:

- **Favourable healing conditions are identified under wet conditions (20±2 °C, 95±5 %RH) and wet-dry cycles (1h submerged in water, 23h dry at 20±2 °C and 65±5 %RH).** While comparable mechanical and aesthetic recovery was achieved under these conditions, moderate-humidity conditions (20±2 °C, 80±5 %RH) failed to promote healing, underscoring the necessity of sufficient water availability for both autogenous and autonomous self-healing.
- **Three-point bending tests with Crack Mouth Opening Displacement (CMOD) control were confirmed as a suitable method for assessing healing performance at the mortar level.** The residual crack width and healing duration were identified as critical governing parameters that must be defined jointly to ensure the accurate detection of autonomous healing.
- **Healing duration was confirmed as a primary governing factor, with results indicating that longer periods favour performance recovery.** Nevertheless, given the limited sample size, this positive trend requires further validation through more extensive testing to establish a statistically robust correlation between time and healing efficiency.
- **Autogenous healing remained dominant for fine cracks (< 0.1 mm); i.e., the mechanical recovery observed in bacteria-based specimens did not significantly differ from that of the reference specimens.** Under the most promising healing conditions, both groups achieved a **full restoration of**

bending stiffness and approximately 33% recovery of flexural strength. In this range, the healing agent's primary contribution lay in improving the consistency of the recovery in flexural stiffness and strength, rather than increasing its magnitude.

- **Bacteria-based specimens achieved full aesthetic recovery for larger cracks (≈ 0.3–0.5 mm), clearly outperforming the reference samples**. This result demonstrates that the healing agent extends the healing capacity beyond natural autogenous limits. Such a finding highlights the critical need to target larger crack widths during testing to ensure the true potential of the autonomous technology is not masked by the inherent healing capabilities of mortars.
- **Recovery follows a directional trend from the surface inwards**. Observations indicate that healing acts first on flexural stiffness and subsequently on flexural strength, confirming that the mechanism proceeds from the outside towards the inside.
- **Watertightness restoration is supported by the successful activation of the healing agent, as evidenced by the deposition of calcium carbonate within the cracks**. The complete filling of cracks with this low-solubility mineral supports the hypothesis of watertightness restoration, even in the absence of direct permeability measurements at this level.
- **The lime/cement ratio was identified as a key factor influencing healing efficiency, as demonstrated by tests across a range of mixtures (0, 0.33, 1, and 3.33)**. Enhanced performance was observed in mortars with high lime content (3.33 lime/cement ratio), probably attributed to greater calcium hydroxide availability for carbonation and superior mechanical compatibility between the healing product (calcium carbonate) and the matrix.
- **The inclusion of the agent introduces no detrimental effects on functional properties, with no adverse impacts on workability or setting time that would restrict practical implementation**. Variations in mechanical properties were found to be composition-dependent; for instance, the high-lime mortar (3.33 L/C ratio) exhibited a 25% increase in the elastic modulus. This highlights the need to precisely adjust mortar formulations to ensure mechanical compatibility.

The investigation at the **brick-mortar level** confirms the feasibility of the PLA-based agent in solid clay brick masonry built with lime-cement masonry mortar, extending mechanical recovery beyond autogenous limits without adverse functional effects:

- **Bond wrench tests with Crack Mouth Opening Displacement (CMOD) control were confirmed as a suitable method for assessing healing performance at the brick-mortar level.**

- **Autogenous healing is confirmed and quantifiable in brick–mortar specimens, proving dominant for cracks below 0.1 mm; i.e., the bond strength recovery in bacteria-based specimens did not significantly differ from that of the reference group.** Under the selected healing condition, both groups achieved approximately **45% restoration of bond strength** in fine cracks.
- **The healing agent effectively extends the repairable range beyond autogenous limits, achieving a mechanical recovery of up to 65% in terms of bond strength for larger cracks.** While reference specimens failed to recover above 0.1 mm crack widths, bacteria-based specimens consistently exhibited measurable recovery for cracks approaching 0.16 mm.
- **Watertightness recovery was verified using an adapted permeability setup, though complete sealing was constrained by crack width variability and healing duration.** High variability in crack width (ranging from 0.2 mm to >1 mm) prevented consistent sealing across the entire crack length within the considered healing period.
- **Localised precipitation in cracks exceeding 1 mm confirms aesthetic restoration.**
- **Wet conditions (20±2 °C, 95±5 %RH) promote healing without leaching, pointing to the proper activation of the agent.** Visual inspection confirmed that wet conditions successfully trigger the healing mechanism without causing the agent to leach out, validating the suitability of the agent in brick-mortar specimens using solid clay bricks and lime- cement mortar.
- **The inclusion of the agent introduces no adverse effects on functional properties.** While permeability and shear response remained unchanged, a significant increase in flexural bond strength was observed; this enhancement does not restrict applicability but suggests that mortar compositions can be adjusted to ensure mechanical compatibility in repointing applications.

The investigation at the **masonry component level** identifies that scale-dependent moisture transport can trigger washout of the agent, making hardening conditions decisive for the correct use of the agent in field applications.

- **Visual inspection revealed extensive leaching in spandrels and wallettes, a phenomenon absent in smaller brick–mortar specimens, identifying a scale-dependent response to hardening conditions.** The reduced drying surface of the mortar joints likely generates steeper moisture gradients, which could drive the highly soluble agent components towards the exterior. This migration is presumably promoted by the high interconnected porosity of the lime mortar, which potentially facilitates the transport of solutes to the surface. These results

highlight that hardening protocols must be specifically adapted to the element's geometry to prevent leaching and ensure the agent remains within the matrix.

- **FTIR analysis confirmed that surface precipitates consist of soluble agent components rather than the intended healing products.** Identifying calcium lactate as the dominant constituent proves that leaching is a result of substrate migration.

From a general methodological perspective,

- **The threshold between autogenous and autonomous healing must be defined, based on the crack width at the end of testing, i.e. after unloading.** Autogenous healing is effective for fine cracks, whereas the autonomous healing triggered by the agent becomes efficient for larger crack widths; therefore, systematic testing should focus on this larger range to effectively isolate the agent's specific contribution from the mortar's natural recovery.
- **The evaluation of healing performance must account for the interplay between healing duration and damage level.** Investigating various time scales is critical to establish the kinetics of the autonomous agent and to determine the time required for effective sealing as crack widths increase.
- **Crack mouth opening displacement (CMOD) controlled testing, as developed here for bond wrench tests on couplets and in-plane bending tests on spandrels, is crucial for minimising experimental scatter, particularly under limited healing durations.** Testing specimens to failure, as performed with shear core testing, induces large crack width variability within individual specimens; since larger cracks require significantly longer to heal, this heterogeneity results in high data dispersion when experimental timeframes are constrained.
- **The adapted permeability setup is a promising and efficient tool for the rapid assessment of watertightness recovery in masonry cores.** While it successfully detected flow reductions due to localized precipitation, longer monitoring periods are essential to fully capture the sealing kinetics and minimize scatter in larger cracks.

7.2 Scientific and societal relevance

From a scientific standpoint, this thesis contributes to the development of self-healing masonry as an emerging research field providing a methodological basis for future research. Building on concepts originally developed for concrete, the work demonstrates that **autonomous self-healing can be effectively activated in masonry materials, composed of solid clay brick and limen-cement mortar**. These findings open up a novel approach to masonry repair and position masonry as a promising new domain for

advanced, engineered self-healing solutions. The **experimental validation of the PLA-based agent** confirms the potential of such approaches, while simultaneously highlighting the need for further research before practical implementation can be realised. Crucially, the thesis aims at establishing a **framework for systematic investigation** rather than proposing a single solution. By demonstrating the transferability of an agent developed for concrete and identifying masonry-specific governing parameters, this work **contributes to the definition of reproducible assessment protocols and provides a foundation for systematic comparison**.

From a societal standpoint, this thesis investigates a strategy that offers transformative advantages, ranging from cost-effective maintenance to the long-term preservation of cultural identity.

- **Economic efficiency**: progressive cracking, even when not structurally critical, often triggers repeated repair cycles that accumulate substantial costs and material loss over time. By enabling autonomous crack sealing, self-healing approaches may reduce intervention frequency and improve resource efficiency throughout the service life of masonry structures.
- **Social reassurance and damage perception**: visible damage can generate concern and uncertainty among building owners, users, and communities. Experiences in regions affected by cumulative damage processes, such as Groningen (the Netherlands), illustrate how even minor but visible cracking may lead to societal tension and loss of confidence, despite the absence of immediate safety issues. In this context, controlling crack progression has implications that extend beyond purely technical performance and relates to how damage is perceived, managed, and addressed over time.
- **Housing availability and circular use of the built stock**: by mitigating deterioration and maintenance downtime, this strategy supports adaptive reuse and keeps existing buildings habitable, offering a sustainable response to the housing crisis while reducing reliance on new construction.
- **Heritage conservation and cultural identity**: extending the durability and service life of historic structures directly contributes to the preservation of cultural heritage and collective memory.

7.3 Recommendations for future research

Building on the findings of this thesis and setting aside the agent-specific limitations identified for the PLA-based system, emerging research topics that could further expand this study and advance the field of self-healing masonry are provided in this section.

A first line of research concerns the **refinement and standardisation of experimental methodologies across material levels**. Establishing reproducible and comparable

testing protocols is essential to assess healing performance and to enable meaningful comparison between different studies, materials, and healing agents. In this context, particular attention should be given to controlled crack induction and width, healing conditions, and assessment criteria that are representative of masonry applications. Furthermore, future work should explore in detail the application of the healing mortar in larger specimens, focusing on hardening procedures that account for geometry-dependent moisture transport to prevent agent leaching and ensure uproper activation.

A second priority is the investigation of self-healing behaviour under **realistic exposure conditions**. Future studies should move beyond optimal healing conditions and consider variable moisture regimes, temperature fluctuations, and wet–dry cycles that characterise in-service environments. Such conditions are expected to strongly influence healing activation and therefore play a key role in assessing the practical relevance of self-healing strategies for masonry.

To support practical adoption, future studies must validate self-healing mortars under **realistic repair conditions**. In particular, experimental validation should be extended from specimens fully built with self-healing mortars, as investigated in this thesis, to repointing scenarios in which self-healing mortars are applied only to the external, superficial portion of the mortar joints. This step is essential to capture the performance of self-healing mortars in realistic repointing applications. In this context, the experimental insights obtained in this thesis could support future modelling work aimed to inform repair decisions. In parallel, validation at larger scales is required to verify the transferability of self-healing performance from small-scale specimens to more representative masonry elements.

Finally, the **long-term performance** of self-healing masonry systems warrants dedicated investigation. This includes assessing durability over extended time periods, the persistence of healing mechanisms, and the response of materials to repeated damage and healing cycles. The experimental framework developed in this work also provides a basis for the comparative evaluation of alternative healing agents, including both masonry-specific systems and agents transferred from other fields. Addressing these topics will support the consolidation of self-healing masonry and facilitate the transition from proof-of-concept studies toward more application-oriented research.

Bibliography

Almssad A et al (2022)
Masonry in the Context of Sustainable Buildings: A Review of the Brick Role in Architecture.
Sustainability 14:14734.
https://doi.org/10.3390/su142214734

Arizzi A et al (2025)
A comprehensive review of the manufacturing process and properties of natural hydraulic limes.
Mater Struct 58:152.
https://doi.org/10.1617/s11527-025-02656-3

ASTM (2014)
Test Method for Static Modulus of Elasticity and Poissons Ratio of Concrete in Compression

ASTM E2167-01 (2008)
Standard Guide for Selection and Use of Stone Consolidants. ASTM International.
https://doi.org/10.1520/E2167-01R08

ASTM E514/E514M-20 (2020)
Test Method for Water Penetration and Leakage Through Masonry

AtïKoğlu MC
A THESIS SUBMITTED TO THE GRADUATE SCHOOL OF NATURAL AND APPLIED SCIENCES OF MIDDLE EAST TECHNICAL UNIVERSITY

Birkeland Ø et al (1963)
Norwegian Test Methods for Rain Penetration through Masonry Walls.
In: Committee C-12 et al. (eds) Symposium on Masonry Testing. ASTM International, p 0

Bowley B (1994)
Calcium silicate bricks.
Struct Surv 12:16–18

Cappellesso VG et al (2023)
Comparison of different types of self-healing concrete under extreme conditions.
MATEC Web Conf 378:08005.
https://doi.org/10.1051/matecconf/202337808005

CEN (1998)
EN 1015-2. Methods of test for mortar for masonry - Part 2: Bulk sampling of mortars and preparation of test mortars

CEN (1999a)
EN 1015-3. Methods of test for mortar for masonry - Part 3- Determination of consistence of fresh mortar (by flow table)

CEN (1999b)
EN 1015-11. Methods of test for mortar for masonry Part 11: Determination of flexural and compressive strength of hardened mortar

CEN (1999c)
EN 1015-10. Methods of test for mortar for masonry - Part 10: Determination of dry bulk density of hardened mortar

CEN (2013)
EN 16302. Conservation of cultural heritage – Test methods – Measurement of water absorption by pipe method.

Çopuroğlu O et al (2013)
Experimental Techniques Used to Verify Healing.
In: de Rooij M et al. (eds) Self-Healing Phenomena in Cement-Based Materials: State-of-the-Art Report of RILEM Technical Committee 221-SHC: Self-Healing Phenomena in Cement-Based Materials. Springer Netherlands, Dordrecht, pp 19–63

Costa C (2015)
Hydraulic Binders.
In: Materials for Construction and Civil Engineering. Springer, Cham, pp 1–52

De Belie N et al (2018)
A Review of Self-Healing Concrete for Damage Management of Structures.
Adv Mater Interfaces 5:.
https://doi.org/10.1002/admi.201800074

De Nardi C et al (2024)
3D-Printed Mini-vascular Networks for Self-healing Lime-based Mortars.
In: Proceedings of the Cardiff University Engineering Research Conference 2023. Cardiff University Press, pp 44–47

De Rooij M et al (eds) (2013)
Self-healing phenomena in cement-based materials.
Springer Netherlands, Dordrecht

Do Rosário Veiga M et al (2019)
Mortars.
In: Long-term Performance and Durability of Masonry Structures. Elsevier, pp 169–208

Dragonetti L et al (2025)
Circular deep renovation versus demolition with reconstruction: Environmental and financial evaluation to support decision making in the construction sector.
Energy Build 336:115610.
https://doi.org/10.1016/j.enbuild.2025.115610

Elert K et al (2002)
Lime Mortars for the Conservation of Historic Buildings.
Stud Conserv 47:62–75.
https://doi.org/10.1179/sic.2002.47.1.62

Elsen J et al (2012)
Hydraulicity in Historic Lime Mortars: A Review.
In: Historic Mortars. Springer, Dordrecht, pp 125–139

Fernandes FM (2019)
Clay bricks.
In: Long-term Performance and Durability of Masonry Structures. Elsevier, pp 3–19

Fernandes FM et al (2010)
Ancient Clay Bricks: Manufacture and Properties.
In: Dan MB et al. (eds) Materials, Technologies and Practice in Historic Heritage Structures. Springer Netherlands, Dordrecht, pp 29–48

Gaggero MB et al (2024)
Innovative Application of Self-Healing Technology to Masonry: A Proof of Concept.
Int J Archit Herit 1–11.
https://doi.org/10.1080/15583058.2024.2380408

Gaggero MB et al (2025)
Exploring Bacteria-Based Self-Healing

Potential in Cement-Lime Mortar Masonry.
In: 18th International Brick and Block Masonry Conference. pp 1011–1020

Gaggero MB et al (2023)
Experimental characterisation of flexural bond behaviour in brick masonry.
Mater Struct 56:62.
https://doi.org/10.1617/s11527-023-02144-6

Ghiassi B et al (2019)
Chapter 7 - Masonry mechanical properties.
In: Ghiassi B et al. (eds) Numerical Modeling of Masonry and Historical Structures. Woodhead Publishing, pp 239–261

Ghiassi B et al (2018)
Long-term Performance and Durability of Masonry Structures: Degradation Mechanisms, Health Monitoring and Service Life Design.
Woodhead Publishing

Giordano FG (2025)
Towards Advanced Lime-Based Mortars: Exploring Microbial Self-healing and Carbonation Strategies.
PhD Thesis, Ghent University

Giordano FG et al (2024)
Bacterially-promoted carbonation of lime-based building materials.
MATEC Web Conf 403:03003.
https://doi.org/10.1051/matecconf/202440303003

Grimm CT (1982)
Water Permeance of Masonry Walls: A Review of the Literature.
In: Masonry: Materials, Design, Construction, and Maintenance. ASTM International, Philadelphia, pp 257–280

Grimm CT (1988)
Water Permeance of Masonry Walls: A Review of the Literature.
Mason Mater Des Constr Maint 68:257–280.
https://doi.org/10.1016/j.jobe.2023.106094

Groot C et al (2022)
RILEM TC 277-LHS report: lime-based mortars for restoration–a review on long-term durability aspects and experience from practice.
Mater Struct 55:1–33.
https://doi.org/10.1617/s11527-022-02052-1

Grosso Giordano F et al (2023)
On the use of non-destructive testing for the measurement of self-healing in lime-based mortars.
Mater Today Proc.
https://doi.org/10.1016/j.matpr.2023.07.367

He S (2025)
Self-healing Strain-hardening Cementitious Composite As Concrete Cover Zone

Heinemann H et al (2009)
Concrete in the Netherlands: Historic Use of Components and Conservation

Huang H et al (2016)
Self-healing in cementitious materials: Materials, methods and service conditions.
Mater Des 92:499–511.
https://doi.org/10.1016/j.matdes.2015.12.091

Hughes DC et al (2009)
Roman cements — Belite cements

calcined at low temperature.
Cem Concr Res 39:77–89.
https://doi.org/10.1016/j.cemconres.2008.11.010

Jessa EK
Communication in Physical Sciences, 2024, 8(4): 667-673

Jonkers HM et al (2015)
Limestone-producing bacteria make concrete self healing.
In: Self Healing Materials. IOS Press, pp 137–148

Jonkers HM et al (2010)
Application of bacteria as self-healing agent for the development of sustainable concrete.
Ecol Eng 36:230–235.
https://doi.org/10.1016/j.ecoleng.2008.12.036

Kahangi Shahreza S (2024a)
Water penetration in cracked clay brick masonry before and after repointing.
Constr Build Mater 420:135631.
https://doi.org/10.1016/j.conbuildmat.2024.135631

Kahangi Shahreza S (2024b)
Water penetration in cracked clay brick masonry before and after repointing.
Constr Build Mater 420:135631.
https://doi.org/10.1016/j.conbuildmat.2024.135631

Kamal MA (2023)
Exploratory study of calcium silicate bricks as a potential material for building construction.
J Constr Built Environ 3:1–12.
https://doi.org/10.10520/ejc-jcbe_v3_n1_a1

Korswagen PA et al (2019)
Crack initiation and propagation in unreinforced masonry specimens subjected to repeated in-plane loading during light damage.
Bull Earthq Eng 17:4651–4687.
https://doi.org/10.1007/s10518-018-00553-5

Korswagen PA (2024)
Quantifying the probability of light damage to masonry structures

Kubica J (2024)
Masonry systems: Past, present and future.
MATEC Web Conf 403:01003.
https://doi.org/10.1051/matecconf/202440301003

Lanas J et al (2004)
Mechanical properties of natural hydraulic lime-based mortars.
Cem Concr Res 34:2191–2201.
https://doi.org/10.1016/j.cemconres.2004.02.005

Lei B et al (2023)
Carbon Emission Reduction Evaluation of End-of-Life Buildings Based on Multiple Recycling Strategies.
Sustainability 15:15711.
https://doi.org/10.3390/su152215711

Lindqvist (2009)
Rilem TC 203-RHM: Repair mortars for historic masonry. Testing of hardened mortars, a process of questioning and interpreting.
Mater Struct 42:853–865.
https://doi.org/10.1617/s11527-008-9455-x

Lourenço PB (2014)
Masonry Structures, Overview.

In: Encyclopedia of Earthquake Engineering. Springer, Berlin, Heidelberg, pp 1–9

Lourenço PB et al (2014)
Characterization and Damage of Brick Masonry.
In: Costa A et al. (eds) Structural Rehabilitation of Old Buildings. Springer Berlin Heidelberg, Berlin, Heidelberg, pp 109–130

Lubelli B et al (2011)
Self-healing of lime based mortars: Microscopy observations on case studies.
HERON 56:75–92

Mack RC (1998)
Repointing Mortar Joints in Historic Masonry Buildings.
U.S. Department of the Interior, National Park Service, Culutral Resources, Heritage Preservation Services

Mack RC et al (1979)
An Introduction to Repointing.
Bull Assoc Preserv Technol 11:44–60. https://doi.org/10.2307/1493799

Maria S (2010)
Methods for porosity measurement in lime-based mortars.
Constr Build Mater 24:2572–2578. https://doi.org/10.1016/j.conbuildmat.2010.05.019

Maurenbrecher P et al (2016)
Repair mortars for historic masonry. State-of-the-art report RILEM TC 203-RHM

McCarthy MJ et al (2019)
9 - Pozzolanas and Pozzolanic Materials.
In: Hewlett PC et al. (eds) Lea's Chemistry of Cement and Concrete (Fifth Edition). Butterworth-Heinemann, pp 363–467

Minke G (2025)
Building with Earth: Design and Technology of a Sustainable Architecture Fifth and revised edition.
Birkhäuser

Mors R et al (2020)
Bacteria-based self-healing concrete: evaluation of full scale demonstrator projects.
RILEM Tech Lett 4:138–144. https://doi.org/10.21809/rilemtechlett.2019.93

Mors RM et al (2017)
Feasibility of lactate derivative based agent as additive for concrete for regain of crack water tightness by bacterial metabolism.
Ind Crops Prod 106:97–104. https://doi.org/10.1016/j.indcrop.2016.10.037

Muhammad NZ et al (2016)
Tests and methods of evaluating the self-healing efficiency of concrete: A review.
Constr Build Mater 112:1123–1132. https://doi.org/10.1016/j.conbuildmat.2016.03.017

Niedostatkiewicz M et al (2024)
CAUSES OF DEFECTS AND DAMAGE TO BRICK MASONRY ELEMENTS IN HISTORIC BUILDINGS.
Civ Environ Eng Rep 34:423–448. https://doi.org/10.59440/ceer/194876

Nijland TG
The volcanic foundation of Dutch architecture: Use of Rhenish tuff and trass in the Netherlands in the past two

millennia

Oliveira DV (2003)
Experimental and numerical analysis of blocky masonry structures under cyclic loading.
doctoralThesis

Papayianni I et al (2006)
Strength–porosity relationships in lime–pozzolan mortars.
Constr Build Mater 20:700–705. https://doi.org/10.1016/j.conbuildmat.2005.02.012

Prosperi A (2025)
Modelling of subsidence induced damage to masonry buildings: Influence of soil heterogeneity on settlement and development of fragility curves.
Delft University of Technology

RILEM TC 25-PEM (1980)
Recommended tests to measure the deterioration of stone and to assess the effectiveness of treatment methods. Mater Struct 13:175–253. https://doi.org/10.1007/BF02473564

Rodriguez-Navarro C et al (2023)
Carbonation mechanisms and kinetics of lime-based binders: An overview.
Cem Concr Res 173:107301

Rossi E (2022)
From waste to self-healing concrete: the missing PHA-link.
Dissertation (TU Delft)

Sánchez A et al (2022)
Mechanical properties of adobe masonry for the rehabilitation of buildings.
Constr Build Mater 333:127330. https://doi.org/10.1016/j.conbuildmat.2022.127330

Sandoval C et al (2016)
Experimental characterization and detailed micro-modeling of multi-perforated clay brick masonry structural response.
Mater Struct 50:34. https://doi.org/10.1617/s11527-016-0888-3

Shellenbarger M (1991)
Tuck Pointing History and Confusion.
APT Bull 23:38. https://doi.org/10.2307/1504338

Shiotani T et al (2024)
Non-destructive inspection technologies for repair assessment in materials and structures.
Dev Built Environ 18:100443. https://doi.org/10.1016/j.dibe.2024.100443

Spaan B et al (2015)
Buildings in the Netherlands by year of construction

TC 203-RHM (Main author: Paul Maurenbrecher) (2012)
RILEM TC 203-RHM: Repair mortars for historic masonry - Requirements for repointing mortars for historic masonry.
Mater Struct 45:1303–1309. https://doi.org/10.1617/s11527-012-9849-7

the brick industry association (2023)
RILEM TUBE TESTING AND BRICK MASONRY

Tziviloglou E (2018)
Biogenic self-healing mortar.

https://doi.org/10.4233/d52fe8b2-8076-4a80-84ad-9030633a39fd

Tziviloglou E et al (2015)
Performance requirements to ensure the crack sealing performance of bacteria-based self-healing concrete.
In: Proceedings of the 9th International Conference on Fracture Mechanics of Concrete and Concrete Structures. IA-FraMCoS

Tziviloglou E et al (2016)
Bio-Based Self-Healing Concrete: From Research to Field Application.
In: Hager MD et al. (eds) Self-healing Materials. Springer International Publishing, Cham, pp 345–385

Válek J et al (2010)
The role of mortar in masonry: an introduction to requirements for the design of repair mortars.
RILEM Publications SARL

Van Balen K (2005)
Carbonation reaction of lime, kinetics at ambient temperature.
Cem Concr Res 35:647–657. https://doi.org/10.1016/j.cemconres.2004.06.020

van Balen K et al (2010)
Repair Mortars for Historic Masonry. From Problem to Intervention: a decision process

van der Zwaag S (2007)
An Introduction to Material Design Principles: Damage Prevention versus Damage Management.
In: van der Zwaag S (ed) Self Healing Materials: An Alternative Approach to 20 Centuries of Materials Science. Springer Netherlands, Dordrecht, pp 1–18

Van Hees RPJ et al (2004)
Characterisation and damage analysis of old mortars.
Mater Struct 37:644–648. https://doi.org/10.1007/BF02483293

Van Mullem T et al (2020)
Addressing the need for standardization of test methods for self-healing concrete: an inter-laboratory study on concrete with macrocapsules.
Sci Technol Adv Mater 21:661–682. https://doi.org/10.1080/14686996.2020.1814117

Van Tittelboom K et al (2013)
Self-Healing in Cementitious Materials—A Review.
Materials 6:2182–2217. https://doi.org/10.3390/ma6062182

Varas MJ et al (2005)
Natural cement as the precursor of Portland cement: Methodology for its identification.
Cem Concr Res 35:2055–2065. https://doi.org/10.1016/j.cemconres.2004.10.045

Wang J et al (2014a)
X-ray computed tomography proof of bacterial-based self-healing in concrete.
Cem Concr Compos 53:289–304. https://doi.org/10.1016/j.cemconcomp.2014.07.014

Wang JY et al (2014b)
Self-healing concrete by use of microencapsulated bacterial spores.
Cem Concr Res 56:139–152. https://doi.org/10.1016/j.cemconres.2013.11.009

Wei S et al (2015)
Biomineralization processes of calcite induced by bacteria isolated from marine

sediments.
Braz J Microbiol 46:455–464.
https://doi.org/10.1590/S1517-838246220140533

White SR et al (2001)
Autonomic healing of polymer composites.
Nature 409:794–797.
https://doi.org/10.1038/35057232

Wiktor V et al (2015)
Field performance of bacteria-based repair system: Pilot study in a parking garage.
Case Stud Constr Mater 2:11–17.
https://doi.org/10.1016/j.cscm.2014.12.004

Wiktor V et al (2011a)
Quantification of crack-healing in novel bacteria-based self-healing concrete.
Cem Concr Compos 33:763–770.
https://doi.org/10.1016/j.cemconcomp.2011.03.012

Wiktor V et al (2011b)
Quantification of crack-healing in novel bacteria-based self-healing concrete.
Cem Concr Compos 33:763–770.
https://doi.org/10.1016/j.cemconcomp.2011.03.012

Young D (2021)
Mortars: materials, mixes and methods : a guide to repointing mortar joints in older buildings : technical guide.
Heritage Council of Victoria, Melbourne, Victoria

Acknowledgments

Looking back, it feels as though a lifetime has passed before reaching this moment. This thesis marks the end of a long journey, one I worked hard for and built step by step across places that shaped me: my hometown in Argentina, my family roots in Italy, and finally the Netherlands, a country that, in ways I did not anticipate, made me feel at home again. Along the way, I was fortunate to meet many people who supported me in different ways. Although it is impossible to name them all, I am deeply grateful to each of them.

I would like to begin by thanking my supervisors, who have supported my growth since 2018. To Paul, thank you for the opportunity to work on this fascinating "self-healing masonry" project, and especially for the freedom and trust you granted me to truly make it my own; your pragmatic advice, your presence during challenging research times, and the way you encouraged me to go further made all the difference. To Rita, thank you for sharing your extensive knowledge on material characterization, for always finding the time to be present when needed, and for helping me refining this work; your commitment to excellence and your attention to detail were both a guide and a constant inspiration to improve. Finally, to Jan, it has been an absolute honor to have you as my promotor; your immense knowledge and sharp perspective on masonry significantly elevated the quality of this work, and I am grateful for your dedication in bringing this innovative research to its highest level. Together, you have been a constant source of guidance and inspiration.

Equally essential to this journey was the Stevin II Laboratory, a place that after so many years became my second home. To the managers, technicians, and student assistants: thank you for your invaluable technical support and for the friendship we built along the way. A very special mention goes to Georgios who welcomed me like family and guided me through all the challenges of the lab. And to Ton: I hope these words reach you, wherever you are; this work would not have been possible without your support, your company, and the joy you brought to every day I spent at Stevin II; thank you for everything, I miss you!

I would also like to thank the many experts and colleagues who contributed their knowledge to specific parts of this research. I am very grateful to Caspar Groot and Barbara Lubelli for their guidance on material selection, and to Rob van der Pluijm and Wienerberger for their support in sourcing the high-porosity bricks. Special thanks also go to Henk Jonkers, Erik Schlangen, Shan He and Emanuele Rossi for helping me navigate the world of bacteria-based self-healing agents. I would also like to thank the staff at the Micro Lab, as well as to Patrik Holthuizen and Franco Grosso, for guiding me through completely new methodologies.

In addition to the academic support, I would like to thank Ines for her dedication in bringing this project to the public eye and for sharing her invaluable expertise in media

A

and communication. Special thanks also go to the administrative staff, Iris, Sandra, Jacqueline, and Jaap, whose kindness and constant availability made TU Delft a much warmer place to work.

To my colleagues and officemates: thank you for sharing both the highs of successful results and the lows of research frustrations. To Navid and Uday for turning laboratory work into a true team effort; your collaboration not only improved the quality of this work but also made the process much more enjoyable. To Michele and Mani for providing valuable numerical insights whenever I needed a different perspective.

I want to thank all the friends that Delft gifted me beyond the academic walls. You made this city a home. A very special mention goes to Manuel and Desa, for making this journey so much more enjoyable. To my paranymph, Yopi: somewhere along the way, you became one of my closest friends; thank you for making everything feel lighter and for always being there, for the fun, the stress, and especially the final stages of this long journey.

To my family, to those present and those in my heart. To my parents, for teaching me to never stop and that it is never too late to start over. To my sister, my lifelong pillar, and my nieces, Margherita and Ludovica. To Sol, Caro, and Flor, my "sisters by choice", always close despite having spent half our lives far apart. To Emanuele: thank you for every moment we have shared and for standing by me through all my highs, lows, and changing moods; but above all, thank you for helping me rediscover myself. And finally, to Bart, my faithful companion who stayed by my side through the longest nights of writing.

Finally, I dedicate this work to my younger self, whose persistence through every challenge made it possible for me to reach this milestone today.

Curriculum Vitae



Maria Belén Gaggero

2026-present	**Postdoc Researcher.** Technische Universiteit Delft, The Netherlands.
2022-2026	**Ph.D. in Structural Mechanics.** Technische Universiteit Delft, The Netherlands.
2019-2022	**Researcher.** Exploring repair and strengthening strategies for unreinforced masonry (bacteria-based self-healing mortar, structural glass window, bed-joint reinforcement). Technische Universiteit Delft, The Netherlands.
2018	**Master's Intership.** Structural health monitoring of "Paraboloide di Casale Monferrato". MastrLAB, Italy.
2016-2019	**Master of Science in Civil Engineering.** Comparison of test methods to determine masonry bond flexural strength. Politecnico di Torino, Italy.
2015-2016	**Bachelor's Internship.** Structural health monitoring for civil structures. Istemi s.a.s., Italy.
2012-2016	**Bachelor of Science in Civil Engineering.** Università degli Studi di Salerno, Italy.
20-08-1991	**Born in Buenos Aires, Argentina.**

CV

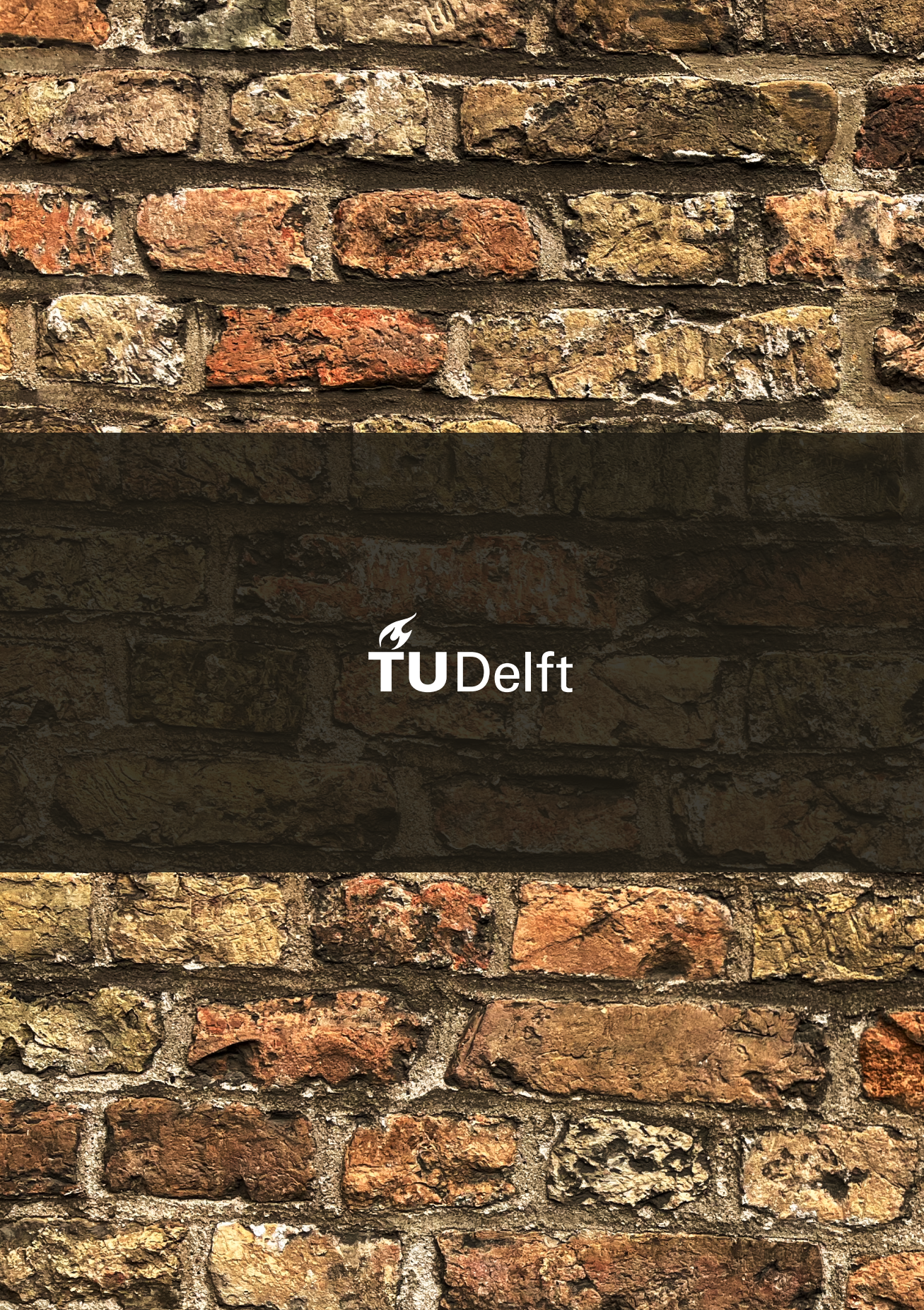
List of Publications

Conference Papers and Journal Articles

- Korswagen, P., **Gaggero, M. B.**, & Rots, J. G. (2025). Experimental Comparison of Cracking in Four Masonry Walls with Different Boundaries and Material. In G. Milani, & B. Ghiassi (Eds.), 18th International Brick and Block Masonry Conference: Proceedings of IB2MaC 2024—Volume 2 (Vol. 2, pp. 322-332). (Lecture Notes in Civil Engineering; Vol. 614). Springer. https://doi.org/10.1007/978-3-031-73310-9_23
- **Gaggero, M. B.**, Korswagen, P. A., Esposito, R., & Rots, J. G. (2025). Exploring Bacteria-Based Self-healing Potential in Cement-Lime Mortar Masonry. In G. Milani, & B. Ghiassi (Eds.), 18th International Brick and Block Masonry Conference: Proceedings of IB2MaC 2024—Volume 2 (Vol. 2, pp. 1011–1020). (Lecture Notes in Civil Engineering; Vol. 614). Springer. https://doi.org/10.1007/978-3-031-73310-9_77
- **Gaggero, M. B.**, Korswagen, P. A., Esposito, R., & Rots, J. G. (2024). Innovative Application of Self-Healing Technology to Masonry: A Proof of Concept. International Journal of Architectural Heritage, 19(5), 598-608. https://doi.org/10.1080/15583058.2024.2380408
- **Gaggero, M. B.**, & Esposito, R. (2023). Experimental characterisation of flexural bond behaviour in brick masonry. Materials and Structures/Materiaux et Constructions, 56(3), Article 62. https://doi.org/10.1617/s11527-023-02144-6
- **Gaggero, M. B.**, Korswagen, P. A., Esposito, R., & Rots, J. G. (2023). Innovative Application of Self-healing Technology to Masonry: A Proof of Concept. In Y. Endo, & T. Hanazato (Eds.), Structural Analysis of Historical Constructions: SAHC 2023 - Volume 1 (Vol. 1, pp. 332-345). (RILEM Bookseries; Vol. 47). Springer. https://doi.org/10.1007/978-3-031-39603-8_28
- **Gaggero, M. B.**, Korswagen, P. A., Esposito, R., & Rots, J. G. (2023). In-Plane Behaviour of Unreinforced Masonry Strengthened with a Structural Glass Window: A Proof of Concept. Buildings, 13(2), 1-13. Article 361. https://doi.org/10.3390/buildings13020361

Extended Abstracts

- **Gaggero, M. B.**, Korswagen, P. A., Esposito, R., & Rots, J. G. (2024). Bacteria-based self-healing agent for masonry repair: applicability to cement-lime mortars. 78-79. Abstract from SUBLime Conference 2024, Funchal, Portugal.


TU Delft